

**INVESTIGATION OF THE ATMOSPHERIC
OZONE FORMATION POTENTIAL OF
TRICHLOROETHYLENE**

Draft Report to the
Halogenated Solvents Industry Alliance

by
William P. L. Carter, Dongmin Luo, and Irina L. Malkina

August 29, 1997

College of Engineering
Center for Environmental Research and Technology
University of California
Riverside, California 92521

SUMMARY

A series of environmental chamber experiments and computer model calculations were carried out to assess the atmospheric ozone formation potential of trichloroethylene (TCE). The experiments consisted of determining the effects of adding TCE on NO oxidation, ozone formation and integrated OH radical levels when irradiated in the presence of NO_x, NO_x and ethane, or in simulated model photochemical smog systems using differing surrogate mixtures to represent the reactive organic gases (ROGs) present in the atmosphere, and using differing ROG/NO_x ratios. The addition of relatively small amounts of ethane slowed down the rates of NO oxidation, O₃ formation, and TCE consumption in TCE - NO_x irradiations. This is explained by chain reactions involving chlorine atoms. TCE had a positive effect on NO oxidation, O₃ formation, and radical levels in simulated photochemical smog systems, though the positive effect on ozone declined to zero in experiments with sufficiently low NO_x/ROG ratios. TCE also enhanced the rate of alkane consumption, also indicating the role of chlorine atoms.

Two chemical mechanisms, with differing assumptions concerning the relative importance of the TCE + ozone reaction, were developed which could predict the effect of TCE on rates of NO oxidation and initial rates of ozone formation in these experiments. However, the mechanisms could not account for the leveling off of O₃ in the added TCE, high ROG/NO_x experiments, the acceleration of ozone formation and leveling off and rapid TCE consumption at the end of one TCE - ethane - NO_x experiment, and they tended to underpredict the apparent Cl atom production in many experiments. It is concluded that there are other secondary reactions occurring in the TCE photooxidation system which are not presently understood.

Atmospheric ozone model calculations were conducted to estimate TCE's ozone impacts for a variety of atmospheric conditions, though the chamber experiments indicated that the model predictions are probably unreliable except for the higher NO_x Maximum Incremental Reactivity (MIR) conditions. The MIR of TCE was found to be approximately 3 times that of ethane on an ozone per gram emitted basis, or approximately 1/4 that of the mixture representing all reactive organic gas emissions. The model predicted that the relative ozone impacts of TCE did not change significantly as NO_x levels are reduced, though based on the chamber experiments it is likely, though not certain, that its relative impacts decline. More laboratory data concerning the identity and reactions of TCE's atmospheric oxidation products are needed before models can be developed which can reliably predict TCE's ozone impacts under the full range of atmospheric conditions.

ACKNOWLEDGEMENTS

The authors gratefully acknowledge Dr. Roger Atkinson for many helpful discussions, Mr. Dennis Fitz for assistance in administering this program, and Mr. Kurt Bumiller and Ms. Kathalena Smihula for assistance in carrying out the experiments. Although this work was funded by the Halogenated Solvents Industry Alliance, the opinions and conclusions expressed in this report are entirely those of the primary author, Dr. William P. L. Carter. Mention of trade names or commercial products do not constitute endorsement or recommendation for use.

TABLE OF CONTENTS

<u>Section</u>	<u>Page</u>
INTRODUCTION	1
EXPERIMENTAL AND DATA ANALYSIS METHODS	3
Overall Experimental Approach	3
Environmental Chamber	4
Experimental Procedures	5
Analytical Methods	6
Characterization Methods	7
Reactivity Data Analysis Methods	7
CHEMICAL MECHANISMS AND MODELING METHODS	10
General Atmospheric Photooxidation Mechanism	10
ClO _x Reactions	11
Atmospheric Reactions of Trichloroethylene	11
TCE Mechanism Used in the Model Simulations	17
Environmental Chamber Simulations	18
Atmospheric Reactivity Simulations	19
RESULTS AND DISCUSSION	20
Summary of Experiments	20
Results of the TCE - NO _x and TCE - Ethene - NO _x Experiments	20
Results of The Reactivity Experiments and Mechanism Evaluations	25
ATMOSPHERIC REACTIVITY CALCULATIONS	33
Scenarios Used for Reactivity Assessment	33
Base Case Scenarios	34
Adjusted NO _x scenarios	36
NO _x Conditions in the Base Case Scenarios	36
Incremental and Relative Reactivities	37
Reactivity Scales	38
Calculated Relative Reactivities of Trichloroethylene	39
CONCLUSIONS	41
REFERENCES	43
APPENDIX A	
LISTING OF THE CHEMICAL MECHANISM	A-1

LIST OF TABLES

<u>Number</u>		<u>page</u>
1.	Chronological listing of all the chamber experiments carried out for this program.	21
2.	Summary of conditions and selected results of the trichloroethylene - NO _x and trichloroethylene - ethane - NO _x chamber experiments.	23
4.	Summary of conditions of base case scenarios used for atmospheric reactivity assessment.	35
5.	Summary of relative incremental reactivities (gram basis) calculated for trichloroethylene, ethane and sum of all emitted VOCs.	40
A-1.	List of species in the chemical mechanism used in the model simulations for this study.	A-1
A-2.	List of reactions in the chemical mechanism used in the model simulations for this study.	A-4
A-3.	Absorption cross sections and quantum yields for photolysis reactions.	A-11
A-4.	Values of chamber-dependent parameters used in the model simulations of the experiments for this study.	A-16

LIST OF FIGURES

<u>Number</u>		<u>page</u>
1.	Experimental and calculated concentration-time plots for selected species in the trichloroethylene - NO _x and the trichloroethylene - ethane - NO _x chamber runs.	24
3.	Summary of conditions and results of the incremental reactivity experiments.	26
2.	Plots of selected results of the mini-surrogate + trichloroethylene experiment DTC-312 . .	27
3.	Plots of selected results of the mini-surrogate + trichloroethylene experiment DTC-305. . .	27
4.	Plots of selected results of the mini-surrogate + trichloroethylene experiment DTC-303. . .	28
5.	Plots of selected results of the mini-surrogate with ethane + trichloroethylene experiment DTC-306.	28
6.	Plots of selected results of the high NO _x full surrogate + trichloroethylene experiment DTC-320.	29
7.	Plots of selected results of the high NO _x full surrogate + trichloroethylene experiment DTC-311.	29
8.	Plots of selected results of the full surrogate + trichloroethylene experiment DTC-308. . .	30
9.	Plots of selected results of the full surrogate + trichloroethylene experiment DTC-307. . .	30
10.	Plots of selected results of the high ROG full surrogate + trichloroethylene experiment DTC-309.	31
11.	Plots of selected results of the low NO _x full surrogate + trichloroethylene experiment DTC-321.	31

INTRODUCTION

Ozone in photochemical smog is formed from the gas-phase reactions of volatile organic compounds (VOCs) and oxides of nitrogen (NO_x) in sunlight. Although Los Angeles has the worst ozone problem in the United States, other areas of the country also have episodes where ozone exceeds the federal air quality standard of 0.12 ppm. Ozone control strategies in the past have focused primarily on VOC controls, though the importance of NO_x control has become recognized in recent years. VOC and NO_x controls have differing effects on ozone formation. NO_x is required for ozone formation, and if the levels of NO_x are low compared to the levels of reactive VOCs, then changing VOC emissions will have relatively little effect on ozone. Since NO_x is removed from the atmosphere more rapidly than VOCs, ozone in areas far downwind from the primary sources tend to be more NO_x limited, and thus less responsive to VOC controls. VOC controls tend to reduce the rate that O_3 is formed when NO_x is present, so VOC controls are the most beneficial in reducing O_3 in the urban source areas, where NO_x is relatively plentiful, and where O_3 yields are determined primarily by how rapidly it is being formed. Because of this, any comprehensive ozone control strategy must involve reduction of emissions of both NO_x and VOCs.

Many different types of VOC compounds are emitted into the atmosphere, each reacting at different rates and having different mechanisms for their reactions. Because of this, they can differ significantly in their effects on ozone formation, or their "reactivity". Some compounds, such as CFCs, do not react in the lower atmosphere at all, and thus make no contribution to ground-level ozone formation. Others, such as methane, react and contribute to ozone formation, but react so slowly that their practical effect on ozone formation is negligible. Obviously, it does not make sense to regulate such compounds as ozone precursors. In recognition of this, the EPA has exempted certain compounds from such regulations on the basis of having "negligible" effects on ozone formation. Although the EPA has no formal policy on what constitutes "negligible" reactivity, in practice it has used the ozone formation potential of ethane as the standard in this regard. This is because ethane is the most reactive of the compounds that the EPA has exempted to date. Therefore, the ozone formation potential of a compound relative to ethane is of particular interest when assessing whether it might be a likely candidate for exemption from regulation as an ozone precursor.

Trichloroethylene (TCE) is a widely used solvent compound which is of interest to the Halogenated Solvents Industry Alliance (HSIA). It is sufficiently volatile that its use might result in it being emitted into the atmosphere, and thus it is subject to regulation as a VOC ozone precursor. However, if TCE can be shown to have negligible ozone reactivity, i.e., have ozone impacts comparable to or less than those of ethane, then it might be appropriate for the EPA to exempt it from such

regulations. To assess this, it is necessary to conduct computer model calculations of the compound's ozone impacts under various atmospheric conditions, and compare them with those calculated for ethane. This was the approach that was employed in our assessments of the reactivities of acetone (Carter et al., 1993a) and the volatile siloxanes (Carter et al., 1992) relative to ethane. However, such estimates of ozone impacts are no more reliable than the chemical mechanisms upon which they are based. Chemical mechanisms can be derived based on laboratory studies, theories, and estimates of the elementary reactions involved (e.g., see Atkinson, 1990, 1994, and references therein), but unless they are evaluated against environmental chamber data, one cannot be confident that the mechanism is complete and is giving accurate predictions. There have been some environmental chamber studies indicating that TCE has a relatively high ozone forming potential (Gay et al, 1976), but these results can be attributed to chain reactions involving chlorine (Cl) atoms which would be unlikely to be important in the atmosphere because of the presence of other pollutants which react with Cl. No predictive mechanism for TCE's atmospheric reactions has been developed or evaluated, and the available environmental chamber data are not sufficiently well characterized or representative of atmospheric conditions to be useful for this purpose.

To improve our ability to assess the ozone impacts of TCE under atmospheric conditions, the HSIA contracted the College of Engineering Center for Environmental Research and Technology (CE-CERT) to develop and evaluate atmospheric reaction mechanism for TCE, to carry out the environmental chamber experiments needed for this purpose, and to use this experimentally-evaluated mechanism to estimate TCE's ozone impacts under varying atmospheric conditions. The results of this study are documented in this report.

EXPERIMENTAL AND DATA ANALYSIS METHODS

Overall Experimental Approach

Two types of environmental chamber experiments were carried out with TCE. The first consisted of irradiations of TCE and oxides of nitrogen (NO_x) in air both with and without ethane, added to partially or completely scavenge Cl atoms. These experiments were used for mechanism evaluation by directly comparing the observed concentration-time profiles for ozone, NO, TCE, and (when present) ethane with those predicted by model calculations. They were carried out because preliminary modeling indicated that their results are highly sensitive to details of the TCE reaction mechanism which was assumed, with the level of added ethane directly affecting the relative importance of the reaction of TCE with chlorine atoms compared to its reactions with hydroxyl (OH) radicals. Ethane was used as the chlorine scavenger because of its relatively simple reaction mechanism and because its reaction with OH radicals are slow compared to its relatively rapid reaction with Cl atoms. The chemical mechanisms and the model simulation methods are discussed in the following section.

Although their sensitivity to mechanistic details made the TCE - NO_x and TCE - ethane - NO_x runs these runs highly useful for mechanism evaluation, they do not represent a very realistic simulation of atmospheric conditions, where significant levels of other reactive organic gas (ROG) pollutants are also present. Therefore, they are not suitable for directly evaluating how well the mechanism predicts ozone impacts in the atmosphere. For this purpose, a second set of experiments, which are referred to as the "incremental reactivity" runs, were carried out. These involve two types of irradiations of model photochemical smog mixtures. The first is a "base case" experiment where a mixture of reactive organic gases (ROGs) representing those present in polluted atmospheres (the "ROG surrogate") is irradiated in the presence of oxides of nitrogen (NO_x) in air. The second is the "test" experiment which consists of repeating the base case irradiation except that the VOC whose reactivity is being assessed is added. The differences between the results of these experiments provide a measure of the atmospheric impact of the test compound, and the difference relative to the amount added is a measure of its reactivity.

Several types of base case experiments were used to provide data concerning the reactivities of the test compound under varying atmospheric conditions. These were as follows:

Mini-Surrogate Experiments. This base case employed a simplified ROG surrogate and relatively low ROG/NO_x ratios. Low ROG/NO_x ratios represent "maximum incremental reactivity" (MIR) conditions, which are most sensitive to VOC effects. This is useful because it provides a sensitive test for the model, and also because it is most important that the model correctly predict a VOC's reactivity under conditions where the atmosphere is most sensitive to the VOCs. The ROG mini-surrogate mixture

employed consisted of ethene, n-hexane, and m-xylene. This same surrogate was employed in our previous studies (Carter et al, 1993a,b; 1995a.), and was found to provide a more sensitive test of the mechanism than the more complex surrogates which more closely represent atmospheric conditions (Carter et al, 1995a). This high sensitivity to mechanistic differences makes the mini-surrogate experiments most useful for mechanism evaluation, while still approximating atmospheric conditions.

Full Surrogate Experiments. This base case employed a more complex ROG surrogate under somewhat higher, though still relatively low, ROG/NO_x conditions. While less sensitive to the mechanism employed, experiments with a more representative ROG surrogate are needed to evaluate the mechanism under conditions that more closely resembling the atmosphere. The ROG surrogate employed was the same as the 8-component "lumped molecule" surrogate as employed in our previous study (Carter et al., 1995a), and consists of n-butane, n-octane, ethene, propene, trans-2-butene, toluene, m-xylene, and formaldehyde. Calculations have indicated that use of this 8-component mixture will give essentially the same results in incremental reactivity experiments as actual ambient mixtures (Carter et al., 1995a).

Full Surrogate Experiments with NO_x or ROG Varied. The base case for these experiments employed the same 8-component lumped molecule surrogate as the full surrogate experiments described above, except that the initial NO_x or ROG levels were varied. These were used to provide data on how well the mechanism could simulate the effects of not only changing the ROG/NO_x ratios, but also of changing the absolute ROG levels. The ROG/NO_x ratio was varied because that has been shown to be an important factor affecting a VOC's impact on ozone formation (Carter and Atkinson, 1989a; Carter, 1994; Carter et al., 1995a). In the case of TCE, the total ROG level was also varied because it might affect how the formation of Cl atoms from the TCE reaction system affect ozone impacts. The ranges in The initial ROG and NO_x reactant concentrations were comparable to those employed in our previous studies (Carter et al. 1995a).

An appropriate set of control and characterization experiments necessary for assuring data quality and characterizing the conditions of the runs for mechanism evaluation were also carried out. These are discussed where relevant in the results or modeling methods sections.

Environmental Chamber

The environmental chamber system employed in this study was the CE-CERT "Dividable Teflon Chamber" (DTC) with a blacklight light source. This consists of two ~5000-liter 2-mil heat-sealed FEP Teflon reaction bags located adjacent to each other and fitted inside an 8'x8'x8' framework, and which uses two diametrically opposed banks of 32 Sylvania 40-W BL black lights as the light source. The lighting system in the DTC was found to provide so much intensity that only half the lights were used for irradiation. The unused black lights were covered with aluminum sheet as well, and were used to bring the chamber up to the temperature it will encounter during the irradiation before the uncovered lights

are turned on. The air conditioner for the chamber room was turned on before and during the experiments. Four air blowers which are located in the bottom of the chamber were used to help cool the chamber as well as mix the contents of the chamber. The CE-CERT DTC is very similar to the SAPRC DTC which is described in detail elsewhere (Carter et al, 1995a,b).

The DTC is designed to allow simultaneous irradiations of the base case and the test experiments under the same reaction conditions. As indicated above, the chamber is actually two adjacent FEP Teflon reaction bags which can be simultaneously irradiated using the same light source and with the same temperature control system. These are referred to as the two “sides” of the chamber (Side A and Side B) in the subsequent discussion. The sides are interconnected with two ports, each with a box fan, which rapidly exchange their contents to assure that base case reactants have equal concentrations in both sides. In addition, a fan is located in each of the reaction bags to rapidly mix the reactants within each chamber. The ports connecting the two reactors can then be closed to allow separate injections on each side, and separate monitoring of each side. This design is optimized for carrying out incremental reactivity experiments such as those for this program.

Experimental Procedures

The reaction bags were flushed with dry air produced by an AADCO air purification system for 14 hours (6pm-8am) on the nights before experiments. The continuous monitors were connected prior to reactant injection and the data system began logging data from the continuous monitoring systems. The reactants were injected as described below (see also Carter et al, 1993b,, 1995b). The common reactants were injected in both sides simultaneously using a three-way (one inlet and two outlets connected to side A and B respectively) bulb of 2 liters in the injection line and were well mixed before the chamber was divided. The contents of each side were blown into the other using two box fans located between them. Mixing fans were used to mix the reactants in the chamber during the injection period, but these were turned off prior to the irradiation. The sides were then separated by closing the ports which connected them, after turning all the fans off to allow their pressures to equalize. After that, reactants for specific sides (the test compound in the case of reactivity experiments) were injected and mixed. The irradiation began by turning on the lights and proceeded for 6 hours. After the run, the contents of the chamber were emptied by allowing the bag to collapse, and then was flushed with purified air. The contents of the reactors were vented into a fume hood.

The procedures for injecting the various types of reactants were as follows. The NO and NO₂ were prepared for injection using a high vacuum rack. Known pressure of NO, measured with MKS Baratron capacitance manometers, were expanded into Pyrex bulbs with known volumes, which were then filled with nitrogen (for NO) or oxygen (for NO₂). The contents of the bulbs were then flushed into the chamber with AADCO air. The other gas reactants were prepared for injection either using a high vacuum rack or a gas-tight syringes whose amounts were calculated. The gas reactants in a gas-tight syringe was

usually diluted to 100-ml with nitrogen in a syringe. The volatile liquid reactants (including TCE) were injected, using a micro syringe, into a 1-liter Pyrex bulb equipped with stopcocks on each end and a port for the injection of the liquid. The port was then closed and one end of the bulb was attached to the injection port of the chamber and the other to a dry air source. The stopcocks were then opened, and the contents of the bulb were flushed into the chamber with a combination of dry air and heat gun for approximately 5 minutes. Formaldehyde was prepared in a vacuum rack system by heating paraformaldehyde in an evacuated bulb until the pressure corresponded to the desired amount of formaldehyde. The bulb was then closed and detached from the vacuum system and its contents were flushed into the chamber with dry air through the injection port.

Analytical Methods

Ozone and nitrogen oxides (NO_x) were continuously monitored using commercially available continuous analyzers with Teflon sample lines inserted directly into the chambers. The sampling lines from each side of the chamber were connected to solenoids which switched from side to side every 10 minutes, so the instruments alternately collected data from each side. Ozone was monitored using a Dasibi 1003AH UV photometric ozone analyzer and NO and total oxides of nitrogen (including HNO₃ and organic nitrates) were monitored using a Teco Model 14B chemiluminescent NO/NO_x monitor. The output of these instruments, along with that from the temperature sensors and the formaldehyde instrument, were attached to a computer data acquisition system, which recorded the data at 10 minutes intervals for ozone, NO and temperature (and at 15 minutes for formaldehyde), using 30 second averaging times. This yielded a sampling interval of 20 minutes for taking data from each side.

The Teco instrument and Dasibi CO analyzer were calibrated with a certified NO and CO source and CSI gas-phase dilution system. It was done prior to chamber experiment for each run. The NO₂ converter efficiency check was carried out in regular intervals. Dasibi ozone analyzer was calibrated against SAPRC transfer standard ozone analyzer using transfer standard method in a interval of three months and was check with CSI ozone generator (set to 400 ppb) for each experiment to assure that the instrument worked properly. The details were discussed elsewhere (Carter et al, 1995b)

Organic reactants other than formaldehyde were measured by gas chromatography with FID and ECD detections as described elsewhere (Carter et al., 1993b; 1995b). GC samples were taken for analysis at intervals from 20 minutes to 30 minutes either using 100 ml gas-tight glass syringes or by collecting the 100 ml sample from the chamber onto Tenax-GC solid adsorbent cartridge. These samples were taken from ports directly connected to the chamber after injection and before irradiation and at regular intervals after irradiation. For analysis of the more volatile species such as TCE and the ROG surrogate components employed in this study, the contents of the syringe were flushed through a 2 ml or 3 ml stainless steel or 1/8' Teflon tube loop and subsequently injected onto the column by turning a gas sample valve.

The calibrations for the GC analyses for most compounds were carried out by sampling from chambers or vessels of known volume into which known amounts of the reactants were injected, as described previously (Carter et al, 1995b).

Characterization Methods

Three temperature thermocouples for each chamber were used to monitor the chamber temperature, two of which were located in the sampling line of continuous analyzers to monitor the temperature in each side. The third one was located in the chamber to monitor chamber temperature. The temperature in these experiment were typically 21-25 C for DTC and 25-30 C for CTC.

The light intensity in the DTC chamber was monitored by periodic NO₂ actinometry experiments utilizing the quartz tube method of Zafonte et al (1977), with the data analysis method modified as discussed by Carter et al. (1995b). The results of these experiments were tracked over time in this chamber since it was first constructed in early 1994, and were fit by a curve where the NO₂ photolysis rate decayed relatively rapidly from its initial values of ~0.31 min⁻¹ when the chamber and lights were new, then declining only slowly during the time of these experiments. A curve through the full set of actinometry results predicted NO₂ photolysis rates in the range of 0.216 - 0.217 min⁻¹ during the time of these experiments, and the results of the actinometry experiments associated with the runs in this study are consistent with this range. The spectrum of the blacklight light source was measured using a LiCor LI-1200 spectra radiometer, and found to be essentially the same as the general blacklight spectrum recommended by Carter et al (1995b) for use in modeling blacklight chamber experiments.

The dilution of the DTC chamber due to sampling is expected to be small because the flexible reaction bags can collapse as samples are withdrawn for analysis. However, some dilution occurs with the aging of reaction bags because of small leaks. Information concerning dilution in an experiment can be obtained from relative rates of decay of added VOCs which react with OH radicals with differing rate constants (Carter et al., 1993b; 1995b). Most experiments had a more reactive compounds such as m-xylene and n-octane present either as a reactant or added in trace amounts to monitor OH radical levels. Trace amounts (~0.1 ppm) of n-butane were also added to experiments if needed to provide a less reactive compound for monitoring dilution. In addition, specific dilution check experiments such as CO irradiations were carried out. Based on these results, the dilution rate was found to be 0.3% per hour in side A, and 0.1% per hour in side B. Note that this alkane tracer method is not a valid measure of dilution in experiments with TCE or other compounds whose reactions can produce Cl atoms.

Reactivity Data Analysis Methods

As indicated above, many of the experiments for this program consisted of simultaneous irradiation of a "base case" reactive organic gas (ROG) surrogate - NO_x mixture in one of the dual reaction chambers, together with an irradiation, in the other reactor, of the same mixture with a TCE added. The results are

analyzed to yield two measures of VOC reactivity: the effect of the added VOC on the amount of NO reacted plus the amount of ozone formed, and integrated OH radical levels. These are discussed in more detail below.

The first measure of reactivity is the effect of the VOC on the change in the quantity $[O_3]-[NO]$, or $([O_3]_t-[NO]_t) - ([O_3]_0-[NO]_0)$, which is abbreviated as $d(O_3-NO)$ in the subsequent discussion. As discussed elsewhere (e.g., Johnson, 1983; Carter and Atkinson, 1987; Carter and Lurmann, 1990, 1991, Carter et al, 1993b, 1995b,c), this gives a direct measure of the amount of conversion of NO to NO_2 by peroxy radicals formed in the photooxidation reactions, which is the process that is directly responsible for ozone formation in the atmosphere. (Johnson calls it "smog produced" or "SP".) The incremental reactivity of the VOC relative to this quantity, which is calculated for each hour of the experiment, is given by

$$IR[d(O_3-NO)]_t^{VOC} = \frac{d(O_3-NO)_t^{test} - d(O_3-NO)_t^{base}}{[VOC]_0} \quad (1)$$

where $d(O_3-NO)_t^{test}$ is the $d(O_3-NO)$ measured at time t from the experiment where the test VOC was added, $d(O_3-NO)_t^{base}$ is the corresponding value from the corresponding base case run, and $[VOC]_0$ is the amount of test VOC added. An estimated uncertainty for $IR[d(O_3-NO)]$ is derived based on assuming an ~3% uncertainty or imprecision in the measured $d(O_3-NO)$ values. This is consistent with the results of the side equivalency test, where equivalent base case mixtures are irradiated on each side of the chamber.

Note that reactivity relative to $d(O_3-NO)$ is essentially the same as reactivity relative to O_3 in experiments where O_3 levels are high, because under such conditions $[NO]_t^{base} \approx [NO]_t^{test} \approx 0$, so a change $d(O_3-NO)$ caused by the test compound is due to the change in O_3 alone. However, $d(O_3-NO)$ reactivity has the advantage that it provides a useful measure of the effect of the VOC on processes responsible for O_3 formation even in experiments where O_3 formation is suppressed by relatively high NO levels.

The second measure of reactivity is the effect of the VOC on the rate of consumption of the other VOCs present in the experiment. For most VOCs, this would be due primarily to the effect of the VOC on OH radical levels, and a quantity called "IntOH" has been defined to measure this (Carter et al, 1993b; 1995c). However, compounds such as TCE also introduce Cl atoms, which also causes enhanced consumption rates for VOCs. This is particularly the case for alkanes, which react at only moderate rates with OH radicals but react with Cl atoms more rapidly than any of the other species present. The effect of TCE on OH radicals and on Cl atoms can be differentiated, at least to some extent, by looking at its effect on consumption rates for VOCs which are consumed to differing extents by each reaction. M-xylene, which is present in both surrogates, has previously been used as the compound of choice for estimating integrated OH radical levels because it reacts relatively rapidly with OH radicals and under normal conditions this is the only reaction which significantly consumes it. Although it also reacts with

Cl atoms, model calculations indicate that it is still consumed primarily by reaction with OH radicals even even in the presence of TCE or other species that introduce Cl atoms. This is because, compared to other organics, the aromatics react relatively rapidly with OH radicals and relatively slowly with Cl atoms, while the opposite is true for the alkanes (see mechanism listing and footnotes in Appendix A). On the other hand, alkanes react quite rapidly with Cl atoms, and provide the main sink for Cl atoms when introduced into surrogate - NO_x systems. Model calculations indicate that reaction with Cl is the major loss process for the n-butane in the full surrogate runs, and for the n-hexane in the mini-surrogate runs, in experiments where a significant Cl atom source such as TCE is present.

For the purposes of mechanism evaluation, the effects of TCE on consumption rates of the ROG surrogate components are measured by quantities referred to as the Relative Consumption Reactivities with respect to the component, which is defined as

$$RCR(tracer)_t = \frac{tracer\ consumption_t^{test} - tracer\ consumption_t^{base}}{[Test\ VOC\ added]} \quad (II)$$

where [Test VOC added] is the amount of TCE added in the test experiment, "tracer" is the ROG surrogate component whose rate of consumption is used as the tracer for OH or Cl levels, [tracer consumption]_t^{test} and [tracer consumption]_t^{base} refer to the amount of consumption of these species up to time = t due to chemical reaction in the base case and added test VOC experiment, respectively, and are defined as

$$tracer\ consumption_t = \ln\left(\frac{[tracer]_0}{[tracer]_t}\right) - t \cdot D, \quad (III)$$

and [tracer]₀ and [tracer]_t refer to the initial and time = t concentration of the radical tracer (m-xylene, n-butane or n-hexane), and D is the average dilution rate for the experiment. The RCR(m-xylene) data thus provide reactivity measures which are sensitive to the effect of the VOC on OH radical levels, while RCR(n-butane) or RCR(n-hexane) indicate of the amounts of Cl atom production caused by the added test VOC.

CHEMICAL MECHANISMS AND MODELING METHODS

General Atmospheric Photooxidation Mechanism

The chemical mechanism used in the environmental chamber and atmospheric model simulations in this study is given in Appendix A to this report. This mechanism is based on that documented by Carter (1990), with a number of updates as discussed below. It can explicitly represent a large number of different types of organic compounds, but it lumps together species reacting with similar rate constants and mechanisms in atmospheric simulations, and it uses a condensed representation for many of the reactive organic products. The reactions of inorganics, CO, formaldehyde, acetaldehyde, peroxyacetyl nitrate, propionaldehyde, peroxypropionyl nitrate, glyoxal and its PAN analog, methylglyoxal and several other product compounds are represented explicitly. In addition, the reactions of unknown photoreactive products formed in the reactions of aromatic hydrocarbons are represented by a model species "AFG2", whose yields and photolysis parameters are adjusted based on fits of model simulations to environmental chamber experiments. A chemical operator approach is used to represent peroxy radical reactions, as discussed in detail by Carter (1990). Generalized reactions with variable rate constants and product yields are used to represent the primary emitted alkane, alkene, aromatic and other VOCs (with rate constants and product yields appropriate for the individual compounds being represented in each simulation); The tables in the Appendix list only those VOCs (or groups of VOCs) used in the simulations in this work. Most of the higher molecular weight oxygenated product species are represented using the "surrogate species" approach, where simpler molecules such as propionaldehyde or 2-butanone are used to represent the reactions of higher molecular weight analogues that are assumed to react similarly.

Several aspects of the Carter (1990) mechanism were updated prior to this work to account for new kinetic and mechanistic information for certain classes of compounds as described by Carter et al. (1993a) and Carter (1995). In addition, further modifications were made to the uncertain portions of the mechanisms for the aromatic hydrocarbons to satisfactorily simulate results of experiments carried out in different chambers. The previously optimized aromatic mechanisms tended to underpredict the rates of NO oxidation and O₃ formation in the aromatic - NO_x experiments carried out in a chamber using a xenon arc light source (Carter et al, 1995c), so the aromatic mechanisms were reoptimized, by adjusting yields of model species used to represent uncharacterized ring-opening products (AFG2 and MGLY), to satisfactorily fit the chamber data. Note that while in the previous mechanisms the model species MGLY represented methylglyoxal alone, in the reoptimized mechanism it is being used to represent uncharacterized products as well. The reoptimized MGLY and AFG2 yields were for toluene were changed from respectively 0.13 and 0.49 to 0.85 and 0.27, and those for m-xylene were changed from 0.37 and 0.75 to 1.55 and 0.51, and the AFG2 photolysis rate was reduced by a factor of 2, relative to those used by the 1993 version of the mechanism (Carter et al, 1993a; Carter 1995). These updated aromatic mechanisms

are still being developed, and a more detailed discussion of them are beyond the scope of this paper. The reactions added to the mechanism to represent the photooxidation of TCE are discussed in more detail below.

ClO_x Reactions

Prior to this study, the general mechanism did not include provisions for representing compounds such as TCE whose photooxidations introduce chlorine atoms into the system. The reactions which were added to the mechanism to account for the presence of Cl are included in the listing in Appendix A, together with the absorption cross-sections used for the photoreactive ClO_x species. Footnotes to the listing in Appendix A indicate the sources of the rate constants and mechanisms assumed. Most of the inorganic reactions and reactions of Cl with the simpler organics were taken from the most recent NASA (1994) or IUPAC (Atkinson et al., 1996) evaluations, and are considered to be reasonably well characterized. In addition, all the absorption cross-sections for the photoreactive ClO_x species were taken from the IUPAC (Atkinson et al., 1996) tabulations. Some reactions expected or calculated to be of negligible importance in these systems (such as ClO + ClO or ClO₂ reactions) have been omitted to simplify the mechanism. (However, we have not carried out a complete sensitivity study, and it is possible that some reactions included on Table 1 could also be neglected.) The greatest uncertainty concerns the reactions of Cl with some of the higher organics, whose mechanisms and (in some cases) rate constants have not been studied. A rate constant of $1 \times 10^{-10} \text{ cm}^3 \text{ molec}^{-1} \text{ s}^{-1}$ is used for organics whose Cl rate constants are unknown, and if the products are unknown they are assumed to be the same as those formed in the corresponding OH reaction, except that HCl is also formed. These assumptions present a source of uncertainty in the model simulations of the reactions of TCE in the presence of mixtures containing these compounds.

Atmospheric Reactions of Trichloroethylene

TCE is expected to react in the atmosphere primarily with OH radicals, though reaction with ozone and NO₃ radicals may also occur to a non-negligible extent. In addition, the reaction of TCE with chlorine atoms can become important, and even dominate, under the conditions of the environmental chamber experiments, and must also be considered. Information is available concerning the rate constants for most of these reactions. For the reaction with OH radicals, the rate constant used for modeling is based on the recommendation of Atkinson (1994), which is

$$\begin{aligned}k(\text{OH} + \text{TCE}) &= 5.63 \times 10^{-13} e^{427/T} \text{ cm}^3 \text{ molec}^{-1} \text{ s}^{-1}, \text{ or} \\k(\text{OH} + \text{TCE}) &= 2.34 \times 10^{-12} \text{ cm}^3 \text{ molec}^{-1} \text{ s}^{-1} \text{ at } 300 \text{ K}.\end{aligned}$$

For the reaction with chlorine atoms, the room-temperature measurements of Atkinson and Aschmann (1987), or

$$k(\text{Cl} + \text{TCE}) = 8.08 \times 10^{-11} \text{ cm}^3 \text{ molec}^{-1} \text{ s}^{-1}$$

was used. The temperature dependence was not determined, but it is likely to be small. For the reaction with NO_3 radicals, the rate constant of Atkinson et al (1987), or

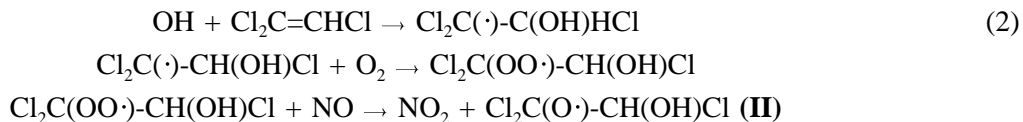
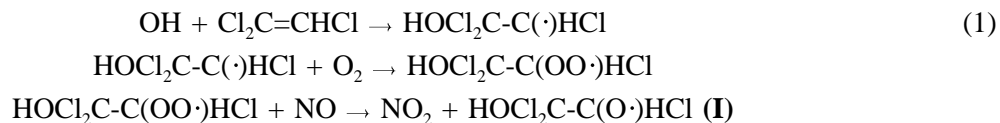
$$k(\text{NO}_3 + \text{TCE}) = 2.81 \times 10^{-16} \text{ cm}^3 \text{ molec}^{-1} \text{ s}^{-1}$$

was used. However, in his review of available data concerning NO_3 kinetics, Atkinson (1991) notes that this value may be subject to uncertainty due to possible interferences caused by chlorine atom formation in this system. The temperature dependence in this rate constant is unknown and was neglected in the model simulations.

For the ozone reaction, there is only an upper limit of $k(\text{O}_3 + \text{TCE}) < 3 \times 10^{-20} \text{ cm}^3 \text{ molec}^{-1} \text{ s}^{-1}$ reported by Atkinson et al (1982). For modeling purposes we use two mechanisms: one assuming a relatively low rate constant of $\sim 1 \times 10^{-21} \text{ cm}^3 \text{ molec}^{-1} \text{ s}^{-1}$, the other where it is treated as an adjustable parameter within the range determined by its upper limit. This is discussed further below.

There are also some data available concerning the mechanism of the atmospheric reactions of trichloroethylene. Tuazon et al. (1988) reported that the products of the $\text{OH} + \text{trichloroethylene}$ reaction are significantly affected by the addition of ethane, indicating that chlorine atoms are formed to a significant extent in this reaction, since ethane acts as a Cl atom scavenger in this system. In a separate study, Kleindienst et al. (1989) reacted TCE with OH radicals in the presence of propene or ethylene, and observed products expected from the reactions of Cl atoms with those compounds. They used their data to derive a Cl atom yield in the $\text{OH} + \text{TCE}$ reaction of $60 \pm 20\%$, though the data were so scattered that this cannot be considered to be quantitative. The major product observed by Tuazon et al (1988) in the presence of the Cl atom scavenger was phosgene, though the yield was only $\sim 40\%$, indicating that other major reaction pathways are not accounted for. Based on the estimated or expected reactions of these radicals (see below), one would have expected that HC(O)Cl and/or HOCHClC(O)Cl , but the yield of the former in the presence of the Cl scavenger was only $\sim 7\%$, while no IR bands attributable to the latter were observed (Tuazon et al, 1988). In the absence of the Cl scavenger, the yield of $\text{CHCl}_2\text{C(O)Cl}$ increased from $\sim 20\%$ to $\sim 50\%$, and the yield of HC(O)Cl also increased to $\sim 50\%$. The latter are the products one would expect from the Cl atom reaction, along with $\sim 100\%$ regeneration of Cl atoms (Tuazon et al. 1988). Significant Cl + trichloroethylene reaction would be expected in the absence of a Cl scavenger because, although trichloroethylene reacts with OH radicals relatively slowly, its Cl atom reaction is quite rapid, as indicated by the rate constants given above.

The reaction of OH radicals with TCE would be expected to proceed by the initial addition of OH radicals to the double bond, followed by the addition of O₂ and reaction with NO to form a chlorinated β-substituted alkoxy radical:



The alternative route for the peroxy + NO reaction,



which becomes increasingly important in the alkane photooxidation systems as the size of the molecule increases (Carter and Atkinson, 1989b, and references therein), is assumed not to be important in the case of TCE. If it were important, one would expect at least some inhibition by TCE of the rates of NO consumption in the initial stages of the incremental reactivity experiments, and this, in fact, was not observed (see Results, below).

The alkoxy radical (I) formed in the above reactions could either decompose via β C-C or C-Cl scission or react with O₂, as follows:



In the case of (II), which cannot react with O₂, the possible decomposition reactions are,



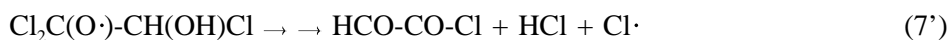
Based on thermochemical considerations and data on relative importances of decomposition vs O₂ reactions with other alkoxy radicals (Atkinson and Carter, 1991), and competing decompositions of

chloroethoxy radicals (Sanhueza et al, 1976; Tuazon et al, 1988) one would expect Reaction (3), decomposition to ultimately yield Cl_2CO , HC(O)Cl and HO_2 , to be the most important process for **(I)**, while for **(II)** Reaction (7), decomposition to form Cl atoms and HOCICH-CO-Cl , is expected to dominate. Note that the latter reaction accounts for the formation of Cl atoms in the TCE photooxidation system, while the former reaction does not.

Unfortunately, the data of Tuazon et al (1988) are not completely consistent with either reactions (3) or (7), though they are no more consistent with any of the other alternatives given above. In particular, in the presence of the Cl atom scavenger, the yield of HC(O)Cl (predicted by Reactions 3 and 6) is only ~7%, and no IR bands attributable to the acid chloride products predicted by Reactions (5) and (7) were observed. However, Tuazon et al (1988) observed that the HC(O)Cl formation was highly variable, and noted that Sanhueza et al (1976) proposed reaction channels involving formation of vibrationally excited HC(O)Cl decomposing to $\text{HCl} + \text{CO}$. In addition, the failure to observe HOCICH-CO-Cl may be due to a rapid elimination of HCl from the α -hydroxy chloride center, giving rise to HCO-CO-Cl . For lack of more reasonable alternatives, and for consistency with both the alkoxy radical estimations cited above and the product data of Tuazon et al (1988), we assume that both of these HCl eliminations are occurring, i.e.,



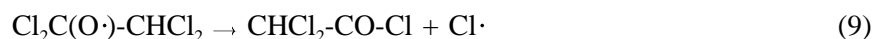
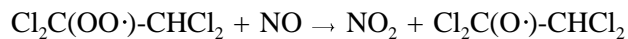
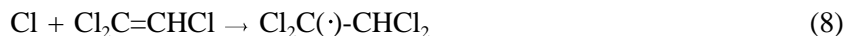
for radical **(I)**, and



for radical **(II)**.

The relative importances of these two processes is unknown, though the ~40% yield of Cl_2CO observed by Tuazon et al (1988) in the presence of the Cl atom trap suggests that Reaction (3') may be occurring approximately that fraction of the time. This is also consistent with the ~60% for chlorine atom production derived by Kieindienst et al (1989), albeit from highly scattered data and with highly uncertain corrections applied. Therefore, this is assumed in the model simulations used in this study.

The reactions of TCE with Cl atoms are expected to proceed via pathways analogous to the OH radical reaction, though addition to the least Cl-substituted end is believed to dominate, and the alkoxy radical formed is believed to react primarily by Cl atom elimination (Sanhueza et al, 1976):



This is consistent with the observations of Tuazon et al (1988) that $\text{CHCl}_2\text{-CO-Cl}$ is a major product formed from the $\text{OH} + \text{TCE}$ system which is suppressed by the addition of a Cl atom scavenger.

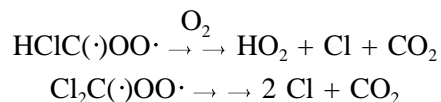
Note that one feature of the above mechanism is that Cl atoms are completely regenerated from the $\text{TCE} + \text{Cl}$ reaction, i.e., that it is not a Cl atom sink. Therefore, if TCE is the major species present in the reaction system which can react with Cl atoms, the TCE photooxidation will be characterized by a chain reaction involving Cl as the chain carrier. This can explain the high reactivity previously observed for TCE (Gay et al, 1976). This also means that addition of other species which react with Cl atoms would have the effect of slowing down the overall TCE photooxidation process. This was examined in our chamber experiments as discussed below.

Although the reaction of TCE with NO_3 radicals is relatively slow, model calculations indicate that this process is not always negligible, and has to be included in the mechanism. The reaction is assumed to proceed analogously to the Cl reactions shown above, giving rise, after an NO to NO_2 conversion, to the formation of Cl atoms and a nitrate-substituted acid chloride. For simplicity and because of the relative small fraction of TCE which reacts via this route, the nitrate-substituted acid chloride is assumed to react similarly to the acid chloride formed in the Cl atom reaction, and thus the radicals and products formed in the NO_3 reaction are lumped with those in the Cl reaction, shown above.

The reactions of TCE with O_3 was also included because model calculations indicate that it may have a non-negligible effect if it occurred with a rate constant near the upper limit determined by Atkinson et al. (1982). The mechanism is unknown, but the initial processes probably involve formation of Crigee-substituted biradicals.

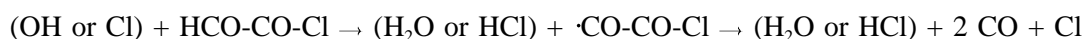


For simplicity and for lack of information otherwise, we assume these two processes are equally important. In addition, it was assumed that both of the Cl-substituted Crigee biradicals undergo complete decomposition,

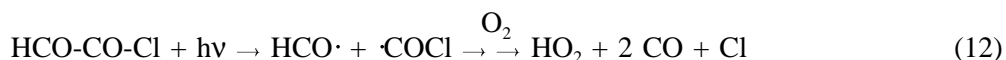


The subsequent reactions of the major TCE reaction products also need to be considered. The major organic products predicted in the OH radical reaction are Cl_2CO and HCO-CO-Cl . Cl_2CO cannot react with OH radicals and its only likely mode of reaction is photolysis. We could not find useful information in the literature about its photolysis under lower atmospheric conditions, but based on the

relatively low absorption cross sections for HC(O)Cl compared to formaldehyde at wavelengths > 300 nm (Atkinson et al, 1996), it is likely that atmospheric photodecomposition of Cl₂CO is not important. Therefore, its reactions are ignored. On the other hand, HCO-CO-Cl is expected to react both with OH radicals and chlorine atoms, and also undergo relatively rapid photolysis, analogously to glyoxal. It's reactions with OH radicals or chlorine atoms are assumed to proceed with rate constants which are half those assumed for glyoxal (for OH) or formaldehyde (for Cl), and are assumed to proceed as follows:

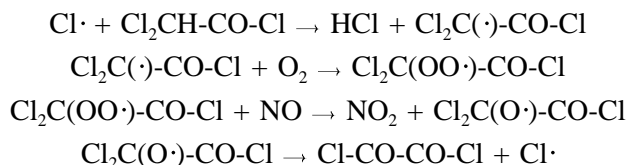


Its photodecomposition is assumed to be similar to that of glyoxal, i.e.,



The absorption cross sections are assumed to be similar to those of glyoxal (see Appendix A). The overall quantum yield is expected to be similar to that for glyoxal, but is treated as an adjustable parameter in the model simulations. Simulations of some of the chamber experiments turned out to be relatively sensitive to this parameter, because Reaction (12) is a non-negligible source of new chlorine atoms at the around the later stages of these experiments.

Finally, the reactions of the products of the TCE + Cl reaction have to be taken into account when modeling the experiments where this reaction is important. Group additivity estimates (Atkinson, 1987; Kwok and Atkinson, 1995) would indicate that Cl₂CH-CO-Cl product would react very slowly with OH radicals, but it's reaction with Cl atoms may be non-negligible. The rate constant is unknown, but based on rate constants for similar species we would be between 0.5-1 x 10⁻¹² cm³ molec⁻¹ s⁻¹. (It turned out that the model simulations of some of the experiments are reasonably sensitive to this rate constant, so it was treated as an adjustable parameter, and the optimized rate constant fell within this range.) The reaction would be expected to result in the ultimate formation of Cl-CO-CO-Cl and regeneration of Cl atoms, as follows:



The Cl-CO-CO-Cl so formed is not expected to react with OH radicals or Cl, but is expected to photolyze at a rate comparable to HCO-CO-Cl, and generate two Cl. atoms.



For the purpose of the model simulations, HCO-CO-Cl and Cl-CO-CO-Cl are assumed to photolyze with the absorption cross sections and overall quantum yield, with former being assumed to be the same as for glyoxal, and the latter being determined by model simulations of the chamber data as discussed later. The quantum yields are probably not exactly the same, but the data are insufficient to determine them separately.

TCE Mechanism Used in the Model Simulations

The reaction listing in Appendix A shows the specific reactions which were incorporated to represent the atmospheric reactions of TCE in the model simulations carried out for this work. The footnotes to the listing give the documentation the rate constants and mechanisms assumed, which, except as indicated below, are based on the data and mechanistic considerations discussed in the previous section. The reactions were represented using the model species and chemical operators in the base mechanism, which as indicated above is an updated version of that of Carter (1990). To properly handle peroxy radicals which react with NO to generate Cl atoms (via formation of an α -chloro alkoxy radical which decomposes by Cl elimination), a new chemical operator, called "RO2-Cl." had to be added. This is analogous to the "RO2-R." operator discussed by Carter (1990) except that it forms Cl atoms rather than HO₂. Use of this operator was compared with model predictions using a mechanism with explicit representations of the various Cl-containing peroxy radicals which are of potential importance in the TCE photooxidation system, and essentially equivalent results were obtained in the simulations of all the experimental measurements carried out for this program.

Model simulations of the environmental chamber experiments, discussed later in this report, would not satisfactorily simulate the experimental results without adjusting or optimizing several uncertain rate constants or product yield parameters. In particular, the model simulations indicated that there must be an additional source of "new" Cl atoms in the TCE photooxidation system than the OH + TCE reaction, and there are a number of alternative possibilities. These include the reaction of TCE with O₃, the photolysis of HCO-CO-CO-Cl (a major assumed OH + TCE product), and reaction of Cl atoms with Cl₂CH-CO-Cl (the main Cl + TCE product) to form Cl-CO-CO-Cl, which subsequently photolyzes. The uncertain parameters which were varied or adjusted were: (1) the rate constant for the O₃ + TCE reaction; (2) the yield of Cl atoms in the OH reaction; (3) the rate constant for the reactions of Cl atoms with Cl₂CH-CO-Cl; (4) the photolysis rates for HCO-CO-CO-Cl and Cl-CO-CO-Cl, which are assumed to be the same; and (5) the yield of Cl atoms from the Cl + TCE reaction.

Assuming that the yield of Cl atoms from the Cl + TCE reaction was much less than 100%, that the reaction of Cl with CH₂CH-CO-Cl was slow, or that the α -dicarbonyl products photolyze slowly resulted in significant underprediction in the O₃ formation and TCE consumption rates in most of these experiments. Therefore, the Cl yield in the Cl + TCE reaction was held at 100% and the rate constants for the other reactions were simultaneously optimized to fit the data. The various optimizations suggested

that the Cl yield in the OH reaction was probably much different than the initially assumed value of 0.6, so that value was used to determine the final values for the other optimized parameters, which are given with the mechanism listing in Appendix A.

The other parameters could not be uniquely determined by the data available, and two alternative optimized mechanisms, based on differing assumptions concerning the TCE + O₃ reaction, were derived. The first mechanism, designated Mechanism "A", assumed that the TCE + O₃ reaction was relatively unimportant, having a relatively rate constant of only 1.0 x 10⁻²¹ cm³ molec⁻¹ s⁻¹. To fit the data the Cl + Cl₂CH-CO-Cl reaction had to be assumed to occur with a relatively high rate constant, to provide the Cl-CO-CO-Cl whose subsequent photolysis would provide the needed new Cl atoms. The best fit rate constant for this reaction for this mechanism was 6.4 x 10⁻¹² cm³ molec⁻¹ s⁻¹, which is which is not a large rate constant for a Cl + VOC reaction, but is high compared to rate constants for the reactions of Cl with other poly-chlorinated compounds (Atkinson et al, 1996). The best fit overall quantum yields for HCO-CO-Cl and Cl-CO-CO-Cl photolysis in this model were 0.074, which is about twice that used for glyoxal, but comparable to that for methylglyoxal (Plum et al, 1983; Atkinson et al, 1996).

The second mechanism, designated Mechanism "B", assumed that the TCE + O₃ reaction might be a non-negligible source of additional Cl atoms, and its rate constant was treated as an adjustable parameter. Best fits were obtained using a TCE + O₃ rate constant of 5.75 x 10⁻²¹, and assuming that the Cl + Cl₂CH-CO-Cl reaction was negligible. Note that this adjusted TCE + O₃ rate constant is not inconsistent with the upper limit value of 3 x 10⁻²⁰ cm³ molec⁻¹ s⁻¹ reported by Atkinson et al (1982). The best fit overall quantum yield for HCO-CO-Cl photolysis in this model was 0.057, which is not greatly different from the value used in Mechanism "A". Note that Cl-CO-CO-Cl is not assumed to be formed in this mechanism, so its photolysis rate is irrelevant. Model simulations using both mechanisms are shown in the presentation of the results.

Environmental Chamber Simulations

The ability of the chemical mechanisms to appropriately simulate the atmospheric impacts of TCE was evaluated by conducting model simulations of the environmental chamber experiments from this study. This requires including in the model appropriate representations of chamber-dependent effects such as wall reactions and characteristics of the light source. The methods used are based on those discussed in detail by Carter and Lurmann (1990, 1991), updated as discussed by Carter et al (1995b,d). The photolysis rates were derived from results of NO₂ actinometry experiments and direct measurements of the spectra of the light source. In the case of the blacklights used in the DTC, the spectrum was assumed to be constant and the blacklight spectrum given by Carter et al (1995b,d) was employed. The thermal rate constants were calculated using the temperatures measured during the experiments, with the small variations in temperature with time during the experiment being taken into account. The computer programs and modeling methods employed are discussed in more detail elsewhere (Carter et al, 1995b).

The specific values of the chamber-dependent parameters used in the model simulations of the experiments for this study are given in Appendix A.

Atmospheric Reactivity Simulations

To estimate its effects on ozone formation under conditions more representative of polluted urban atmospheres, incremental reactivities, defined as the change in O₃ caused by adding small amounts of a compound to the emissions, were calculated for ethane, TCE, and several other representative compounds for various simulated atmospheric pollution scenarios. Carter (1994a) used a series of single-day EKMA box model scenarios (EPA, 1984) derived by the EPA to represent 39 different urban ozone exceedence areas around the United States (Baugues, 1990), to develop various reactivity scales to quantify impacts of VOCs on ozone formation in various environments. It was found that NO_x levels are the most important factor affecting differences in relative ozone impacts among VOCs, and that the ranges of relative reactivities in the various scales can be reasonably well represented by ranges in relative reactivities in three "averaged conditions" scenarios representing three different NO_x conditions. These scenarios were derived by averaging the inputs to the 39 EPA scenarios, except for the NO_x emissions. In the "maximum reactivity" scenario, the NO_x inputs were adjusted such that the final O₃ level is most sensitive to changes in VOC emissions; in the "maximum ozone" scenario the NO_x inputs were adjusted to yield the highest maximum O₃ concentration; and in the "equal benefit" scenario the NO_x inputs were adjusted such that relative changes in VOC and NO_x emissions had equal effect on ozone formation. As discussed by Carter (1994a), there represent respectively the high, medium and low ranges of NO_x conditions which are of relevance when assessing VOC control strategies for reducing ozone.

The chemical mechanisms used for these atmospheric simulations were the same as used to simulate the chamber experiments, except that the reactions representing chamber effects were removed, and the reactions for the full variety of VOCs emitted into the scenarios (Carter, 1994a) were represented (see Appendix A). Most of the emitted VOCs (other than the test compound whose reactivity is being calculated) are not represented in the model explicitly, but are represented using lumped model species whose rate constants and product yield parameters are derived based on the mixture of compounds they represent. The rate constants and mechanistic parameters for the emitted species in the scenarios were the same as those used previously (Carter, 1994a; Carter et al, 1993a), except for the aromatics, whose unknown photoreactive product yields were reoptimized in a manner analogous to that discussed above for toluene and m-xylene (unpublished results from this laboratory). The listings on Appendix A give the lumped model species used to represent the emissions into the scenarios, indicate the types of species each is used to represent, and give their rate constants and product yield parameters.

RESULTS AND DISCUSSION

Summary of Experiments

Table 1 gives a chronological listing of all the experiments carried out for this program. These consisted primarily of the TCE - NO_x, TCE - ethane - NO_x, and the incremental reactivity experiments, whose results are discussed in more detail in the following sections. In addition, several characterization runs were carried out to determine the chamber-dependent inputs needed for the model simulations of the experiments, control experiments were conducted to assure consistency with previous results, and side equivalency tests were conducted to assure that essentially equivalent results were obtained when equal mixtures were simultaneously irradiated in each of the dual reaction bags.

Table 1 summarizes relevant results from these characterization and control runs. Their results were generally as expected based on our previous experience with these and similar chambers in our laboratories (Carter et al., 1995b and references therein). Good side equivalency was observed when equivalent surrogate - NO_x, propene - NO_x, CO - NO_x, or n-butane - NO_x mixtures were simultaneously irradiated in the dual reactors. The results of the n-butane - NO_x and the purified CO - NO_x experiments, which are highly sensitive to the magnitude of the chamber radical source assumed in the model (see Table A-4 in Appendix A), were sufficiently well simulated by the model to indicate that the model was appropriately representing this effect for these runs. The actinometry results agreed with the extrapolated values based on results of previous determinations (see Table A-4) to within the variability of these determinations.

Results of the TCE - NO_x and TCE - Ethene - NO_x Experiments

Table 1 lists the initial reactant concentrations, 3- and 6-hour ozone yields, and t=6 hour fractions of TCE and ethane reacted in the TCE - NO_x and TCE - ethane - NO_x chamber experiments, and concentration-time profiles for O₃, NO, TCE and ethane for those experiments are shown on Figure 1. Results of model calculations, discussed below, are also shown on Figure 1.

Run DTC-313 consisted of a simultaneous irradiation of equal amounts of both TCE and NO_x on both sides of the chamber, with ~100 ppb ethane added to one side. The TCE - NO_x experiment formed a substantial amount (~300 ppb) of ozone, and approximately 1/3 of the initially present TCE reacted. However, the addition of only 100 ppb of ethane significantly decreased both the amount of ozone formation and TCE consumption. This is despite the fact that ethane has a positive effect on O₃ formation when added in sufficient quantities to ROG surrogate - NO_x - air irradiations, though the effect would be small with only 100 ppb added because of its slow reaction with OH radicals. These results are attributed to the role of Cl atoms in the TCE - NO_x photooxidation system. In the absence of other

Table 1. Chronological listing of the environmental chamber experiments carried out for this program.

RunID	Date	Title	Comments
DTC-299	11/29/95	n-butane - NOx	Control run to measure the chamber radical source. Some indication of leakage on Side A, and Side A also had a slightly higher NO consumption rate. NO consumption rate on Side A was well fit by predictions of chamber model. NO consumption rate on Side B was slightly lower than predicted by chamber model, but results were within the experimental variability.
DTC-300	1/19/96	NO ₂ Actinometry	Measured NO ₂ photolysis rate was 0.216 min ⁻¹ , in good agreement with the prediction of the curve fit to the full set of actinometry results through run 356, which was 0.218 min ⁻¹ .
DTC-301	1/24/96	Propene + NOx	Control run for comparison with other propene runs carried out in this and other chambers. The model slightly overpredicted the ozone formation rate, but the results were within the normal range. Good side equivalency was observed.
DTC-302	1/25/96	Mini-surrogate + NOx	Control run and side equivalency test. Good side equivalency observed. Ozone formation rate slightly slower than predicted by model, but results within the normal range.
DTC-303	1/26/96	Mini-surrogate + TCE (B)	See Table 3 and Figure 4.
DTC-304	1/30/96	n-Butane - NOx	Control run to measure the chamber radical source. Very good side equivalency, and NO consumption rates on both sides were well fit by predictions of chamber model.
DTC-305	1/31/96	Mini-surrogate + TCE (A)	See Table 3 and Figure 3.
DTC-306	2/1/96	Modified Mini-surrogate + TCE (B)	10 ppm ethane present on both sides, along with mini-surrogate components. Results on Table 3 and Figure 5..
DTC-307	2/2/96	Full surrogate + TCE (A)	Initial formaldehyde was twice the normal amount due to an injection error. Run still usable. Results on Table 3 and Figure 9.
DTC-308	2/6/96	Full surrogate + TCE (B)	See Table 3 and Figure 8.
DTC-309	2/7/96	Full surrogate (higher ROG) + TCE (A)	Total amounts of base ROG components increased to examine effects of variable conditions. No formaldehyde data, so initial formaldehyde had to be estimated based on amount injected. Results on Table 3 and Figure 10.

Table 1 (continued)

RunID	Date	Title	Comments
DTC-310	2/8/96	CO + NO _x	Control run to measure chamber radical source. Results rejected because CO may not have been purified, and concentrations above the reliable operating range of the CO monitor.
DTC-311	2/9/96	Full surrogate (higher NO _x) + TCE (B)	Initial NO _x levels increased to examine effects of variable conditions. Results on Table 3 and Figure 7.
DTC-312	2/13/96	mini-surrogate + ethane (B) or TCE (A)	Due to a misunderstanding, 18.2 ppm of ethane was injected on one side, and 1.0 ppm of TCE was injected on the other. Rates of NO oxidation and ozone formation were similar on both sides, and only slightly higher than base case experiments.
DTC-313	2/15/96	TCE - NO _x + ethane (B)	Same amounts of TCE and NO _x injected on both sides, but with 0.1 ppm ethane on Side A. The small amount of ethane caused a decrease in the rate of NO oxidation, O ₃ formation, and TCE consumption. See Table 2 and Figure 1.
DTC-314	2/16/96	Trichloroethene + Ethane + NO _x	Same amounts of TCE and NO _x injected on both sides, but with 0.1 ppm ethane on Side A, and ~5 ppm on Side B.. The higher amount of ethane caused a slowed down the rates of NO oxidation, O ₃ formation, and TCE consumption. See Table 2 and Figure 1.
DTC-316	2/22/96	CO + NO _x	Control run to measure chamber radical source. CO was purified. Results were in good agreement with predictions of chamber model.
DTC-320	2/29/96	Full surrogate (higher NO _x) + TCE (A)	Same base case as DTC-311. Results on Table 3 and Figure 6.
DTC-321	3/1/96	Full surrogate (Reduced NO _x) + TCE (B)	Initial NO _x reduced to examine effects of varying conditions. Results on Table 3 and Figure 11.
DTC-322	3/4/96	CO + NO _x	Control run to measure chamber radical source. Results were in good agreement with predictions of chamber model.
DTC-326	3/11/96	NO ₂ Actinometry	Measured NO ₂ photolysis rate was 0.212 min ⁻¹ , in good agreement with the prediction of the curve fit to the full set of actinometry results through run 356, which was 0.217 min ⁻¹ .

Table 2. Summary of conditions and selected results of the trichloroethylene - NO_x and trichloroethylene - ethane - NO_x chamber experiments.

Run	Initial Conc. (ppm)			Ozone (ppm)		Fraction Reacted	
	TCE	NO _x	Ethane	3 hour	6 hour	TCE	Ethane
DTC-313 (A)	1.5	0.23	-	0.06	0.30	34%	-
DTC-313 (B)	1.5	0.23	0.11	0.01	0.08	13%	8%
DTC-314 (A)	3.8	0.22	0.12	0.36	0.76	69%	50%
DTC-314 (B)	3.7	0.22	4.6	0.01	0.14	7%	3%

Table 2. Summary of conditions and selected results of the trichloroethylene - NO_x and trichloroethylene - ethane - NO_x chamber experiments.

VOCs which react with the Cl atoms, most of the Cl atoms formed in the OH + TCE reaction end up reacting with TCE, which regenerates Cl atoms. Thus there is a chain reaction with Cl atoms as the chain carrier causing the consumption of TCE and the formation of peroxy radicals which convert NO to NO₂ and cause ozone formation. However, when ethane is added, some of the Cl atoms reacts with ethane, which results in a net sink for Cl atoms. Even though most of the Cl is still reacting with the TCE (which is present in higher concentrations than ethane and also reacts slightly faster with Cl), the relatively small amount reacting with ethane is net sink process, while the reaction with TCE is not, and thus the ethane reaction has a large effect on the chain length and the overall Cl atom concentrations.

Run DTC-314 consists of simultaneous irradiations of a the same TCE - NO_x mixture, with the TCE level increased by a factor of 2.5 compared to the previous run, with varying amounts of ethane added. The amount of ethane and NO_x in run DTC-314(A) is the same as in DTC-313(B), and thus comparing the two runs shows the effects of increasing the TCE while holding the other reactant levels constant. Figure 1 shows that increasing the TCE increases the rate of NO oxidation and O₃ formation, but that eventually the O₃ peaks and begins to decline, and around the same time there is an acceleration in the rate of consumption of both the TCE and the added ethane. Because of this acceleration starting around the time of the O₃ peak, the fraction of TCE which was consumed in this experiment was even higher than in the TCE - NO_x experiments with the lower amount of initial TCE, even without the added ethane inhibiting Cl atom levels. As discussed below, the model could not adequately simulate this behavior.

Run DTC-314(B) had a sufficiently high amount of added ethane that most of the TCE consumption was calculated to be due to its reaction with OH radicals. Thus, it can serve as a test for the TCE + OH mechanism which is less sensitive to uncertainties in the TCE + Cl reactions. As expected, the higher amounts of added ethane significantly slowed down the rates of NO oxidation, O₃ formation, and TCE consumption.

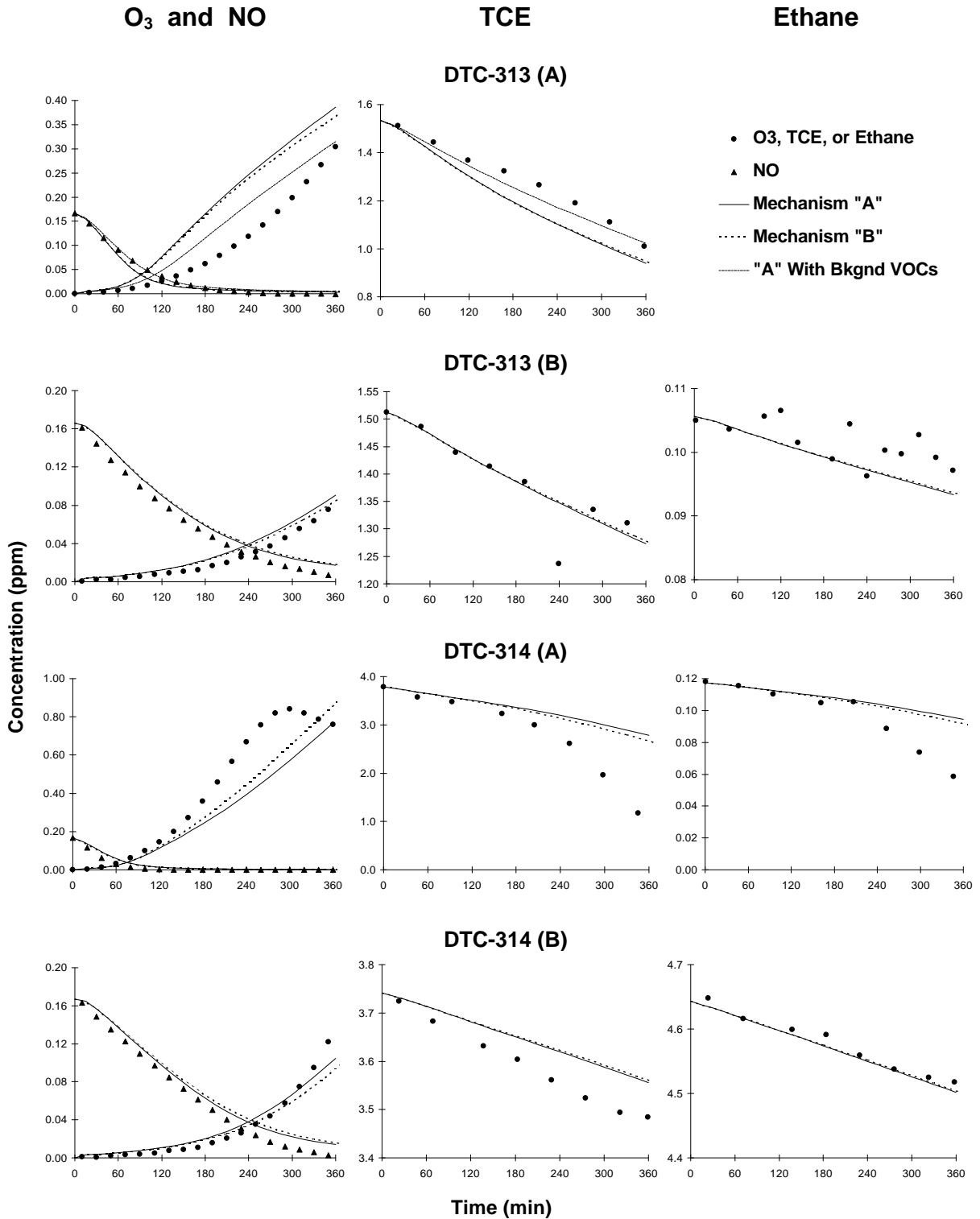


Figure 1. Experimental and calculated concentration-time plots for selected species in the trichloroethylene - NO_x and trichloroethylene - ethane - NO_x chamber runs.

Figure 1 shows the results of the model simulations using the two optimized TCE mechanism developed in this work. Note that simulations of run DTC-313(A) were highly sensitive to the amounts of background VOC species which were assumed to be present, since background VOCs act as Cl atom sinks and tend to slow down the TCE consumption and ozone formation processes. For optimization purposes it was assumed that background levels of methane, ethane, and n-butane of 2 ppm, 5 ppb and 2 ppb, respectively, were present in the experiment, and the simulations of this run on Figure 1 show the results of the calculations both with and without these assumed background contaminants. These background levels did not affect the results of the simulations of the other experiments, nor of the simulations of the reactivity experiments discussed in the following sections, because their effects are small compared to the effects of the much higher levels of added VOCs. Since the actual background levels were not measured and are uncertain, this presents an uncertainty in the optimization using the data for this run. However, the values of the optimized parameters do not change significantly when data from run DTC-313(A) are removed from the optimizations.

Figure 1 shows that seen that optimized models gives reasonably good simulations of the experiments with the higher ethane/TCE ratio, and fair simulations to the results of the TCE - NO_x run and the first half of the high TCE/low ethane run DTC-314(A), with model "B" performing slightly better in this regard. In particular, they correctly predict the relatively rapid rate of O₃ formation and TCE consumption in the run without added ethane, the inhibiting effect of adding small amounts of ethane, and the rate of NO oxidation, O₃ formation, and TCE consumption in the experiment where large amounts of added ethane suppress the TCE + Cl reaction.

However, both models underpredicted the rate of O₃ formation in the second half of run DTC-314(A), and neither correctly simulated acceleration in TCE and ethane consumption and the decline in the O₃ concentration around t = 5 hours. No other chemically reasonable adjustment to the model could correctly simulate this behavior, other than assuming rate constants for the NO₃ + TCE reaction which are inconsistent with laboratory data, or assuming unreasonably high rate constants for reactions of O₃ with the various TCE oxidation products. There is apparently some process occurring in the later stages of this experiment, presumably involving some reactions of one or more TCE products introducing more Cl atoms into the system, which is not being represented in this model. More definitive and complete product data are needed to elucidate this.

Results of The Reactivity Experiments and Mechanism Evaluations

Summaries of the conditions and results of the incremental reactivity experiments are given on Table 3, and figures 2 through 11 give time series plots relevant measurements used for mechanism evaluation. These include concentrations of d(O₃-NO), m-xylene and n-hexane or n-butane in the base case and test experiments, and the d(O₃-NO) incremental reactivities and relative consumption reactivities

Table 3. Summary of conditions and results of the incremental reactivity experiments.

Run	Initial Reactants (ppm)			t=6 d(O ₃ -NO) (ppm)			m-Xylene consumption (t=5)			Alkane Consumption (t=5)		
	NOx	Surg [a]	TCE	Base	Test	IR [b]	Base	Test	RCR	Base	Test	RCR
Mini-Surrogate												
DTC-312 (A)	0.32	5.5	1.0	0.77	0.76	-0.009	0.51	0.69	0.18	0.12	0.27	0.14
DTC-305 (A)	0.32	5.3	2.0	0.66	0.76	0.049	0.56	0.58	0.01	0.13	0.26	0.06
DTC-303 (B)	0.33	5.5	10.0	0.59	0.94	0.035	0.51	0.56	0.00	0.14	0.47	0.03
Mini-Surrogate + 9 ppm Ethane												
DTC-306 (B)	0.32	5.5	2.0	0.72	0.79	0.033	0.57	0.62	0.02	0.15	0.18	0.01
Full Surrogate - High NOx												
DTC-320 (A)	0.28	3.8	0.8	0.52	0.59	0.083	0.78	0.96	0.24	0.09	0.28	0.26
DTC-311 (B)	0.28	3.7	1.4	0.52	0.66	0.098	0.82	0.98	0.12	0.14	0.23	0.06
Full Surrogate												
DTC-308 (B)	0.16	3.7	0.9	0.48	0.47	-0.011	1.07	0.92	-0.16	0.15	0.20	0.05
DTC-307 (A)	0.16	3.8	2.0	0.50	0.49	-0.005	1.02	0.84	-0.09	0.11	0.26	0.07
Full Surrogate - High ROG												
DTC-309 (A)	0.16	5.1	1.5	0.50	0.47	-0.020	0.91	0.76	-0.10	0.10	0.19	0.07
Full Surrogate - Low NOx												
DTC-321 (B)	0.10	3.8	1.3	0.33	0.34	0.008	0.64	0.36	-0.21	0.16	0.16	0.00

Notes

[a] Total base ROG surrogate in ppmC.

[b] Incremental reactivity

Table 3. Summary of conditions and results of the incremental reactivity experiments.

(RCR's) derived from the differences between the two sides. Results of model calculations are also shown.

Table 3 shows that TCE has a relatively low incremental reactivities with respect to $d(O_3-NO)$, which is close to zero and even slightly negative by the end of the run in the experiments carried out under lower NO_x conditions. The effect of TCE on the m-xylene consumption rates indicate that TCE tends to slightly enhance OH radical levels under low ROG/NO_x conditions, but to inhibit integrated OH when the ROG/NO_x ratio is high. This tendency to inhibit integrated OH under high ROG/NO_x conditions is consistent with the reactivity trends observed for many VOCs, including some, such as carbon monoxide, whose mechanisms involve no radical initiation and termination processes (Carter et al, 1995a). The fact that TCE slightly enhances OH radical levels under higher NO_x conditions suggests that it does not have significant radical termination processes in its mechanism.

Table 3 and Figures 2 through 11 also show that for most experiments the addition of TCE enhances the rates of consumptions of the alkanes present in the ROG surrogate, indicating the formation

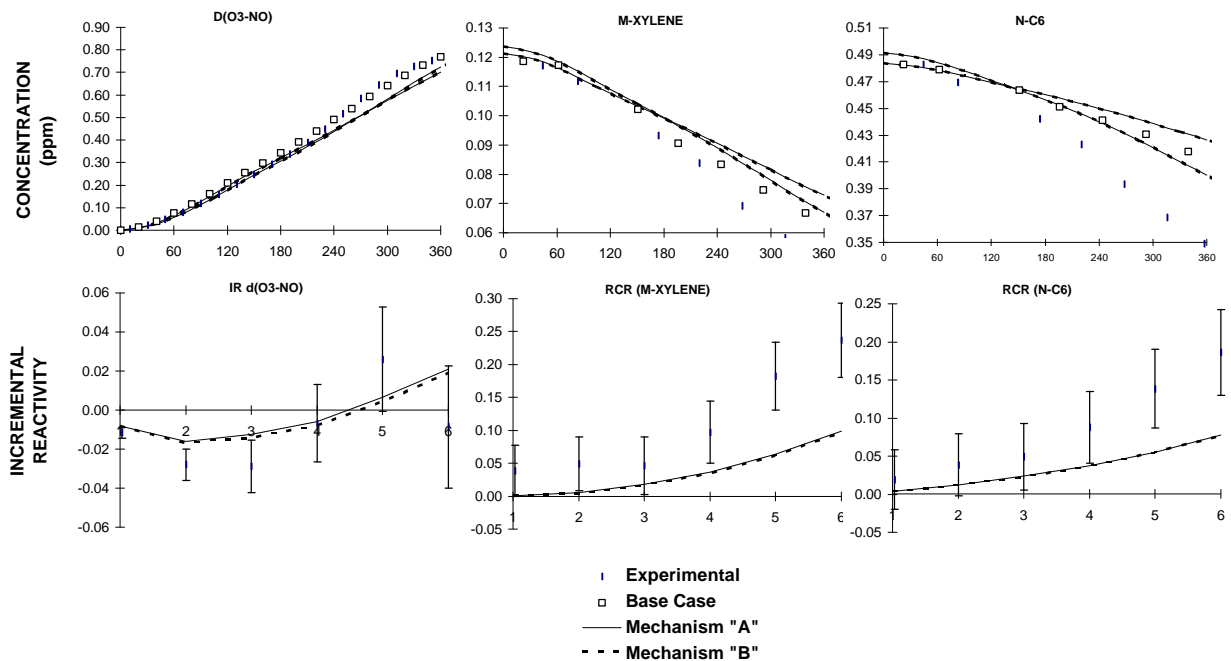


Figure 2. Plots of selected results of the mini-surrogate + trichloroethylene experiment DTC-312

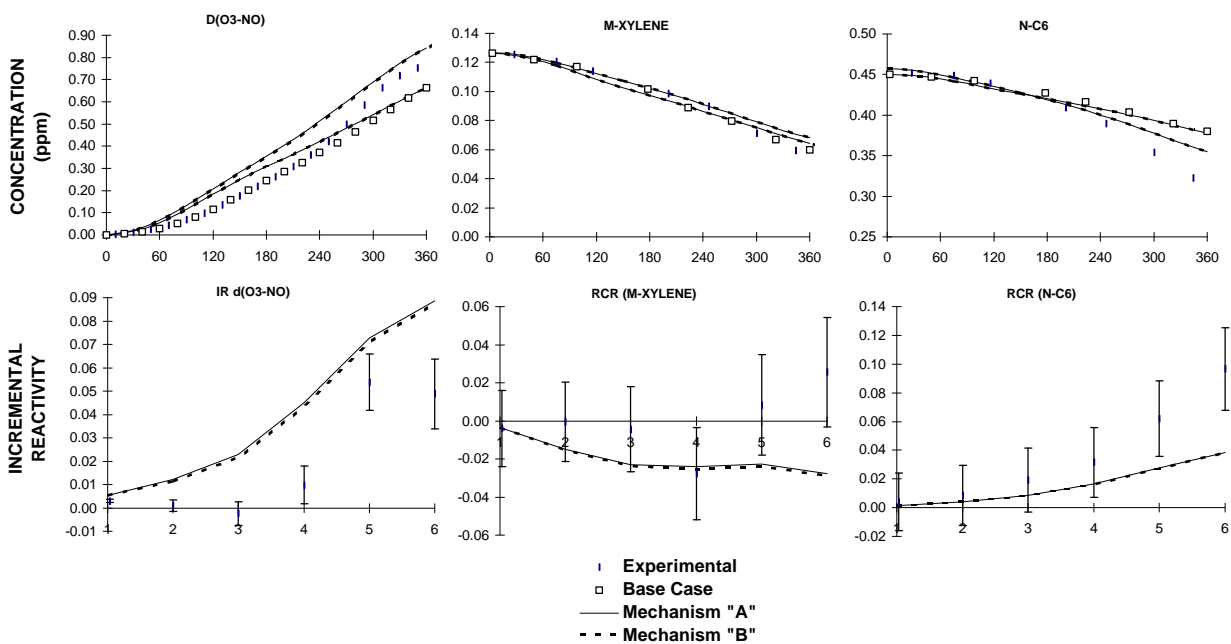


Figure 3. Plots of selected results of the mini-surrogate + trichloroethlene experiment DTC-305.

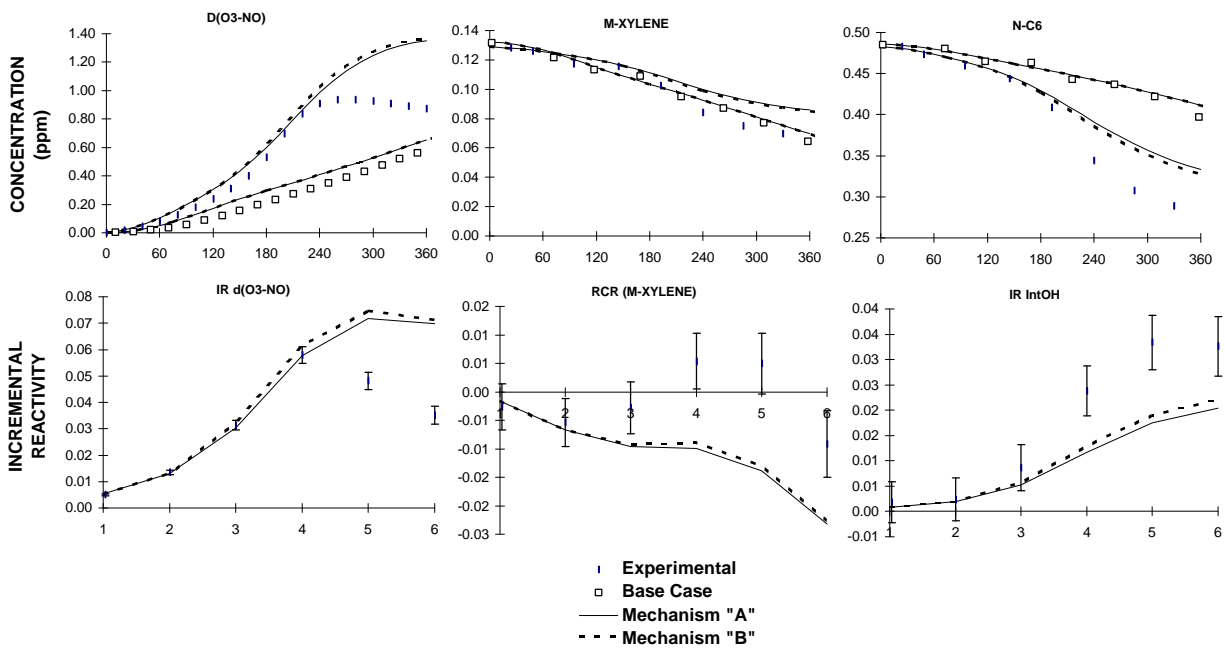


Figure 4. Plots of selected results of the mini-surrogate + trichloroethylene experiment DTC-303.

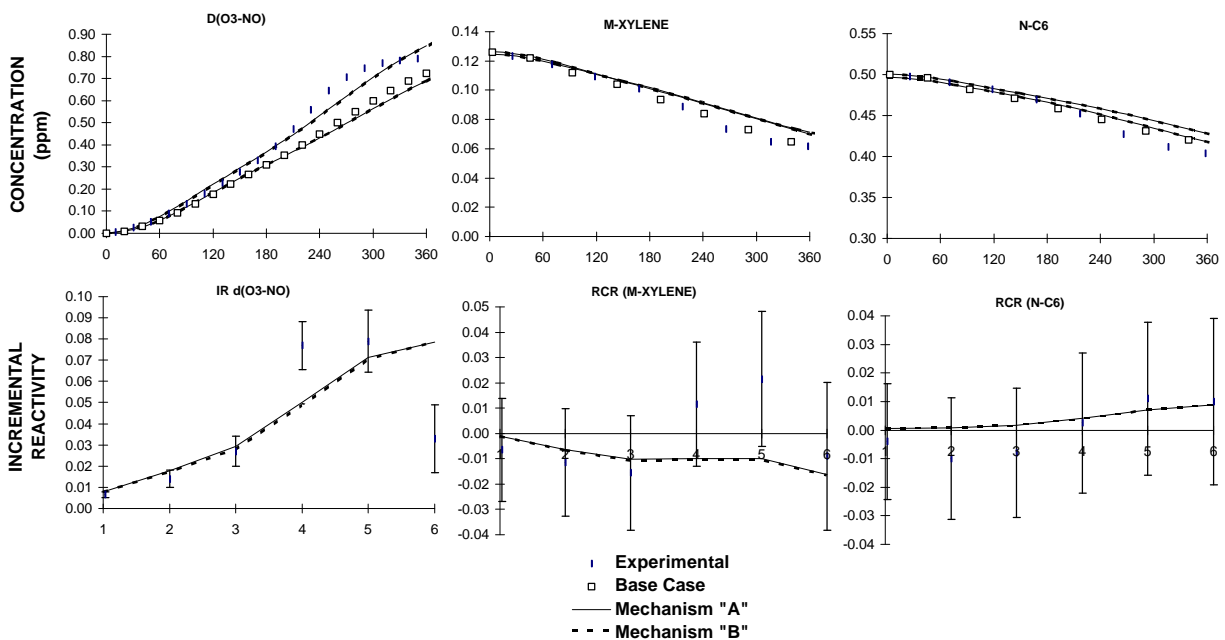


Figure 5. Plots of selected results of the mini-surrogate with ethane + trichloroethylene experiment DTC-306.

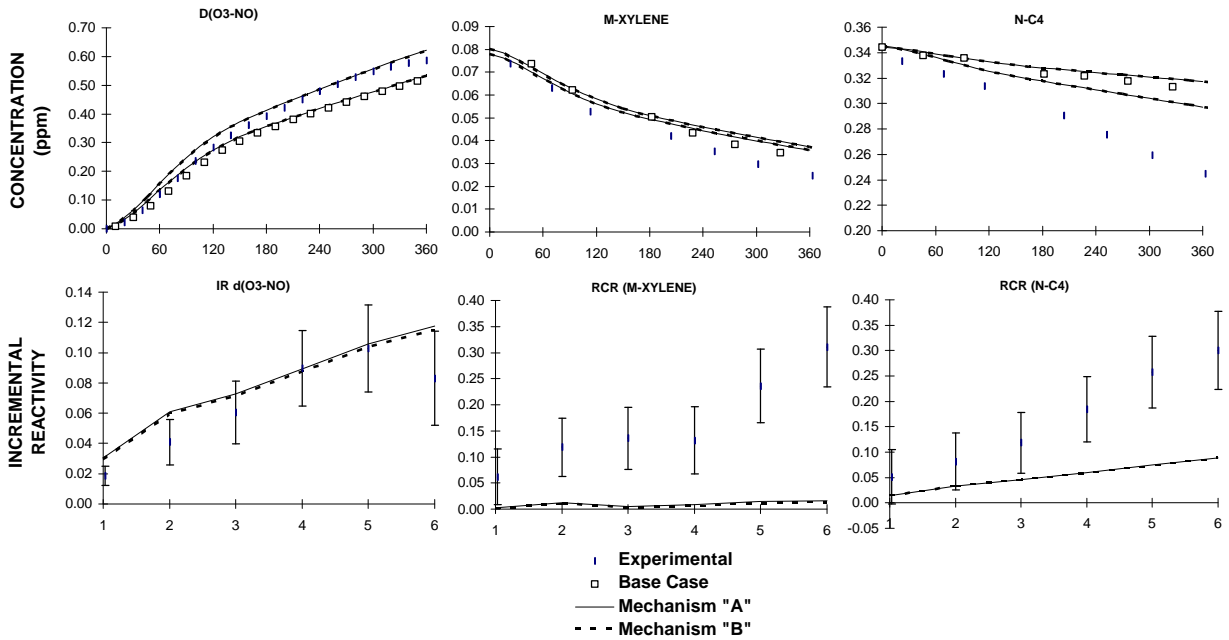


Figure 6. Plots of selected results of the high NO_x full surrogate + trichloroethylene experiment DTC-320.

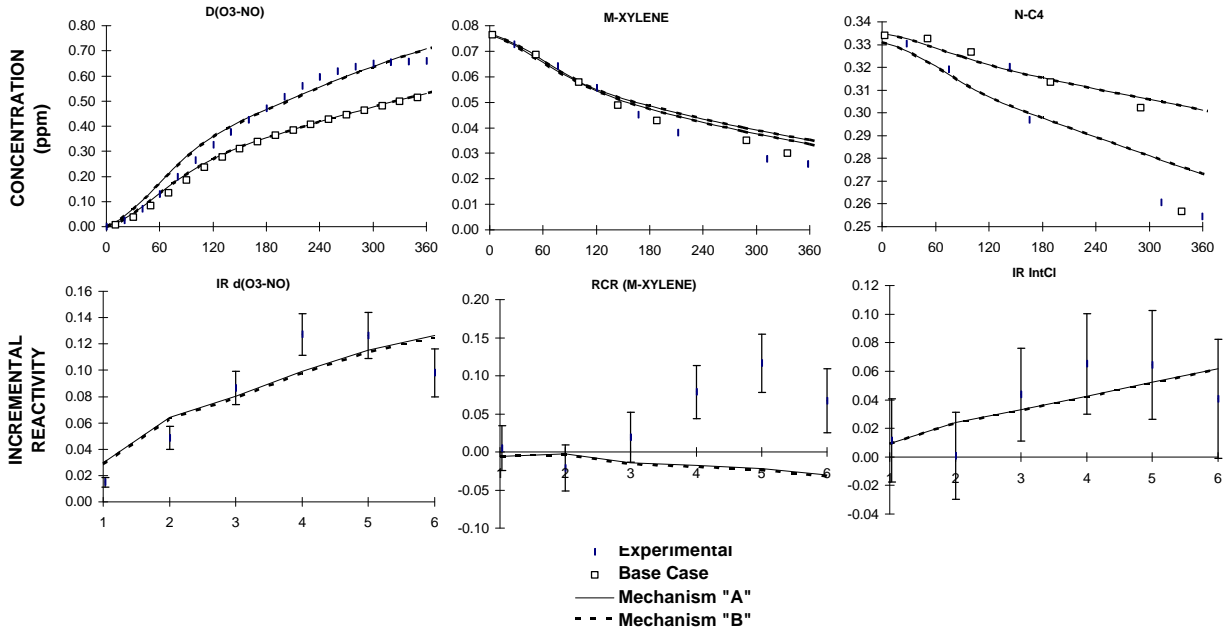


Figure 7. Plots of selected results of the high NO_x full surrogate + trichloroethylene experiment DTC-311.

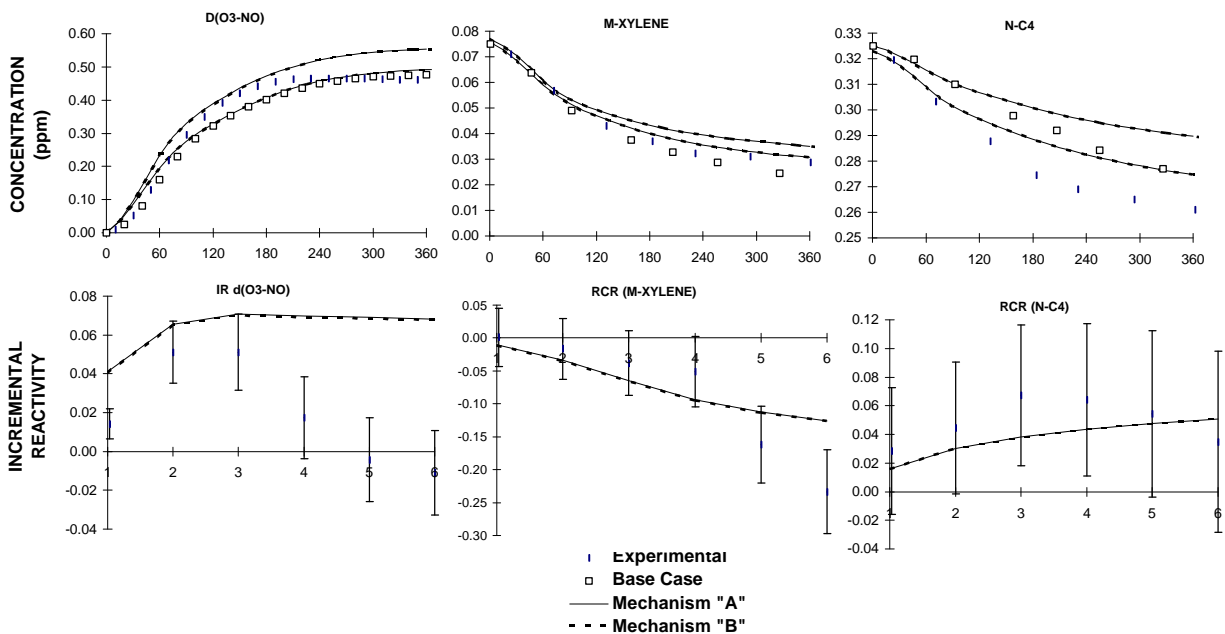


Figure 8. Plots of selected results of the full surrogate + trichloroethylene experiment DTC-308.

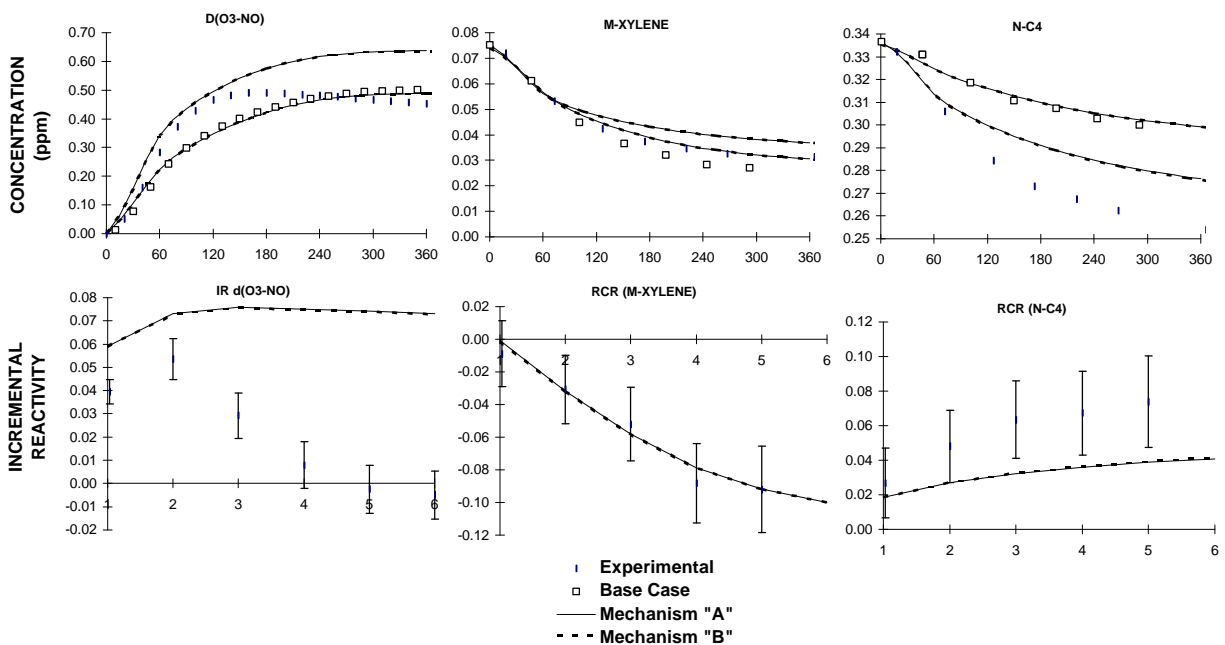


Figure 9. Plots of selected results of the full surrogate + trichloroethylene experiment DTC-307.

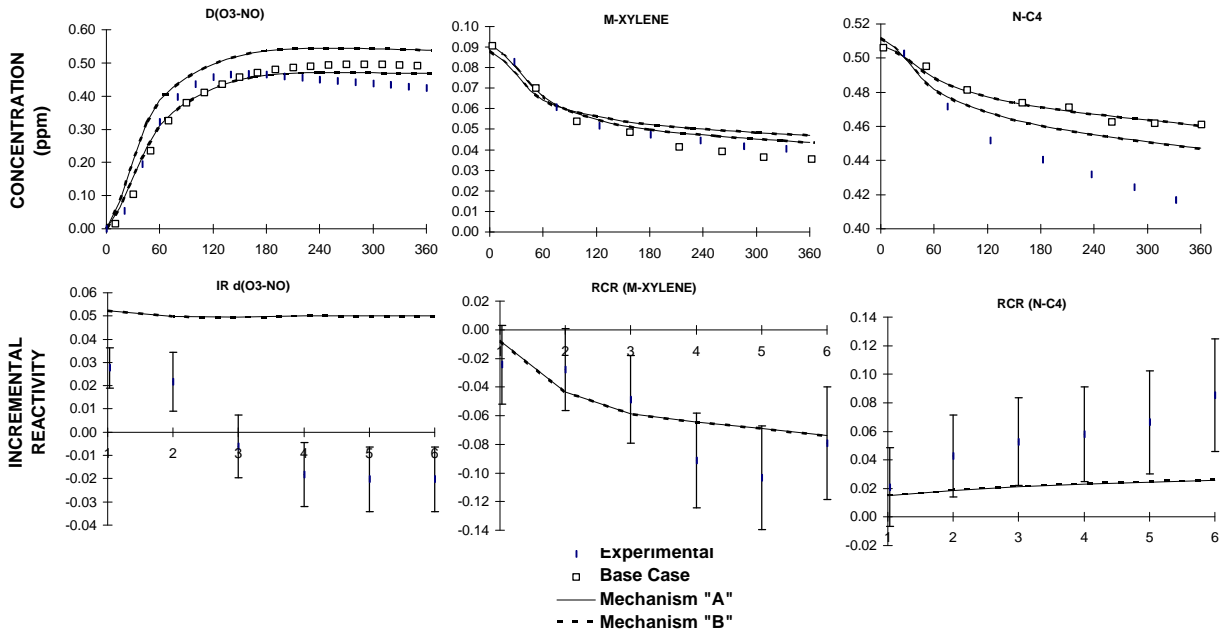


Figure 10. Plots of selected results of the high ROG full surrogate + trichloroethylene experiment DTC-309.

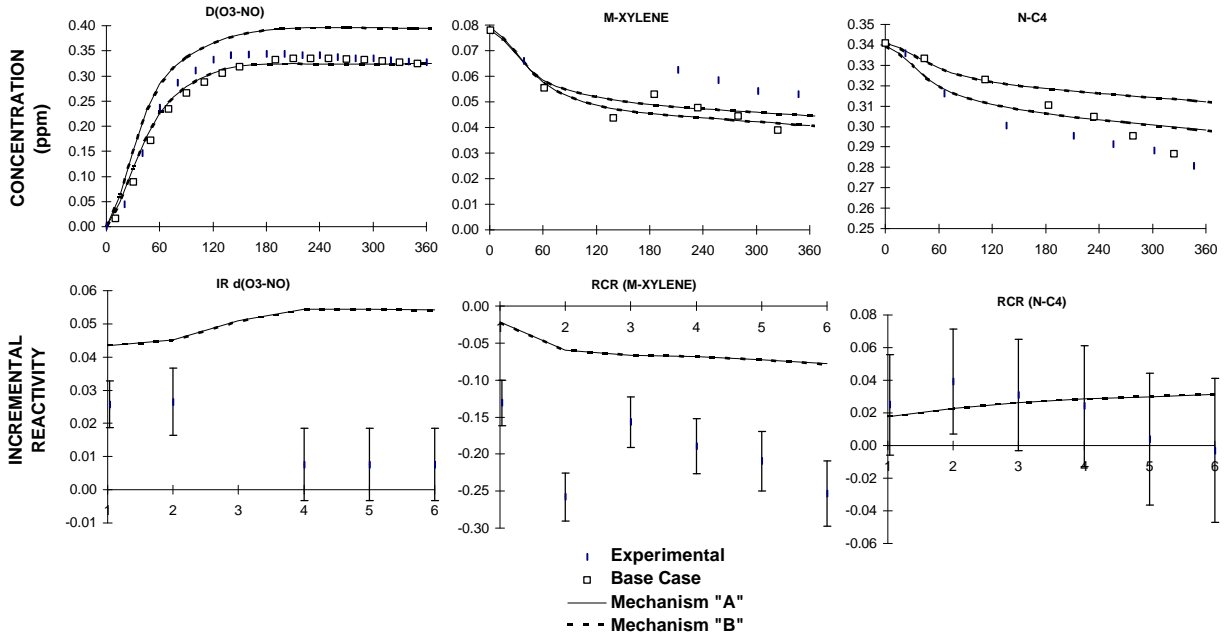


Figure 11. Plots of selected results of the low NO_x full surrogate + trichloroethylene experiment DTC-321.

of Cl atoms. The effect on alkane consumption increases as the amount of added TCE is increased, but the relative effect, or RCR(alkane), decreases with amount of added TCE.

The results of the model simulations of the reactivity experiments are shown on Figures 1-11. The model simulates the base case experiments reasonably well, though there may be a slight bias towards overpredicting $d(\text{O}_3\text{-NO})$ formation and m-xylene consumption rates in some experiments. This bias is cancelled out when comparing experimental and model predicted incremental reactivities or relative consumption rates, as shown on the bottom plots sets of plots on the figures. The TCE mechanisms simulate moderately well the effects of TCE on the $d(\text{O}_3\text{-NO})$ formation rates in most of the experiments, though there are several notable exceptions. In mini-surrogate runs DTC-305 and 306 there is an increase in the rate of O_3 formation after about 3 or 4 hours of irradiation which is not well simulated by the model, and in mini-surrogate runs DTC-306 and (especially) DTC-303 there is a decline in O_3 near the end of the experiment which the model does not simulate. The model performs reasonably well simulating the effect of TCE on O_3 formation and NO oxidation in the full surrogate runs carried out at relatively high NO_x levels or low ROG/ NO_x conditions. However, in the lower NO_x or higher ROG/ NO_x runs, while the model correctly predicts the positive effect of the added TCE on the initial NO oxidation and O_3 formation rates, it does not correctly simulate the experimental observation that the O_3 formation stops earlier and O_3 begins to decline on the added TCE side, resulting in the final ozone being comparable to or lower than on the base case side. Instead, the model incorrectly predicts that TCE has a positive effect on O_3 at all times in these experiments. No reasonable adjustment of the mechanism could be found to improve model performance in this regard.

The model simulates the effects of TCE on m-xylene consumption rates reasonably well in some runs, but tends to underpredict it in others. Perhaps more significantly, the model consistently underpredicts the effect of TCE on in almost all experiments where a measurable effect was observed. This indicates that TCE is introducing more Cl atoms into the system than can be accounted for by this mechanism. This may be related to discrepancies observed with the simulations of O_3 in the later stages of the lower NO_x or higher ROG or added TCE experiments, or the failure of the model to predict the acceleration of O_3 formation and TCE and ethane consumption at the end of the TCE + ethane experiment DTC-314(A).

ATMOSPHERIC REACTIVITY CALCULATIONS

Incremental reactivities of VOCs have been shown to be highly dependent on environmental conditions, so reactivities measured in environmental chamber experiments cannot necessarily be assumed to be exactly the same as those under atmospheric conditions (Carter and Atkinson, 1989a; Carter et al, 1995a). The only method available to obtain quantitative estimates of incremental reactivities of VOCs in ambient air pollution episodes is to conduct airshed model simulations of the episodes. Since these simulations cannot be any more reliable than the chemical mechanisms used, the major objective of this program was to assess the reliability of the TCE mechanism for use in such simulations. This was discussed in the previous sections. Although the alternative TCE photooxidation mechanisms developed in this work did not successfully simulate all the experimental observations, they performed quite well in simulating the effects of TCE on O₃ formation under low ROG/NO_x experiments, indicating that they may not give unreliable predictions in airshed where these conditions prevail. Furthermore, since the mechanisms always overpredicted the effect of TCE on O₃ under high ROG/NO_x conditions, they might be useful for indicating upper limit reactivities for TCE under those conditions.

Scenarios Used for Reactivity Assessment

The set of airshed scenarios employed to assess the reactivity of TCE for this study is the same as those used for calculating the MIR and other reactivity scales (Carter, 1994a; Carter et al, 1993a). The objective is to use a set of scenarios which represents, as much as possible, a comprehensive distribution of the environmental conditions where unacceptable levels of ozone are formed. Although a set of scenarios has not been developed for the specific purpose of VOC reactivity assessment, the EPA developed an extensive set of scenarios for conducting analyses of effects of ROG and NO_x controls on ozone formation using the EKMA modeling approach (Gipson et al., 1981; Gipson and Freas, 1983; EPA, 1984; Gery et al., 1987; Baugues, 1990). The EKMA approach involves the use of single-cell box models to simulate how the ozone formation in one day episodes is affected by changes in ROG and NO_x inputs. Although single-cell models cannot represent realistic pollution episodes in great detail, they can represent dynamic injection of pollutants, time-varying changes of inversion heights, entrainment of pollutants from aloft as the inversion height raises, and time-varying photolysis rates, temperatures, and humidities (Gipson and Freas, 1981; EPA, 1984; Gipson, 1984; Hogo and Gery, 1988). Thus, they can be used to simulate a wide range of the chemical conditions which affect ozone formation from ROG and NO_x, and which affect VOC reactivity. Therefore, at least to the extent they are suitable for their intended purpose, an appropriate set of EKMA scenarios should also be suitable for assessing reactivities over a wide range of conditions.

Base Case Scenarios

The set of EKMA scenarios used in this study were developed by the United States EPA for assessing how various ROG and NO_x control strategies would affect ozone nonattainment in various areas of the country (Baugues, 1990). The characteristics of these scenarios and the methods used to derive their input data are described in more detail elsewhere (Baugues, 1990; Carter, 1993). Briefly, 39 urban areas in the United States were selected based on geographical representativeness of ozone nonattainment areas and data availability, and a representative high ozone episode was selected for each. The initial NMOC and NO_x concentrations, the aloft O₃ concentrations, and the mixing height inputs were based on measurement data for the various areas, the hourly emissions in the scenarios were obtained from the National Acid Precipitation Assessment Program emissions inventory (Baugues, 1990), and biogenic emissions were also included. Table 4 gives a summary of the urban areas represented and other selected characteristics of the scenarios.

Several changes to the scenario inputs were made based on discussions with the California ARB staff and others (Carter, 1993). Two percent of the initial NO_x and 0.1% of the emitted NO_x in all the scenarios was assumed to be in the form of HONO. The photolysis rates were calculated using solar light intensities and spectra calculated by Jeffries (1991) for 640 meters, the approximate mid-point of the mixed layer during daylight hours. The composition of the NMOCs entrained from aloft was based on the analysis of Jeffries et al (1989). The composition of the initial and emitted reactive organics was derived as discussed below. Complete listings of the input data for the scenarios are given elsewhere (Carter, 1993).

This set of 39 EKMA scenarios are referred to as "base case" to distinguish them from the scenarios derived from them by adjusting NO_x inputs to yield standard conditions of NO_x availability as discussed below. No claim is made as to the accuracy of these scenarios in representing any real episode, but they are a result of an effort to represent, as accurately as possible given the available data and the limitations of the formulation of the EKMA model, the range of conditions occurring in urban areas throughout the United States. When developing general reactivity scales it is more important that the scenarios employed represent a realistic distribution of chemical conditions than accurately representing the details of any one particular episode.

The Base ROG mixture is the mixture of reactive organic gases used to represent the chemical composition of the initial and emitted anthropogenic reactive organic gases from all sources in the scenarios. Consistent with the approach used in the original EPA scenarios, the same mixture was used for all scenarios. The speciation for this mixture was derived by Croes (1991) based on an analysis of the EPA database (Jeffries et al. 1989) for the hydrocarbons and the 1987 Southern California Air Quality Study (SCAQS) database for the oxygenates (Croes et al., 1994; Lurmann et al., 1992). This mixture consists of 52% (by carbon) alkanes, 15% alkenes, 27% aromatics, 1% formaldehyde, 2% higher

Table 4. Summary of conditions of base case scenarios used for atmospheric reactivity assessment.

City, State	Calc. Max O ₃ (ppb)	ROG /NO _x	NO _x /NO _x ^{MOR}	Final Height (km)	Init.+Emit Base ROG (mmol m ⁻²)	Aloft O ₃ (ppb)
Atlanta, GA	178	7.3	0.7	2.1	12	63
Austin, TX	174	9.3	0.5	2.1	11	85
Baltimore, MD	323	5.2	1.1	1.2	17	84
Baton Rouge, LA	245	6.8	1.0	1.0	11	62
Birmingham, AL	237	6.9	0.6	1.8	13	81
Boston, MA	194	6.5	0.6	2.6	14	105
Charlotte, NC	143	7.8	0.3	3.0	7	92
Chicago, IL	280	11.6	0.5	1.4	25	40
Cincinnati, OH	197	6.4	0.8	2.8	17	70
Cleveland, OH	250	6.6	1.0	1.7	16	89
Dallas, TX	210	4.7	1.3	2.3	18	75
Denver, CO	209	6.3	1.2	3.4	29	57
Detroit, MI	236	6.8	0.8	1.8	17	68
El Paso, TX	186	6.6	1.1	2.0	12	65
Hartford, CT	169	8.4	0.5	2.3	11	78
Houston, TX	305	6.1	1.0	1.7	25	65
Indianapolis, IN	210	6.6	0.9	1.7	12	52
Jacksonville, FL	156	7.6	0.7	1.5	8	40
Kansas City, MO	154	7.1	0.6	2.2	9	65
Lake Charles, LA	290	7.4	0.7	0.5	7	40
Los Angeles, CA	576	7.6	1.0	0.5	23	100
Louisville, KY	209	5.5	0.9	2.5	14	75
Memphis, TN	224	6.8	0.7	1.8	15	58
Miami, FL	133	9.6	0.4	2.7	9	57
Nashville, TN	165	8.1	0.5	1.6	7	50
New York, NY	361	8.1	0.8	1.5	39	103
Philadelphia, PA	240	6.2	1.0	1.8	19	53
Phoenix, AZ	273	7.6	1.0	3.3	40	60
Portland, OR	164	6.5	0.7	1.6	6	66
Richmond, VA	232	6.2	0.8	1.9	16	64
Sacramento, CA	201	6.6	0.9	1.1	7	60
St Louis, MO	319	6.1	1.1	1.6	26	82
Salt Lake City, UT	183	8.5	0.6	2.2	11	85
San Antonio, TX	131	3.9	1.1	2.3	6	60
San Diego, CA	195	7.1	1.0	0.9	8	90
San Francisco, CA	308	4.8	1.8	0.7	25	70
Tampa, FL	230	4.4	1.1	1.0	8	68
Tulsa, OK	224	5.3	0.9	1.8	15	70
Washington, DC	275	5.3	0.9	1.4	13	99

aldehydes, 1% ketones, and 2% acetylene. The detailed composition of this mixture is given elsewhere (Carter, 1993).

Adjusted NO_x scenarios

Incremental reactivities in the base case scenarios would be expected to vary widely, since incremental reactivities depend on the ROG/NO_x ratio, and that ratio varies widely among the base case scenarios. To obtain reactivity scales for specified NO_x conditions, separate sets of scenarios, designated MIR (for Maximum Incremental Reactivity), MOR (for maximum ozone reactivity), and Equal Benefit Incremental Reactivity (EBIR) were developed (Carter, 1984). In the MIR scenarios, the NO_x inputs were adjusted so the base ROG mixture (and most other VOCs) have their highest incremental reactivity. This is representative of the highest NO_x conditions of relevance to VOC reactivity assessment because at higher NO_x levels O₃ yields become significantly suppressed, but is also the condition where O₃ is most sensitive to VOC emissions. In the MOR scenarios, the NO_x inputs were adjusted to yield the highest ozone concentration. In the EBIR scenarios, the NO_x inputs were adjusted so that the relative effects of NO_x reductions and total ROG reductions on peak ozone levels were equal. This represents the lowest NO_x condition of relevance for VOC reactivity assessment, because O₃ formation becomes more sensitive to NO_x emissions than VOC emissions at lower NO_x levels. The changes in the base case ROG/NO_x ratios which yielded the MOR scenarios are given in Table 3. As discussed by Carter (1994a) the MIR and EBIR ROG/NO_x ratios are respectively ~1.5 and ~0.7 times those for the MOR scenarios in all cases. Note that set of incremental reactivities calculated for the MIR and EBIR scenarios are referred to as the MIR or EBIR scales, while those calculated for MOR scenarios are referred to as MOIR, for Maximum Ozone Incremental Reactivity, scale.

For this study, the MIR, MOIR, and EBIR reactivities were calculated using the "averaged conditions" scenarios with the corresponding adjusted NO_x conditions. As discussed by Carter (1994a), averaged conditions scenarios have all inputs derived by averaging the corresponding inputs of the base case scenarios, except that the NO_x inputs were adjusted to yield the specified NO_x conditions as discussed above. This is slightly different than the approach used by Carter (1994a) to derive the MIR, MOIR, and EBIR scales, which involved adjusting NO_x conditions separately for each of the 39 base case scenarios, and then averaging the reactivities derived from them. Since Carter (1994a) showed that both approaches yield essentially the same result. For this work use of the averaged conditions approach was preferred because it is computationally much more straightforward, and gives an equally a good indication of how the relative reactivities of compounds vary with varying NO_x conditions.

NO_x Conditions in the Base Case Scenarios

The variability of ROG/NO_x ratios in the base case scenarios suggest a variability of reactivity characteristics in the base case scenarios. However, as discussed previously (Carter, 1994a), the ROG/NO_x ratio is also variable in the MIR or MOR scenarios, despite the fact that the NO_x inputs in these

scenarios are adjusted to yield a specified reactivity characteristic. Thus, the ROG/NO_x ratio, by itself, is not necessarily a good predictor of reactivity characteristics of a particular scenario. The NO_x/NO_x^{MOR} ratio is a much better predictor of this, with values greater than 1 indicating relatively high NO_x conditions where ozone formation is more sensitive to VOCs, and values less than 1 indicating NO_x-limited conditions. NO_x/NO_x^{MOR} ratios less than 0.7 represent conditions where NO_x control is a more effective ozone control strategy than ROG control (Carter, 1994a). Note that more than half of the base case scenarios represent NO_x-limited conditions, and ~25% of them represent conditions where NO_x control is more beneficial than VOC control. A relatively small number of scenarios represent MIR or near-MIR conditions. However, as discussed elsewhere (Carter, 1994a), this set of scenarios is based on near-worst-case conditions for ozone formation in each of the airsheds. Had scenarios representing less-than-worst-case conditions been included, one might expect a larger number of MIR or near MIR scenarios. This is because NO_x is consumed more slowly on days with lower light intensity or temperature, and thus the scenario is less likely to become NO_x-limited.

Incremental and Relative Reactivities

The incremental reactivity of a VOC in an airshed scenario is the change in ozone caused by adding the VOC to the emissions, divided by the amount of VOC added, calculated for sufficiently small amounts of added VOC that the incremental reactivity is independent of the amount added. The procedure used to calculate incremental reactivities in a scenario was as discussed in detail elsewhere (Carter, 1993, 1994a,b). The incremental reactivities depend on how the amount of VOC added are quantified. In this work, the added VOC was quantified on a mass basis, since this is how VOCs are regulated. In addition, the incremental reactivities also depend on how ozone impacts are quantified (Carter, 1994a). In this work, two different ozone quantifications were used, resulting in two different incremental reactivities being calculated for a VOC in a scenario. These are discussed below.

The "Ozone Yield" incremental reactivities measure the effect of the VOC on the total amount of ozone formed in the scenario at the time of its maximum concentration. In this work, this is quantified as grams O₃ formed per gram VOC added. This gives the same ratios of incremental reactivities as reactivities calculated from peak ozone concentrations, but is preferred because it permits magnitudes of reactivities in scenarios with differing dilutions to be compared on the same basis. Most previous recent studies of incremental reactivity (Dodge, 1984; Carter and Atkinson, 1987, 1989a, Chang and Rudy, 1990; Jeffries and Crouse, 1991) have all been based on ozone yield or peak ozone concentration reactivities.

The ozone yield incremental reactivities do not necessarily measure the effect of the VOC on exposure to unacceptable levels of ozone because it does not measure how long high levels of ozone are present. A quantification which reflects this is integrated ozone over the standard, which is defined as the sum of the hourly ozone concentrations for the hours when ozone exceeds the standard in the base case scenarios (Carter 1994a). In the previous work (Carter, 1994a), we used the California ozone standard

of 90 ppb, but in this work we will use the national standard of 0.12 ppm. Reactivities relative to this quantification of ozone are referred to by the abbreviation "IntO₃>0.12" reactivities.

Relative reactivities are ratios of incremental reactivities to incremental reactivities of some standard VOC or mixture. Since these are the quantities which usually are the most relevant to control strategy applications, the results in this work will be given in terms of relative reactivities. In our previous work (Carter 1991, 1994a), we used the incremental reactivity of the base ROG mixture, i.e., the mixture representing ROG pollutants from all sources, as the standard to define relative reactivities. However, because of the tendency within the EPA to consider ethane as the standard to define exempt vs controlled VOCs, in this work we will present reactivity ratios where ethane is used as the standard.

Reactivity Scales

A reactivity scale is a set of incremental or relative reactivities for a particular scenario or group of scenarios. Two types of reactivity scales will be discussed here, "base case" scales and adjusted NO_x scales. Base case scales are simply the set of incremental or relative reactivities in the 39 base case scenarios. Two sets of base case scales are derived — those based ozone yield reactivities and those based on IntO₃>0.12 reactivities. In the previous work (Carter, 1991, 1994a) we derived various multi-scenario scales from the individual base case scales by averaging or other procedures, to evaluate alternative approaches for developing single reactivity scales for applications requiring single scales. However, the decision of whether to exempt a VOC should not be made based on relative reactivities of a single scale, but on a knowledge of the range of relative reactivities for a variety of conditions. Thus in this work we present the distribution of base case relative reactivities for the 39 individual scenarios rather than developing aggregated or optimum scales which represent the distribution by single numbers.

The adjusted NO_x incremental reactivity scales refer to the MIR (Maximum Incremental Reactivity), MOIR (maximum Ozone Incremental Reactivity), or the EBIR (Equal Benefit Incremental Reactivity) scales. In this work, these consist of ozone yield incremental reactivities in averaged conditions scenarios where NO_x inputs were adjusted to yield MIR, MOR or EBIR conditions, respectively. Relative reactivities in these scales are ratios of incremental reactivities in these scales. Reactivities in the MIR scale are of interest because the California Air Resources Board utilized an MIR scale to calculate reactivity adjustment factors in its clean fuels/low emissions vehicle regulations (CARB, 1993). The justification for using this scale in applications requiring a single scale (such as the CARB vehicle regulations) is that it reflects conditions where ozone is most sensitive to changes in VOC emissions, and complements NO_x control, which is most effective for reducing ozone under conditions where the MIR scale is least applicable (Carter, 1994a). The MOIR scale is preferred by many as an alternative for such applications because it reflects conditions which are most favorable for ozone, and is more representative of the distribution of conditions in the base case scenarios (Carter 1994a). Most other alternative reactivity scales which might be appropriate for assessing VOC control strategies (i.e.,

excluding scales representing highly NO_x-limited conditions where ozone is more sensitive to NO_x than VOCs) tend to fall in the range defined by the MIR and MOIR scales. Since the EBIR scale represents lower NO_x conditions where O₃ is less sensitive to VOCs, its use in applications requiring a single scale has not been considered. However, it is useful for assessing how reactivities depend on NO_x conditions.

Note that the MIR, MOIR, EBIR and base case scales derived in this work are somewhat different from those calculated previously (Carter, 1994a; Carter et al, 1993a) because an updated chemical mechanism was used. The updates to the mechanism were discussed in the previous section. In addition, as indicated above, for computational efficiency the MIR, MOIR and EBIR scales were calculated using a single averaged conditions scenario, rather than the average of the adjusted NO_x base case scenarios as done previously (Carter, 1994a).

Calculated Relative Reactivities of Trichloroethylene

Table 5 lists the ozone yield and IntO₃>0.12 reactivities trichloroethylene relative to ethane and relative to the total of all emitted VOCs for the base case and the adjusted NO_x averaged conditions scenarios. Calculations were carried out using both of the alternative TCE photooxidation mechanisms, though as expected based on the simulations of the reactivity experiments the differences were extremely minor. Both mechanism predict that TCE between 2-3 times more reactive than ethane, and 1/4 to 1/3 as reactive as the total of all emissions, on an ozone formed per gram basis, regardless of whether ozone is quantified by peak ozone yield or integrated ozone over the standard. Compared to the average of all emissions, The model predicts that the reactivity relative to ethane decreases slightly as NO_x becomes more limited, though the opposite is observed for the predicted reactivities relative to the total of all emissions, and the dependence of relative reactivities on NO_x levels and other scenario conditions is not large compared to many other VOCs (e.g., see Carter, 1994).

Note that the chemical mechanisms used in these calculations consistently underpredicted the effects of TCE on peak ozone yields in experiments where NO_x is limited, suggesting that the model may be overpredicting TCE's ozone impacts in the Maximum Ozone, Equal Benefit, and in many if not most of the base case scales. However, the model also consistently underpredicted the apparent Cl atom production from TCE, suggesting that there may be some circumstances, perhaps not represented in our chamber experiments, where TCE's ozone impacts may be underpredicted. Therefore, the ozone impact estimates for TCE under the MOIR, EBIR, and lower NO_x base case conditions are probably not reliable. Nevertheless, the mechanisms did perform quite well in simulating TCE's ozone impacts in the chamber experiments representing relatively low ROG/NO_x, "maximum reactivity" conditions, so we can probably have more confidence of the reactivity predictions for TCE in the MIR scale.

Table 5. Summary of calculated relative incremental reactivities (gram basis) for trichloroethylene, ethane, and the total of all emitted VOCs.

Scenario	Relative to the Total of Emitted VOCS (Base ROG)						Relative to Ethane					
	O ₃ Yield Reactivity			IntO ₃ >0.12 Reactivity			O ₃ Yield Reactivity			IntO ₃ >0.12 Reactivity		
	TCE		Ethane	TCE		Ethane	TCE		Base ROG	TCE		Base ROG
	A	B		A	B		A	B		A	B	
<u>Averaged Conditions</u>												
Max React (MIR)	0.24	0.22	0.08	0.22	0.21	0.07	2.9	2.8	12.4	3.0	2.8	13.5
Max Ozone (MOIR)	0.30	0.29	0.15	0.25	0.23	0.10	2.0	1.9	6.8	2.5	2.4	10.2
Equal Benefit (EBIR)	0.34	0.33	0.19	0.28	0.27	0.12	1.8	1.7	5.3	2.3	2.2	8.1
<u>Base Case</u>												
Average	0.32	0.31	0.17	0.27	0.26	0.12	2.0	1.9	6.3	2.4	2.3	9.2
St.Dev	14%	14%	23%	14%	14%	25%	22%	21%	38%	18%	18%	30%
ATL GA	0.33	0.32	0.17	0.29	0.27	0.12	1.9	1.9	6.0	2.4	2.3	8.4
AUS TX	0.35	0.34	0.19	0.30	0.29	0.14	1.8	1.8	5.2	2.2	2.1	7.3
BAL MD	0.29	0.28	0.15	0.22	0.21	0.09	1.9	1.8	6.6	2.6	2.4	11.5
BAT LA	0.35	0.34	0.15	0.30	0.28	0.10	2.3	2.2	6.6	2.9	2.7	9.8
BIR AL	0.37	0.36	0.23	0.27	0.26	0.13	1.6	1.5	4.3	2.1	2.0	7.6
BOS MA	0.32	0.32	0.20	0.26	0.25	0.12	1.6	1.6	4.9	2.1	2.0	8.0
CHA NC	0.32	0.32	0.21	0.29	0.29	0.17	1.5	1.5	4.8	1.8	1.7	6.0
CHI IL	0.50	0.49	0.27	0.40	0.39	0.17	1.9	1.8	3.8	2.4	2.3	6.0
CIN OH	0.31	0.30	0.19	0.25	0.24	0.12	1.6	1.6	5.3	2.1	2.0	8.2
CLE OH	0.30	0.29	0.15	0.24	0.22	0.09	2.0	2.0	6.8	2.7	2.5	11.3
DAL TX	0.29	0.28	0.12	0.26	0.24	0.09	2.5	2.4	8.6	2.8	2.6	10.9
DEN CO	0.28	0.26	0.11	0.24	0.22	0.07	2.6	2.5	9.4	3.2	3.0	13.8
DET MI	0.32	0.31	0.20	0.26	0.25	0.13	1.6	1.6	5.1	2.1	2.0	7.9
ELP TX	0.29	0.28	0.11	0.25	0.24	0.08	2.6	2.5	8.9	3.2	3.0	12.7
HAR CT	0.32	0.32	0.20	0.28	0.27	0.14	1.6	1.6	4.9	2.0	1.9	7.0
HOU TX	0.33	0.32	0.18	0.26	0.24	0.11	1.8	1.7	5.4	2.3	2.2	9.0
IND IN	0.30	0.29	0.16	0.26	0.25	0.11	1.9	1.8	6.4	2.5	2.3	9.5
JAC FL	0.34	0.32	0.16	0.32	0.30	0.14	2.1	2.0	6.2	2.2	2.2	7.1
KAN MO	0.31	0.30	0.20	0.27	0.26	0.14	1.6	1.5	5.1	1.9	1.9	7.1
LAK LA	0.41	0.39	0.22	0.34	0.32	0.13	1.9	1.8	4.6	2.5	2.4	7.6
LOS CA	0.33	0.32	0.15	0.24	0.23	0.08	2.2	2.2	6.7	2.9	2.7	11.9
LOU KY	0.32	0.31	0.19	0.29	0.27	0.13	1.7	1.7	5.4	2.2	2.1	7.6
MEM TN	0.34	0.33	0.20	0.28	0.27	0.13	1.7	1.6	4.9	2.1	2.0	7.5
MIA FL	0.33	0.32	0.18	0.32	0.31	0.17	1.8	1.8	5.5	1.9	1.8	5.9
NAS TN	0.37	0.36	0.23	0.33	0.32	0.19	1.6	1.5	4.3	1.7	1.7	5.2
NEW NY	0.39	0.39	0.17	0.27	0.26	0.09	2.3	2.3	5.8	3.0	2.9	11.4
PHI PA	0.31	0.30	0.17	0.26	0.24	0.11	1.8	1.8	6.0	2.3	2.2	9.0
PHO AZ	0.31	0.30	0.16	0.24	0.22	0.09	1.9	1.8	6.2	2.5	2.4	10.6
POR OR	0.32	0.31	0.18	0.30	0.28	0.14	1.8	1.7	5.7	2.1	2.0	7.1
RIC VA	0.30	0.30	0.18	0.25	0.24	0.11	1.7	1.6	5.4	2.2	2.1	8.7
SAC CA	0.32	0.31	0.17	0.28	0.26	0.12	1.9	1.8	5.9	2.4	2.2	8.5
SAI MO	0.29	0.28	0.14	0.22	0.21	0.08	2.1	2.0	7.1	2.7	2.5	12.3
SAL UT	0.32	0.31	0.19	0.26	0.25	0.12	1.7	1.7	5.4	2.3	2.1	8.6
SAN TX	0.30	0.28	0.13	0.28	0.27	0.12	2.4	2.3	8.0	2.5	2.3	8.6
SDO CA	0.30	0.29	0.12	0.27	0.25	0.09	2.6	2.4	8.5	2.9	2.7	11.0
SFO CA	0.20	0.19	0.05	0.19	0.18	0.05	3.7	3.6	18.3	3.9	3.6	20.1
TAM FL	0.31	0.29	0.13	0.26	0.24	0.09	2.3	2.2	7.5	2.9	2.7	10.9
TUL OK	0.30	0.29	0.18	0.25	0.23	0.11	1.7	1.6	5.6	2.2	2.1	9.0
WAS DC	0.32	0.31	0.19	0.25	0.23	0.11	1.7	1.6	5.2	2.2	2.1	8.9

CONCLUSIONS

The decision whether it is appropriate to regulate a compound as an ozone precursor requires a qualitative assessment of its ozone impacts under a variety of environmental conditions. This involves developing a chemical mechanism for the compounds atmospheric reactions which can be reliably used in airshed models to predict its atmospheric reactivity. Until this study, there was no chemical mechanism available for simulating the atmospheric reactions of trichloroethylene, and thus reactivity estimates for this compound could not be made. The objective of this study was to develop such a mechanism and provide the data needed to verify its predictive capabilities. This program made significant towards meeting this objective, allowing estimates to be made of TCE's relative ozone impacts under the relatively high NO_x conditions where VOCs have the greatest impacts on ozone formation. However, it is clear that we do not understand all the aspects of atmospheric reactions of trichloroethylene which might affect ozone formation, particularly those affecting predictions of its ozone impacts under the lower NO_x conditions where peak ozone concentrations are formed.

This work has confirmed previous laboratory and chamber studies that chlorine atom formation is a significant factor in the atmospheric photooxidation of TCE. A chemical mechanism has been developed to account for the effect of TCE on rates of NO oxidation and initial rates of ozone formation under a variety of conditions, at least up to the time that peak ozone concentrations are approached. Several uncertain mechanistic parameters, concerning primarily secondary reactions of some of TCE's expected oxidation products, had to be adjusted to obtain satisfactory simulations of these data, and more than one set of optimum parameters were obtained which yielded essentially the same predictions in atmospheric simulations. However, no reasonable adjustments of the uncertain aspects of the mechanism resulted in a model which could successfully simulate an acceleration in O_3 formation and TCE consumption and then O_3 consumption observed in one TCE + ethane + NO_x experiment, or could simulate the leveling off or decline in ozone concentrations in the higher ROG/ NO_x added TCE experiments, or could predict the full amount of apparent Cl atom production observed in most experiments. Thus it is apparent that there are other secondary reactions occurring in the TCE photooxidation system which are not presently understood.

Since the mechanisms developed in this work performed best in simulating ozone formation in the experiments representing maximum incremental reactivity conditions, they can be expected to be most reliable in predicting MIR reactivities. Under these conditions, TCE is predicted to form three times as much ozone per gram emitted than ethane, indicating that it is probably not negligibly reactive under the criterion currently used by the EPA. On the other hand, it is clearly not highly reactive, having a predicted MIR reactivity only 1/4 of that of the mixture of all emissions. The ambiguities in the

mechanisms concerning the set of parameters to adjust to fit the data had only a very minor impact on the MIR predictions, indicating that this is probably not a large source of uncertainty. The mechanisms also predict that TCE's ozone impacts relative to ethane or the mixture of all emissions are only slightly affected by changes in NO_x conditions, but this prediction is probably incorrect, and it is more likely that TCE's relative ozone impacts decrease significantly with decreasing NO_x . However, we cannot be absolutely confident of this because of the underprediction of the effect of TCE on Cl atom levels, whose formation may enhance ozone levels under some situations. It is concluded that more fundamental mechanistic data are needed TCE's atmospheric reactions we can reliably predict its ozone impacts under the full range of atmospheric conditions.

REFERENCES

- Aschmann, S. A. and R. Atkinson (1995): "Rate Constants for the Gas-Phase Reactions of Alkanes with Cl Atmos at 296 ± 2 K," *Int. J. Chem. Kinet.*, 27, 613-622.
- Atkinson, R. (1987): "A Structure-Activity Relationship for the Estimation of Rate Constants for the Gas-Phase Reactions of OH Radicals with Organic Compounds," *Int. J. Chem. Kinet.*, 19, 799-828.
- Atkinson, R. (1989): "Kinetics and Mechanisms of the Gas-Phase Reactions of the Hydroxyl Radical with Organic Compounds," *J. Phys. Chem. Ref. Data*, Monograph no 1.
- Atkinson, R. (1994): "Gas-Phase Tropospheric Chemistry of Organic Compounds," *J. Phys. Chem. Ref. Data*, Monograph No. 2.
- Atkinson, R. and S. M. Aschmann (1985): *Int. J. Chem. Kinet.* 17, 33.
- Atkinson, R., S. M. Aschmann, A. M. Winer, and J. N. Pitts, Jr. (1982): *Int. J. chem. Kinet.* 14, 13.
- R. Atkinson and S. M. Aschmann (1987): "Kinetics of the Gas-Phase Reactions of Cl Atoms with Chloroethenes at 298 ± 2 K and Atmospheric Pressure," *Int. J. Chem. Kinet.* 19, 1097-1105.
- Atkinson, R., S. M. Aschmann, and M. A. Goodman (1987): *Int J. Chem. Kinet.* 19, 299.
- Atkinson, R., D. L. Baulch, R. A. Cox, R. F. Hampson, Jr., J. A. Kerr, M. J. Rossi, and J. Troe (1996): "Evaluated Kinetic, Photochemical and Heterogeneous Data for Atmospheric Chemistry: Supplement V., IUPAC Subcommittee on Gas Kinetic Data Evaluation for Atmospheric Chemistry," *J. Phys. Chem. Ref. Data*, in press.
- Atkinson, R. (1989): "Kinetics and Mechanisms of the Gas-Phase Reactions of the Hydroxyl Radical with Organic Compounds," *J. Phys. Chem. Ref. Data*, Monograph no 1.
- Atkinson, R. (1991): "Kinetics and Mechanisms of the Gas-Phase Reactions of the NO_3 Radical with Organic Compounds," *J. Phys. Chem. Ref. Data*, 20, 459-507.
- Atkinson, R. and W. P. L. Carter (1984): "Kinetics and Mechanisms of the Gas-Phase Reactions of Ozone with Organic Compounds under Atmospheric Conditions," *Chem. Rev.* 1984, 437-470.
- Atkinson, R. and W. P. L. Carter (1992): "Reactions of Alkoxy Radicals under Atmospheric Conditions: The Relative Importance of Decomposition versus Reaction with O_2 ," *J. Atm. Chem.*, 13, 195-210.
- Atkinson, R. and W. P. L. Carter (1992): "Reactions of Alkoxy Radicals under Atmospheric Conditions: The Relative Importance of Decomposition versus Reaction with O_2 ," *J. Atm. Chem.*, 13, 195-210.

- Baugues, K. (1990): "Preliminary Planning Information for Updating the Ozone Regulatory Impact Analysis Version of EKMA," Draft Document, Source Receptor Analysis Branch, Technical Support Division, U. S. Environmental Protection Agency, Research Triangle Park, NC, January.
- Campbell, I. M. and P. E. Parkinson (1978): Chem. Phys. Lett. 53, 385.
- CARB (1993): "Proposed Regulations for Low-Emission Vehicles and Clean Fuels — Staff Report and Technical Support Document," California Air Resources Board, Sacramento, CA, August 13, 1990. See also Appendix VIII of "California Exhaust Emission Standards and Test Procedures for 1988 and Subsequent Model Passenger Cars, Light Duty Trucks and Medium Duty Vehicles," as last amended September 22, 1993. Incorporated by reference in Section 1960.1 (k) of Title 13, California Code of Regulations.
- Calvert, J. G., and J. N. Pitts, Jr. (1966): Photochemistry, John Wiley and Sons, New York.
- Carter, W. P. L. (1990): "A Detailed Mechanism for the Gas-Phase Atmospheric Reactions of Organic Compounds," Atmos. Environ., 24A, 481-518.
- Carter, W. P. L. (1991): "Development of Ozone Reactivity Scales for Volatile Organic Compounds", EPA-600/3-91/050, August.
- Carter, W. P. L. (1993): "Development and Application of an Up-To-Date Photochemical Mechanism for Airshed Modeling and Reactivity Assessment," Draft final report for California Air Resources Board Contract No. A934-094, April 26.
- Carter, W. P. L. (1994a): "Development of Ozone Reactivity Scales for Volatile Organic Compounds," J. Air & Waste Manage. Assoc., 44, 881-899.
- Carter, W. P. L. (1994b): "Calculation of Reactivity Scales Using an Updated Carbon Bond IV Mechanism," Draft Report Prepared for Systems Applications International Under Funding from the Auto/Oil Air Quality Improvement Research Program, April 12.
- Carter, W. P. L. (1995): "Computer Modeling of Environmental Chamber Measurements of Maximum Incremental Reactivities of Volatile Organic Compounds," Atmos. Environ., 29, 2513-2517.
- Carter, W. P. L. and R. Atkinson (1987): "An Experimental Study of Incremental Hydrocarbon Reactivity," Environ. Sci. Technol., 21, 670-679
- Carter, W. P. L. and R. Atkinson (1989a): "A Computer Modeling Study of Incremental Hydrocarbon Reactivity", Environ. Sci. Technol., 23, 864.
- Carter, W. P. L. and R. Atkinson (1989b): "Alkyl Nitrate Formation from the Atmospheric Photooxidation of Alkanes; a Revised Estimation Method," J. Atm. Chem. 8, 165-173.
- Carter, W. P. L., and F. W. Lurmann (1990): "Evaluation of the RADM Gas-Phase Chemical Mechanism," Final Report, EPA-600/3-90-001.

- Carter, W. P. L. and F. W. Lurmann (1991): "Evaluation of a Detailed Gas-Phase Atmospheric Reaction Mechanism using Environmental Chamber Data," *Atm. Environ.* 25A, 2771-2806.
- Carter, W. P. L., D. Luo, I. L. Malkina, and J. A. Pierce (1993a): "An Experimental and Modeling Study of the Photochemical Ozone Reactivity of Acetone," Final Report to Chemical Manufacturers Association Contract No. KET-ACE-CRC-2.0. December 10.
- Carter, W. P. L., J. A. Pierce, I. L. Malkina, D. Luo and W. D. Long (1993b): "Environmental Chamber Studies of Maximum Incremental Reactivities of Volatile Organic Compounds," Report to Coordinating Research Council, Project No. ME-9, California Air Resources Board Contract No. A032-0692; South Coast Air Quality Management District Contract No. C91323, United States Environmental Protection Agency Cooperative Agreement No. CR-814396-01-0, University Corporation for Atmospheric Research Contract No. 59166, and Dow Corning Corporation. April 1.
- Carter, W. P. L., D. Luo, I. L. Malkina, and J. A. Pierce (1995a): "Environmental Chamber Studies of Atmospheric Reactivities of Volatile Organic Compounds. Effects of Varying ROG Surrogate and NO_x," Final report to Coordinating Research Council, Inc., Project ME-9, California Air Resources Board, Contract A032-0692, and South Coast Air Quality Management District, Contract C91323. March 24.
- Carter, W. P. L., D. Luo, I. L. Malkina, and D. Fitz (1995b): "The University of California, Riverside Environmental Chamber Data Base for Evaluating Oxidant Mechanism. Indoor Chamber Experiments through 1993," Report submitted to the U. S. Environmental Protection Agency, EPA/AREAL, Research Triangle Park, NC., March 20..
- Carter, W. P. L., J. A. Pierce, D. Luo, and I. L. Malkina (1995c): "Environmental Chamber Study of Maximum Incremental Reactivities of Volatile Organic Compounds," *Atmos. Environ.* 29, 2499-2511.
- Carter, W. P. L., D. Luo, I. L. Malkina, and J. A. Pierce (1995d): "Environmental Chamber Studies of Atmospheric Reactivities of Volatile Organic Compounds. Effects of Varying Chamber and Light Source," Final report to National Renewable Energy Laboratory, Contract XZ-2-12075, Coordinating Research Council, Inc., Project M-9, California Air Resources Board, Contract A032-0692, and South Coast Air Quality Management District, Contract C91323, March 26.
- Chang, T. Y. and S. J. Rudy (1990): "Ozone-Forming Potential of Organic Emissions from Alternative-Fueled Vehicles," *Atmos. Environ.*, 24A, 2421-2430.
- Croes, B. E., Technical Support Division, California Air Resources Board, personal communication (1991).
- Croes, B. E., et al. (1994): "Southern California Air Quality Study Data Archive," Research Division, California Air Resources Board.
- Dodge, M. C. (1984): "Combined effects of organic reactivity and NMHC/NO_x ratio on photochemical oxidant formation -- a modeling study," *Atmos. Environ.*, 18, 1657.

- EPA (1984): "Guideline for Using the Carbon Bond Mechanism in City-Specific EKMA," EPA-450/4-84-005, February.
- Gay, B. W., P. L. Hanst, J. J. Bufalini, and R. C. Noonan (1976): "Atmospheric Oxidation of Chlorinated Ethylenes," Environ. Sci. Technol. 10, 58-67.
- Gery, M. W., R. D. Edmond and G. Z. Whitten (1987): "Tropospheric Ultraviolet Radiation. Assessment of Existing Data and Effects on Ozone Formation," Final Report, EPA-600/3-87-047, October.
- Gipson, G. L., W. P. Freas, R. A. Kelly and E. L. Meyer, "Guideline for Use of City-Specific EKMA in Preparing Ozone SIPs, EPA-450/4-80-027, March, 1981.
- Gipson, G. L. and W. P. Freas (1983): "Use of City-Specific EKMA in the Ozone RIA," U. S. Environmental Protection Agency, July.
- Gipson, G. L. (1984): "Users Manual for OZIPM-2: Ozone Isopleth Plotting Package With Optional Mechanism/Version 2," EPA-450/4-84-024, August.
- Hogo, H. and M. W. Gery (1988): "Guidelines for Using OZIPM-4 with CBM-IV or Optional Mechanisms. Volume 1. Description of the Ozone Isopleth Plotting Package Version 4", Final Report for EPA Contract No. 68-02-4136, Atmospheric Sciences Research Laboratory, Research Triangle Park, NC. January.
- Jeffries, H. E., K. G. Sexton, J. R. Arnold, and T. L. Kale (1989): "Validation Testing of New Mechanisms with Outdoor Chamber Data. Volume 2: Analysis of VOC Data for the CB4 and CAL Photochemical Mechanisms," Final Report, EPA-600/3-89-010b.
- Jeffries, H. E. and R. Crouse (1991): "Scientific and Technical Issues Related to the Application of Incremental Reactivity. Part II: Explaining Mechanism Differences," Report prepared for Western States Petroleum Association, Glendale, CA, October.
- Jeffries, H. E. (1991): "UNC Solar Radiation Models," unpublished draft report for EPA Cooperative Agreements CR813107, CR813964 and CR815779". Undated.
- Johnson, G. M. (1983): "Factors Affecting Oxidant Formation in Sydney Air," in "The Urban Atmosphere -- Sydney, a Case Study." Eds. J. N. Carras and G. M. Johnson (CSIRO, Melbourne), pp. 393-408.
- Kwok and Atkinson (1995) estimation OH
- Lurmann, F. W. and H. H. Main (1992): "Analysis of the Ambient VOC Data Collected in the Southern California Air Quality Study," Final Report to California Air Resources Board Contract No. A832-130, February.
- NASA (1994): "Chemical Kinetics and Photochemical Data for Use in Stratospheric Modeling, Evaluation Number 11," JPL Publication 94-26, Jet Propulsion Laboratory, Pasadena, California, December.

- Pitts, J. N., Jr., E. Sanhueza, R. Atkinson, W. P. L. Carter, A. M. Winer, G. W. Harris, and C. N. Plum (1984): "An Investigation of the Dark Formation of Nitrous Acid in Environmental Chambers," *Int. J. Chem. Kinet.*, 16, 919-939.
- Plum, C. N., Sanhuesa, E., Atkinson, R., Carter W. P. L. and Pitts, J. N., Jr. (1983): "OH Radical Rate Constants and Photolysis Rates of α -Dicarbonyls," *Environ. Sci. Technol.* 17, 479-484.
- Sanhueza, E., I. C. Hisatsune, and J. Heicklen (1976): *Chem. Rev.* 76, 801.
- Schonle, G., H. D. Knauth, R. N. Schindler (1979); *J. Phys. Chem.* 83, 3297
- E. C. Tuzaon, R. Atkinson, S. M. Aschmann, M. A. Goodman, and A. M. Winer (1988): "Atmospheric Reactions of Chloroethanes with the OH Radical," *Int. J. Chem. Kinet.*, 20, 241-265.
- Tuazon, E. C., R. Atkinson, C. N. Plum, A. M. Winer, and J. N. Pitts, Jr. (1983): "The Reaction of Gas-Phase N_2O_5 with Water Vapor," *Geophys. Res. Lett.* 10, 953-956.
- Wallington, T. J., P. Dagaut, R. Liu, and M. J. Kurylo (1988a): *Int. J. Chem. Kinet.* 20, 177.
- Wallington, T. J., L. M. Skewes, and W. O. Siegl (1988b): *J. Photochem. Photobiol. A:Chem*, 45, 33.
- Zafonte, L., P. L. Rieger, and J. R. Holmes (1977): "Nitrogen Dioxide Photolysis in the Los Angeles Atmosphere," *Environ. Sci. Technol.* 11, 483-487.

APPENDIX A
LISTING OF THE CHEMICAL MECHANISM

The chemical mechanism used in the environmental chamber and atmospheric model simulations discussed in this report is given in Tables A-1 through A-4. Table A-1 lists the species used in the mechanism, Table A-2 gives the reactions and rate constants, Table A-3 gives the parameters used to calculate the rates of the photolysis reactions, and Table A-4 gives the values and derivations of the chamber-dependent parameters used when modeling the environmental chamber experiments. Footnotes to Table A-2 indicate the format used for the reaction listing.

Table A-1. List of species in the chemical mechanism used in the model simulations for this study.

Name	Description
Constant Species.	
O2	Oxygen
M	Air
H2O	Water
Active Inorganic Species.	
O3	Ozone
NO	Nitric Oxide
NO2	Nitrogen Dioxide
NO3	Nitrate Radical
N2O5	Nitrogen Pentoxide
HONO	Nitrous Acid
HNO3	Nitric Acid
HNO4	Peroxynitric Acid
HO2H	Hydrogen Peroxide
Cl2	Chlorine
ClNO	ClONO
ClONO	ClONO ₂
ClNO2	ClNO ₂
ClO	Chlorine Oxide
ClONO2	Chlorine Nitrate
Active Radical Species and Operators.	
HO2.	Hydroperoxide Radicals
RO2.	Operator to Calculate Total Organic Peroxy Radicals
RCO3.	Operator to Calculate Total Acetyl Peroxy Radicals
CL.	Chlorine Atoms

Table A-1, (continued)

Name	Description
Active Reactive Organic Product Species.	
CO	Carbon Monoxide
HCHO	Formaldehyde
CCHO	Acetaldehyde
RCHO	Lumped C3+ Aldehydes
ACET	Acetone
MEK	Lumped Ketones
PHEN	Phenol
CRES	Cresols
BALD	Aromatic aldehydes (e.g., benzaldehyde)
GLY	Glyoxal
MGLY	Methyl Glyoxal
AFG1	Reactive Aromatic Fragmentation Products from benzene and naphthalene
AFG2	Other Reactive Aromatic Fragmentation Products
AFG3	Aromatic Fragmentation Products used in adjusted m-xylene mechanism
RNO3	Organic Nitrates
NPHE	Nitrophenols
ISOPROD	Lumped isoprene product species
PAN	Peroxy Acetyl Nitrate
PPN	Peroxy Propionyl Nitrate
GPAN	PAN Analogue formed from Glyoxal
PBZN	PAN Analogues formed from Aromatic Aldehydes
-OOH	Operator Representing Hydroperoxy Groups
HCO-CO-CL	Product formed from the OH + TCE reaction
CL2CH-CO-CL	Product formed from the Cl + TCE reaction
CL-CO-CO-CL	Product formed from the Cl + Cl ₂ CH-CO-Cl reaction
Non-Reacting Species	
CO ₂	Carbon Dioxide
-C	"Lost Carbon"
-N	"Lost Nitrogen"
H ₂	Hydrogen
HCL	Hydrogen Chloride
Steady State Species and Operators.	
HO.	Hydroxyl Radicals
O	Ground State Oxygen Atoms
O*1D2	Excited Oxygen Atoms
RO2-R.	Peroxy Radical Operator representing NO to NO ₂ conversion with HO ₂ formation.
RO2-N.	Peroxy Radical Operator representing NO consumption with organic nitrate formation.
RO2-NP.	Peroxy Radical Operator representing NO consumption with nitrophenol formation
R2O2.	Peroxy Radical Operator representing NO to NO ₂ conversion.

Table A-1, (continued)

Name	Description
RO2-CL.	Peroxy Radical Operator representing NO to NO ₂ conversion with Cl formation.
CCO-O2.	Peroxy Acetyl Radicals
C2CO-O2.	Peroxy Propionyl Radicals
HCOCO-O2.	Peroxyacyl Radical formed from Glyoxal
BZ-CO-O2.	Peroxyacyl Radical formed from Aromatic Aldehydes
HOCOO.	Intermediate formed in Formaldehyde + HO ₂ reaction
C2(C)-O.	T-Butoxy Radicals.
BZ-O.	Phenoxy Radicals
BZ(NO2)-O.	Nitratophenoxy Radicals
HOCOO.	Radical Intermediate formed in the HO ₂ + Formaldehyde system.
(HCHO2)	Excited Criegee biradicals formed from =CH ₂ groups
(CCHO2)	Excited Criegee biradicals formed from =CHCH ₃ groups
(RCHO2)	Excited Criegee biradicals formed from =CHR groups, where R not CH ₃
(C(C)CO2)	Excited Criegee biradicals formed from =C(CH ₃) ₂ groups
(C(R)CO2)	Excited Criegee biradicals formed from =C(CH ₃)R or CR ₂ groups
(BZCHO2)	Excited Criegee biradicals formed from styrenes
Primary organic species represented explicitly	
CH4	Methane (EKMA simulations only)
ETHANE	Ethane (Ethane reactivity simulations only)
N-C4	n-Butane (Chamber simulations only)
N-C6	n-Hexane (Chamber simulations only)
N-C8	n-Octane (Chamber simulations only)
ETHE	Ethene
ISOP	Isoprene (EKMA Simulations only)
APIN	α-Pinene (EKMA Simulations only)
UNKN	Unknown biogenics. (EKMA Simulations only)
PROPENE	Propene (Chamber simulations only)
T-2-BUTE	<u>trans</u> -2-Butene (Chamber simulations only)
TOLUENE	Toluene (Chamber simulations only)
M-XYLENE	m-Xylene (Chamber simulations only)
CL3-ETHE	Trichloroethylene
Lumped species used to represent the Base ROG mixture in the EKMA model simulations.	
ALK1	Alkanes and other saturated compounds with $k_{OH} < 10^4 \text{ ppm}^{-1} \text{ min}^{-1}$.
ALK2	Alkanes and other saturated compounds with $k_{OH} \geq 10^4 \text{ ppm}^{-1} \text{ min}^{-1}$.
ARO1	Aromatics with $k_{OH} < 2 \times 10^4 \text{ ppm}^{-1} \text{ min}^{-1}$.
ARO2	Aromatics with $k_{OH} \geq 2 \times 10^4 \text{ ppm}^{-1} \text{ min}^{-1}$.
OLE2	Alkenes (other than ethene) with $k_{OH} < 7 \times 10^4 \text{ ppm}^{-1} \text{ min}^{-1}$.
OLE3	Alkenes with $k_{OH} \geq 7 \times 10^4 \text{ ppm}^{-1} \text{ min}^{-1}$.

Table A-2. List of reactions in the chemical mechanism used in the model simulations for this study.

Kinetic Parameters [a]				Notes [c]	Reactions [b]
k(300)	A	Ea	B		
<u>Inorganic Reactions</u>					
(Phot. Set = NO2)					NO2 + HV = NO + O
6.00E-34	6.00E-34	0.00	-2.30		O + O2 + M = O3 + M
9.69E-12	6.50E-12	-0.24	0.00		O + NO2 = NO + O2
1.55E-12				(Falloff Kinetics)	O + NO2 = NO3 + M
k0 =	9.00E-32	0.00	-2.00		
kINF =	2.20E-11	0.00	0.00		
	F= 0.60	n= 1.00			
1.88E-14	2.00E-12	2.78	0.00		O3 + NO = NO2 + O2
3.36E-17	1.40E-13	4.97	0.00		O3 + NO2 = O2 + NO3
2.80E-11	1.70E-11	-0.30	0.00		NO + NO3 = 2 NO2
1.92E-38	3.30E-39	-1.05	0.00		NO + NO + O2 = 2 NO2
1.26E-12				(Falloff Kinetics)	NO2 + NO3 = N2O5
k0 =	2.20E-30	0.00	-4.30		
kINF =	1.50E-12	0.00	-0.50		
	F= 0.60	n= 1.00			
k = kEQ x	k(NO2 + NO3),	kEQ =			N2O5 + #k(reverse) = NO2 + NO3
5.53E+10	9.09E+26	22.26	0.00		
1.00E-21				(No T Dependence)	N2O5 + H2O = 2 HNO3
4.17E-16	2.50E-14	2.44	0.00		NO2 + NO3 = NO + NO2 + O2
	(Phot. Set = NO3NO)				NO3 + HV = NO + O2
	(Phot. Set = NO3NO2)				NO3 + HV = NO2 + O
	(Phot. Set = O3O3P)				O3 + HV = O + O2
	(Phot. Set = O3OLD)				O3 + HV = O*1D2 + O2
2.20E-10				(No T Dependence)	O*1D2 + H2O = 2 HO.
2.92E-11	1.92E-11	-0.25	0.00		O*1D2 + M = O + M
4.81E-12				(Falloff Kinetics)	HO. + NO = HONO
k0 =	7.00E-31	0.00	-2.60		
kINF =	1.50E-11	0.00	-0.50		
	F= 0.60	n= 1.00			
	(Phot. Set = HONO)				HONO + HV = HO. + NO
1.13E-11				(Falloff Kinetics)	HO. + NO2 = HNO3
k0 =	2.60E-30	0.00	-3.20		
kINF =	2.40E-11	0.00	-1.30		
	F= 0.60	n= 1.00			
1.03E-13	6.45E-15	-1.65	0.00		HO. + HNO3 = H2O + NO3
2.40E-13				(No T Dependence)	HO. + CO = HO2. + CO2
6.95E-14	1.60E-12	1.87	0.00		HO. + O3 = HO2. + O2
8.28E-12	3.70E-12	-0.48	0.00		HO2. + NO = HO. + NO2
1.37E-12				(Falloff Kinetics)	HO2. + NO2 = HNO4
k0 =	1.80E-31	0.00	-3.20		
kINF =	4.70E-12	0.00	-1.40		
	F= 0.60	n= 1.00			
k = kEQ x	k(HO2 + NO2),	kEQ =			HNO4 + #k(reverse) = HO2. + NO2
7.92E+10	4.76E+26	21.66	0.00		
4.61E-12	1.30E-12	-0.75	0.00		HNO4 + HO. = H2O + NO2 + O2
2.08E-15	1.10E-14	0.99	0.00		HO2. + O3 = HO. + 2 O2
1.73E-12	2.20E-13	-1.23	0.00		HO2. + HO2. = HO2H + O2
5.00E-32	1.90E-33	-1.95	0.00		HO2. + HO2. + M = HO2H + O2
3.72E-30	3.10E-34	-5.60	0.00		HO2. + HO2. + H2O = HO2H + O2 + H2O
2.65E-30	6.60E-35	-6.32	0.00		HO2. + HO2. + H2O = HO2H + O2 + H2O
1.73E-12	2.20E-13	-1.23	0.00		NO3 + HO2. = HNO3 + O2
5.00E-32	1.90E-33	-1.95	0.00		NO3 + HO2. + M = HNO3 + O2
3.72E-30	3.10E-34	-5.60	0.00		NO3 + HO2. + H2O = HNO3 + O2 + H2O
2.65E-30	6.60E-35	-6.32	0.00		NO3 + HO2. + H2O = HNO3 + O2 + H2O
	(Phot. Set = H2O2)				HO2H + HV = 2 HO.
1.70E-12	3.30E-12	0.40	0.00		HO2H + HO. = HO2. + H2O
9.90E-11	4.60E-11	-0.46	0.00		HO. + HO2. = H2O + O2
<u>Peroxy Radical Operators</u>					
7.68E-12	4.20E-12	-0.36	0.00		RO2. + NO = NO
2.25E-11				(Falloff Kinetics)	RCO3. + NO = NO
k0 =	5.65E-28	0.00	-7.10		
kINF =	2.64E-11	0.00	-0.90		
	F= 0.27	n= 1.00			
1.04E-11				(Falloff Kinetics)	RCO3. + NO2 = NO2
k0 =	2.57E-28	0.00	-7.10		
kINF =	1.20E-11	0.00	-0.90		
	F= 0.30	n= 1.00			
4.90E-12	3.40E-13	-1.59	0.00		RO2. + HO2. = HO2. + RO2-HO2-PROD
4.90E-12	3.40E-13	-1.59	0.00		RCO3. + HO2. = HO2. + RO2-HO2-PROD
1.00E-15				(No T Dependence)	RO2. + RO2. = RO2-RO2-PROD
1.09E-11	1.86E-12	-1.05	0.00		RO2. + RCO3. = RO2-RO2-PROD
1.64E-11	2.80E-12	-1.05	0.00		RCO3. + RCO3. = RO2-RO2-PROD
	(Same k as for RO2.)				RO2-R. + NO = NO2 + HO2.

Table A-2 (continued)

Kinetic Parameters [b]				Notes [d]	Reactions [c]
k(300)	A	Ea	B		
(Same k as for RO2.))				RO2-R. + HO2. = -OOH
(Same k as for RO2.))				RO2-R. + RO2. = RO2. + 0.5 HO2.
(Same k as for RO2.))				RO2-R. + RCO3. = RCO3. + 0.5 HO2.
(Same k as for RO2.))				RO2-N. + NO = RNO3
(Same k as for RO2.))				RO2-N. + HO2. = -OOH + MEK + 1.5 -C
(Same k as for RO2.))				RO2-N. + RO2. = RO2. + 0.5 HO2. + MEK + 1.5 -C
(Same k as for RO2.))				RO2-N. + RCO3. = RCO3. + 0.5 HO2. + MEK + 1.5 -C
(Same k as for RO2.))				R2O2. + NO = NO2
(Same k as for RO2.))				R2O2. + HO2. =
(Same k as for RO2.))				R2O2. + RO2. = RO2.
(Same k as for RO2.))				R2O2. + RCO3. = RCO3.
(Same k as for RO2.))				RO2-XN. + NO = -N
(Same k as for RO2.))				RO2-XN. + HO2. = -OOH
(Same k as for RO2.))				RO2-XN. + RO2. = RO2. + 0.5 HO2.
(Same k as for RO2.))				RO2-XN. + RCO3. = RCO3. + HO2.
(Same k as for RO2.))				RO2-NP. + NO = NPHE
(Same k as for RO2.))				RO2-NP. + HO2. = -OOH + 6 -C
(Same k as for RO2.))				RO2-NP. + RO2. = RO2. + 0.5 HO2. + 6 -C
(Same k as for RO2.))				RO2-NP. + RCO3. = RCO3. + HO2. + 6 -C
<u>Excited Criegee Biradicals</u>					
(fast)					(HCHO2) = 0.7 HCOOH + 0.12 "HO. + HO2. + CO" + 0.18 "H2 + CO2"
(fast)					(CCHO2) = 0.25 CCOOH + 0.15 "CH4 + CO2" + 0.6 HO. + 0.3 "CCO-O2. + RCO3." + 0.3 "RO2-R. + HCHO + CO + RO2."
(fast)					(RCHO2) = 0.25 CCOOH + 0.15 CO2 + 0.6 HO. + 0.3 "C2CO-O2. + RCO3." + 0.3 "RO2-R. + CCHO + CO + RO2." + 0.55 -C
(fast)					(C(C)CO2) = HO. + R2O2. + HCHO + CCO-O2. + RCO3. + RO2.
(fast)					(C(R)CO2) = HO. + CCO-O2. + CCHO + R2O2. + RCO3. + RO2.
(fast)					(CYCCO2) = 0.3 "HO. + C2CO-O2. + R2O2. + RCO3. + RO2." + 0.3 RCHO + 4.2 -C
(fast)					(BZCHO2) = 0.5 "BZ-O. + R2O2. + CO + HO."
(fast)					(C:CC(C)O2) = HO. + R2O2. + HCHO + C2CO-O2. + RO2. + RCO3.
(fast)					(C:C(C)CHO2) = 0.75 RCHO + 0.25 ISOPROD + 0.5 -C
(fast)					(C2(O2)CHO) = HO. + R2O2. + HCHO + HCOCO-O2. + RO2. + RCO3.
(fast)					(HOCCHO2) = 0.6 HO. + 0.3 "CCO-O2. + RCO3." + 0.3 "RO2-R. + HCHO + CO + RO2." + 0.8 -C
(fast)					(HCOCHO2) = 0.12 "HO2. + 2 CO + HO." + 0.74 -C + 0.51 "CO2 + HCHO"
(fast)					(C2(O2)COH) = HO. + MGLY + HO2. + R2O2. + RO2.
<u>Organic Product Species</u>					
(Phot. Set = CO2H)					-OOH + HV = HO2. + HO.
1.81E-12	1.18E-12	-0.25	0.00		HO. + -OOH = HO.
3.71E-12	1.79E-12	-0.44	0.00		HO. + -OOH = RO2-R. + RO2.
(Phot. Set = HCHONEWR)					HCHO + HV = 2 HO2. + CO
(Phot. Set = HCHONEWM)					HCHO + HV = H2 + CO
9.76E-12	1.13E-12	-1.29	2.00		HCHO + HO. = HO2. + CO + H2O
7.79E-14	9.70E-15	-1.24	0.00		HCHO + HO2. = HOCOO.
1.77E+02	2.40E+12	13.91	0.00		HOCOO. = HO2. + HCHO
(Same k as for RO2.))				HOCOO. + NO = -C + NO2 + HO2.
6.38E-16	2.80E-12	5.00	0.00		HCHO + NO3 = HNO3 + HO2. + CO
1.57E-11	5.55E-12	-0.62	0.00		CCHO + HO. = CCO-O2. + H2O + RCO3.
(Phot. Set = CCHOR)					CCHO + HV = CO + HO2. + HCHO + RO2-R. + RO2.
2.84E-15	1.40E-12	3.70	0.00		CCHO + NO3 = HNO3 + CCO-O2. + RCO3.
1.97E-11	8.50E-12	-0.50	0.00		RCHO + HO. = C2CO-O2. + RCO3.
(Phot. Set = RCHO)					RCHO + HV = CCHO + RO2-R. + RO2. + CO + HO2.
2.84E-15	1.40E-12	3.70	0.00		NO3 + RCHO = HNO3 + C2CO-O2. + RCO3.
2.23E-13	4.81E-13	0.46	2.00		ACET + HO. = R2O2. + HCHO + CCO-O2. + RCO3. + RO2.
(Phot. Set = ACET-93C)					ACET + HV = CCO-O2. + HCHO + RO2-R. + RCO3. + RO2.
1.16E-12	2.92E-13	-0.82	2.00		MEK + HO. = H2O + 0.5 "CCHO + HCHO + CCO-O2. + C2CO-O2." + RCO3. + 1.5 "R2O2. + RO2."
(Phot. Set = KETONE)					MEK + HV = CCO-O2. + CCHO + RO2-R. + RCO3. + RO2.
(Overall q.y = 0.1)					
2.07E-12	2.19E-11	1.41	0.00		RNO3 + HO. = NO2 + 0.155 MEK + 1.05 RCHO + 0.48 CCHO + 0.16 HCHO + 0.11 -C + 1.39 "R2O2. + RO2."

Table A-2 (continued)

Kinetic Parameters [b]				Notes [d]	Reactions [c]
k(300)	A	Ea	B		
1.14E-11	(Phot. Set = GLYOXAL1) (Phot. Set = GLYOXAL2) (Overall q.y = 0.029) (No T Dependence) (Same k as for CCHO)				GLY + HV = 0.8 HO2. + 0.45 HCHO + 1.55 CO GLY + HV = 0.13 HCHO + 1.87 CO GLY + HO. = 0.6 HO2. + 1.2 CO + 0.4 "HCOCO-O2. + RCO3." GLY + NO3 = HNO3 + 0.6 HO2. + 1.2 CO + 0.4 "HCOCO-O2. + RCO3."
1.72E-11	(Phot. Set = MEGLYOX1) (Phot. Set = MEGLYOX2) (No T Dependence) (Same k as for CCHO)				MGLY + HV = HO2. + CO + CCO-O2. + RCO3. MGLY + HV + 0.107 = HO2. + CO + CCO-O2. + RCO3. MGLY + HO. = CO + CCO-O2. + RCO3. MGLY + NO3 = HNO3 + CO + CCO-O2. + RCO3.
1.14E-11	(No T Dependence) (Phot. Set = ACROLEIN) (Overall q.y = 0.029)				HO. + AFG1 = HCOCO-O2. + RCO3. AFG1 + HV = HO2. + HCOCO-O2. + RCO3.
1.72E-11	(No T Dependence) (Phot. Set = ACROLEIN)				HO. + AFG2 = C2CO-O2. + RCO3. AFG2 + HV = HO2. + CO + CCO-O2. + RCO3.
2.63E-11	(No T Dependence)				HO. + PHEN = 0.15 RO2-NP. + 0.85 RO2-R. + 0.2 GLY + 4.7 -C + RO2.
3.60E-12	(No T Dependence)				NO3 + PHEN = HNO3 + BZ-O.
4.20E-11	(No T Dependence)				HO. + CRES = 0.15 RO2-NP. + 0.85 RO2-R. + 0.2 MGLY + 5.5 -C + RO2.
2.10E-11	(No T Dependence)				NO3 + CRES = HNO3 + BZ-O. + -C
1.29E-11	(No T Dependence) (Phot. Set = BZCHO) (Overall q.y = 0.05)				BALD + HO. = BZ-CO-O2. + RCO3. BALD + HV = 7 -C
2.61E-15	1.40E-12 3.75 0.00				BALD + NO3 = HNO3 + BZ-CO-O2.
3.60E-12	(No T Dependence) (Same k as for BZ-O.) (Same k as for RO2.) (Same k as for BZ-O.)				NPHE + NO3 = HNO3 + BZ(NO2)-O. BZ(NO2)-O. + NO2 = 2 -N + 6 -C BZ(NO2)-O. + HO2. = NPHE BZ(NO2)-O. = NPHE
6.50E-04	(Same k as for RCO3.) (Same k as for RCO3.) (Falloff Kinetics) k0 = 4.90E-03 23.97 0.00 kINF = 4.00E+16 27.08 0.00 F = 0.30 n = 1.00				CCO-O2. + NO = CO2 + NO2 + HCHO + RO2-R. + RO2. CCO-O2. + NO2 = PAN CCO-O2. + HO2. = -OOH + CO2 + HCHO CCO-O2. + RO2. = RO2. + 0.5 HO2. + CO2 + HCHO CCO-O2. + RCO3. = RCO3. + HO2. + CO2 + HCHO PAN = CCO-O2. + NO2 + RCO3.
8.40E-12	(Same k as for RCO3.) (No T Dependence) (Same k as for RCO3.) (Same k as for RCO3.) (Same k as for RCO3.)				C2CO-O2. + NO = CCHO + RO2-R. + CO2 + NO2 + RO2. C2CO-O2. + NO2 = PPN C2CO-O2. + HO2. = -OOH + CCHO + CO2 C2CO-O2. + RO2. = RO2. + 0.5 HO2. + CCHO + CO2 C2CO-O2. + RCO3. = RCO3. + HO2. + CCHO + CO2 PPN = C2CO-O2. + NO2 + RCO3.
6.78E-04	1.60E+17 27.97 0.00 (Same k as for RCO3.) (Same k as for PAN)				HCOCO-O2. + NO = NO2 + CO2 + CO + HO2. HCOCO-O2. + NO2 = GPAN HCOCO-O2. + HO2. = -OOH + CO2 + CO HCOCO-O2. + RO2. = RO2. + 0.5 HO2. + CO2 + CO HCOCO-O2. + RCO3. = RCO3. + HO2. + CO2 + CO GPAN = HCOCO-O2. + NO2 + RCO3.
3.53E-11	(Same k as for RCO3.) 1.30E-11 -0.60 0.00 (Same k as for RO2.)				BZ-CO-O2. + NO = BZ-O. + CO2 + NO2 + R2O2. + RO2. BZ-O. + NO2 = NPHE BZ-O. + HO2. = PHEN BZ-O. = PHEN
1.00E-03	(No T Dependence)				BZ-CO-O2. + NO2 = PBZN
8.40E-12	(No T Dependence) (Same k as for RCO3.) (Same k as for RCO3.) (Same k as for RCO3.)				BZ-CO-O2. + HO2. = -OOH + CO2 + PHEN BZ-CO-O2. + RO2. = RO2. + 0.5 HO2. + CO2 + PHEN BZ-CO-O2. + RCO3. = RCO3. + HO2. + CO2 + PHEN PBZN = BZ-CO-O2. + NO2 + RCO3.
2.17E-04	1.60E+15 25.90 0.00				
3.36E-11	(No T Dependence)				ISOPROD + HO. = 0.293 CO + 0.252 CCHO + 0.126 HCHO + 0.041 GLY + 0.021 RCHO + 0.168 MGLY + 0.314 MEK + 0.503 RO2-R. + 0.21 CCO-O2. + 0.288 C2CO-O2. + 0.21 R2O2. + 0.713 RO2. + 0.498 RCO3. + -0.112 -C
7.11E-18	(No T Dependence)				ISOPROD + O3 = 0.02 CCHO + 0.04 HCHO + 0.01 GLY + 0.84 MGLY + 0.09 MEK + 0.66 (HCHO2) + 0.09 (HCOCHO2) + 0.18 (HOCCHO2) + 0.06 (C2(O2)CHO) + 0.01 (C2(O2)COH) + -0.39 -C
	(Phot. Set = ACROLEIN)				ISOPROD + HV + 0.0036 = 0.333 CO + 0.067 CCHO + 0.9 HCHO +

Table A-2 (continued)

Kinetic Parameters [b]				Notes [d]	Reactions [c]
k(300)	A	Ea	B		
1.00E-15	(No T Dependence)				0.033 MEK + 0.333 HO2. + 0.7 RO2-R. + 0.267 CCO-O2. + 0.7 C2CO-O2. + 0.7 RO2. + 0.967 RCO3. + -0.133 -C ISOPROD + NO3 = 0.643 CO + 0.282 HCHO + 0.85 RNO3 + 0.357 RCHO + 0.925 HO2. + 0.075 C2CO-O2. + 0.075 R2O2. + 0.925 RO2. + 0.075 RCO3. + 0.075 HNO3 + -2.471 -C
<u>Hydrocarbon Species Represented Explicitly</u>					
2.56E-12	1.36E-12	-0.38	2.00		N-C4 + HO. = 0.076 RO2-N. + 0.924 RO2-R. + 0.397 R2O2. + 0.001 HCHO + 0.571 CCHO + 0.14 RCHO + 0.533 MEK + -0.076 -C + 1.397 RO2.
5.63E-12	1.35E-11	0.52	0.00		N-C6 + HO. = 0.185 RO2-N. + 0.815 RO2-R. + 0.738 R2O2. + 0.02 CCHO + 0.105 RCHO + 1.134 MEK + 0.186 -C + 1.738 RO2.
8.76E-12	3.15E-11	0.76	0.00		N-C8 + HO. = 0.333 RO2-N. + 0.667 RO2-R. + 0.706 R2O2. + 0.002 RCHO + 1.333 MEK + 0.998 -C + 1.706 RO2.
8.43E-12	1.96E-12	-0.87	0.00		ETHENE + HO. = RO2-R. + RO2. + 1.56 HCHO + 0.22 CCHO
1.68E-18	9.14E-15	5.13	0.00		ETHENE + O3 = HCHO + (HCHO2)
2.18E-16	4.39E-13	4.53	2.00		ETHENE + NO3 = R2O2. + RO2. + 2 HCHO + NO2
7.42E-13	1.04E-11	1.57	0.00		ETHENE + O = RO2-R. + HO2. + RO2. + HCHO + CO
2.60E-11	4.85E-12	-1.00	0.00		PROPENE + HO. = RO2-R. + RO2. + HCHO + CCHO
1.05E-17	5.51E-15	3.73	0.00		PROPENE + O3 = 0.6 HCHO + 0.4 CCHO + 0.4 (HCHO2) + 0.6 (CCHO2)
9.74E-15	4.59E-13	2.30	0.00		PROPENE + NO3 = R2O2. + RO2. + HCHO + CCHO + NO2
4.01E-12	1.18E-11	0.64	0.00		PROPENE + O = 0.4 HO2. + 0.5 RCHO + 0.5 MEK + -0.5 -C
6.30E-11	1.01E-11	-1.09	0.00		T-2-BUTE + HO. = RO2-R. + RO2. + 2 CCHO
1.95E-16	6.64E-15	2.10	0.00		T-2-BUTE + O3 = CCHO + (CCHO2)
3.92E-13	1.10E-13	-0.76	2.00		T-2-BUTE + NO3 = R2O2. + RO2. + 2 CCHO + NO2
2.34E-11	2.26E-11	-0.02	0.00		T-2-BUTE + O = 0.4 HO2. + 0.5 RCHO + 0.5 MEK + 0.5 -C
9.88E-11	2.54E-11	-0.81	0.00		ISOP + HO. = 0.088 RO2-N. + 0.912 RO2-R. + 0.629 HCHO + 0.912 ISOPROD + 0.079 R2O2. + 1.079 RO2. + 0.283 -C
1.34E-17	7.86E-15	3.80	0.00		ISOP + O3 = 0.4 HCHO + 0.6 ISOPROD + 0.55 (HCHO2) + 0.2 (C:CC(C)O2) + 0.2 (C:C(C)CHO2) + 0.05 -C
3.60E-11	(No T Dependence)				ISOP + O = 0.75 "ISOPROD + -C" + 0.25 "C2CO-O2. + RCO3. + 2 HCHO + RO2-R. + RO2."
6.81E-13	3.03E-12	0.89	0.00		ISOP + NO3 = 0.8 "RCHO + RNO3 + RO2-R." + 0.2 "ISOPROD + R2O2. + NO2" + RO2. + -2.2 -C
1.50E-19	(No T Dependence)				ISOP + NO2 = 0.8 "RCHO + RNO3 + RO2-R." + 0.2 "ISOPROD + R2O2. + NO" + RO2. + -2.2 -C
5.31E-11	1.21E-11	-0.88	0.00		APIN + HO. = RO2-R. + RCHO + RO2. + 7 -C
1.00E-16	9.90E-16	1.37	0.00		APIN + O3 = 0.05 HCHO + 0.2 CCHO + 0.5 RCHO + 0.61 MEK + 0.075 CO + 0.05 CCO-O2. + 0.05 C2CO-O2. + 0.1 RCO3. + 0.105 HO2. + 0.16 HO. + 0.135 RO2-R. + 0.15 R2O2. + 0.285 RO2. + 5.285 -C
6.10E-12	1.19E-12	-0.97	0.00		APIN + NO3 = NO2 + R2O2. + RCHO + RO2. + 7 -C
3.00E-11	(No T Dependence)				APIN + O = 0.4 HO2. + 0.5 MEK + 0.5 RCHO + 6.5 -C
6.57E-11	(No T Dependence)				UNKN + HO. = RO2-R. + RO2. + 0.5 HCHO + RCHO + 6.5 -C
5.85E-17	(No T Dependence)				UNKN + O3 = 0.135 RO2-R. + 0.135 HO2. + 0.075 R2O2. + 0.21 RO2. + 0.025 CCO-O2. + 0.025 C2CO-O2. + 0.05 RCO3. + 0.275 HCHO + 0.175 CCHO + 0.5 RCHO + 0.41 MEK + 0.185 CO + 5.925 -C + 0.11 HO.
4.30E-12	(No T Dependence)				UNKN + NO3 = R2O2. + RO2. + 0.5 HCHO + RCHO + 6.5 -C + NO2
2.90E-11	(No T Dependence)				UNKN + O = 0.4 HO2. + 0.5 RCHO + 0.5 MEK + 6.5 -C
5.91E-12	1.81E-12	-0.70	0.00		TOLUENE + HO. = 0.085 BALD + 0.26 CRES + 0.118 GLY + 0.847 MGLY + 0.276 AFG2 + 0.74 RO2-R. + 0.26 HO2. + 0.981 -C + 0.74 RO2.
2.36E-11	(No T Dependence)				M-XYLENE + HO. = 0.04 BALD + 0.18 CRES + 0.108 GLY + 1.554 MGLY + 0.505 AFG2 + 0.82 RO2-R. + 0.18 HO2. + 0.068 -C + 0.82 RO2.
<u>Lumped Species used in EKMA Simulations [d]</u>					
3.46E-12	2.56E-12	-0.18	0.00		ALK1 + HO. = 0.911 RO2-R. + 0.074 RO2-N. + 0.005 RO2-XN. + 0.011 HO2. + 0.575 R2O2. + 1.564 RO2. + 0.065 HCHO + 0.339 CCHO + 0.196 RCHO + 0.322 ACET + 0.448 MEK + 0.024 CO + 0.025 GLY + 0.051 -C
9.14E-12	5.12E-12	-0.35	0.00		ALK2 + HO. = 0.749 RO2-R. + 0.249 RO2-N. + 0.002 RO2-XN. +

Table A-2 (continued)

Kinetic Parameters [b]				Notes [d]	Reactions [c]
k(300)	A	Ea	B		
					0.891 R2O2. + 1.891 RO2. + 0.029 HCHO + 0.048 CCHO + 0.288 RCHO + 0.028 ACET + 1.105 MEK + 0.043 CO + 0.018 CO2 + 1.268 -C
5.87E-12	(No T Dependence)				ARO1 + HO. = 0.742 RO2-R. + 0.258 HO2. + 0.742 RO2. + 0.015 PHEN + 0.244 CRES + 0.08 BALD + 0.124 GLY + 0.681 MGLY + 0.11 AFG1 + 0.244 AFG2 + 1.857 -C
3.22E-11	1.20E-11	-0.59	0.00		ARO2 + HO. = 0.82 RO2-R. + 0.18 HO2. + 0.82 RO2. + 0.18 CRES + 0.036 BALD + 0.068 GLY + 1.02 MGLY + 0.532 AFG2 + 2.588 -C
3.17E-11	2.22E-12	-1.59	0.00		OLE2 + HO. = 0.858 RO2-R. + 0.142 RO2-N. + RO2. + 0.858 HCHO + 0.252 CCHO + 0.606 RCHO + 1.267 -C
1.08E-17	1.42E-15	2.91	0.00		OLE2 + O3 = 0.6 HCHO + 0.635 RCHO + 0.981 -C + 0.4 (HCHO2) + 0.529 (CCHO2) + 0.071 (RCHO2)
1.16E-14	1.99E-13	1.69	0.00		OLE2 + NO3 = R2O2. + RO2. + HCHO + 0.294 CCHO + 0.706 RCHO + 1.451 -C + NO2
4.11E-12	4.51E-12	0.06	0.00		OLE2 + O = 0.4 HO2. + 0.5 RCHO + 0.5 MEK + 1.657 -C
6.23E-11	4.54E-12	-1.56	0.00		OLE3 + HO. = 0.861 RO2-R. + 0.139 RO2-N. + RO2. + 0.24 HCHO + 0.661 CCHO + 0.506 RCHO + 0.113 ACET + 0.086 MEK + 0.057 BALD + 0.848 -C
1.70E-16	1.77E-15	1.40	0.00		OLE3 + O3 = 0.203 HCHO + 0.358 CCHO + 0.309 RCHO + 0.061 MEK + 0.027 BALD + 0.976 -C + 0.076 (HCHO2) + 0.409 (CCHO2) + 0.279 (RCHO2) + 0.158 (C(C)CO2 + 0.039 (C(R)CO2 + 0.04 (BZCHO2)
1.07E-12	3.19E-13	-0.72	0.00		OLE3 + NO3 = R2O2. + RO2. + 0.278 HCHO + 0.767 CCHO + 0.588 RCHO + 0.131 ACET + 0.1 MEK + 0.066 BALD + 0.871 -C + NO2
2.52E-11	8.66E-12	-0.64	0.00		OLE3 + O = 0.4 HO2. + 0.5 RCHO + 0.5 MEK + 2.205 -C
<u>TCE Reactions [e]</u>					
2.34E-12	5.63E-13	-0.85	0.00	1,2	HO. + CL3-ETHE = 0.4 {CL2CO + CO + HCL + RO2-R.} + 0.6 {RO2-CL. + HCO-CO-CL + HCL} + RO2.
8.08E-11	(No T Dependence)			2,3	CL. + CL3-ETHE = RO2-CL. + CL2CH-CO-CL
2.81E-16	(No T Dependence)			4,5	NO3 + CL3-ETHE = RO2-CL. + CL2CH-CO-CL + RO2. + -N
1.00E-21	(No T Dependence)			6	O3 + CL3-ETHE = 0.5 {CL2CO + CLCHO + HO2.} + CO2 + 1.5 CL.
5.75E-21					
6.40E-12	(No T Dependence)			2,7	CL2CH-CO-CL + CL. = HCL + CL-CO-CO-CL + RO2-CL. + RO2.
0.0					
5.70E-12	(No T Dependence)			8	HCO-CO-CL + HO. = H2O + 2 CO + CL.
3.66E-11	4.10E-11	0.07	0.00	9	HCO-CO-CL + CL. = HCL + 2 CO + CL.
	(Phot. Set = GLYOXAL)			10	HCO-CO-CL + HV = 2 CO + CL. + HO2.
	(Overall q.y. = 0.074)				
	(Overall q.y. = 0.057)				
	(Same k as for HCO-CO-CL)			11	CL-CO-CO-CL + HV = 2 {CO + CL.}
	(Same k as for RO2.)			12	RO2-CL. + NO = NO2 + CL.
	(Same k as for RO2.)				RO2-CL. + HO2. = -OOH
	(Same k as for RO2.)				RO2-CL. + RO2. = RO2. + 0.5 CL.
	(Same k as for RO2.)				RO2-CL. + RCO3. = RCO3. + 0.5 CL.
<u>Other ClOx Reactions [f]</u>					
	(Phot. Set = CL2)				CL2 + HV = 2 CL.
	(Phot. Set = CLNO)				CLNO + HV = CL. + NO
9.05E-32	(No T Dependence)			13	CL. + NO + M = CLNO + M
1.60E-11	(Falloff Kinetics)			13	CL. + NO2 = CLONO
k0 =	1.30E-30	0.00	-2.00		
kINF =	1.00E-10	0.00	-1.00		
	F = 0.6				
3.52E-12	(Falloff Kinetics)			13	CL. + NO2 = CLONO2
k0 =	1.80E-31	0.00	-2.00		
kINF =	1.00E-10	0.00	-1.00		
	F = 0.6				
	(Phot. Set = CLONO)				CLONO + HV = CL. + NO2
	(Phot. Set = CLNO2)				CLNO2 + HV = CL. + NO2
3.17E-11	1.80E-11	-0.34	0.00		CL. + HO2. = HCL + O2
9.15E-12	4.10E-11	0.89	0.00		CL. + HO2. = CLO. + HO.
1.22E-11	2.90E-11	0.52	0.00		CL. + O3 = CLO. + O2
2.40E-11	(No T Dependence)				CL. + NO3 = CLO. + NO2
1.65E-11	6.20E-12	-0.58	0.00		CLO. + NO = CL. + NO2
2.06E-12	(Falloff Kinetics)				CLO. + NO2 = CLONO2
k0 =	1.60E-31	0.00	-3.40		

Table A-2 (continued)

Kinetic Parameters [b]				Notes [d]	Reactions [c]
k(300)	A	Ea	B		
kINF =	2.00E-11	0.00	0.00		
	F= 0.5				
k = kEQ x k(CLO.+NO2), kEQ =	4.02E+08	5.20E+25	23.49	3.40	14
(Phot. Set = CLONO2)					CLONO2 = CLO. + NO2
1.16E-11	6.80E-12	-0.32	0.00		CLONO2 + HV = 0.9 {CL. + NO3} + 0.1 {O + CLONO}
4.90E-12	4.60E-13	-1.41	0.00		CL. + CLONO2 = CL2 + NO3
(Phot. Set = HOCL)					CLO. + HO2. = HOCL + O2
(neglected)				15	HOCL + HV = HO. + CL. CLO. + CLO. = products
<u>Cl + VOC and Cl + VOC Product Reactions Added to Mechanism</u>					
1.07E-13	9.60E-12	2.68	0.00		CL. + CH4 = HCL + HCHO + RO2-R. + RO2.
5.90E-11	8.10E-11	0.19	0.00		CL. + ETHANE = HCL + CCHO + RO2-R. + RO2.
1.94E-10	(No T Dependence)			16	CL. + N-C4 = HCL + 0.076 RO2-N. + 0.924 RO2-R. + 0.397 R2O2. + 0.001 HCHO + 0.571 CCHO + 0.14 RCHO + 0.533 MEK + -0.076 -C + 1.397 RO2.
2.99E-10	(No T Dependence)			16	CL. + N-C6 = HCL + 0.185 RO2-N. + 0.815 RO2-R. + 0.738 R2O2. + 0.02 CCHO + 0.105 RCHO + 1.134 MEK + 0.186 -C + 1.738 RO2.
4.05E-10	(No T Dependence)			16	CL. + N-C8 = HCL + 0.333 RO2-N. + 0.667 RO2-R. + 0.706 R2O2. + 0.002 RCHO + 1.333 MEK + 0.998 -C + 1.706 RO2.
5.82E-11	(No T Dependence)			17,18	CL. + TOLUENE = HCL + RO2-R. + BALD + RO2.
1.20E-10	(No T Dependence)			18,19	CL. + M-XYLENE = HCL + RO2-R. + BALD + RO2. + -C
1.03E-10	(Falloff Kinetics)				CL. + ETHENE = RO2-R. + RO2. + HCHO + HCLCO
k0 =	1.60E-29	0.00	-3.50		
kINF =	3.00E-10	0.00	0.00		
	F= 0.6				
2.41E-10	(No T Dependence)			17	CL. + PROPENE = RO2-R. + RO2. + 0.5 {HCLCO + HCHO + CLCCHO + CCHO}
2.70E-10	(No T Dependence)			20	CL. + T-2-BUTE = RO2-R. + RO2. + CCHO + CLCCHO
7.32E-11	8.20E-11	0.07	0.00		CL. + HCHO = HCL + HO2. + CO
7.20E-11	(No T Dependence)				CL. + CCHO = HCL + CCO-O2. + RCO3.
1.20E-10	(No T Dependence)				CL. + RCHO = HCL + C2CO-O2. + RCO3.
3.50E-12	(No T Dependence)				CL. + ACET = HCL + R2O2. + HCHO + CCO-O2. + RCO3.+RO2.
1.00E-10	(No T Dependence)			21	CL. + MEK = HCL + 0.5 {CCHO + HCHO + CCO-O2. + C2CO-O2.} + RCO3. + 1.5 {R2O2. + RO2.}
1.00E-10	(No T Dependence)			21	CL. + RNO3 = HCL + NO2 + 0.155 MEK + 1.05 RCHO + 0.48 CCHO + 0.16 HCHO + 0.11 -C + 1.39 {R2O2. + RO2.}
1.00E-10	(No T Dependence)			21	CL. + GLY = HCL + 0.6 HO2. + 1.2 CO + 0.4 {HCOCO-O2. + RCO3.}
1.00E-10	(No T Dependence)			21	CL. + MGLY = HCL + CO + CCO-O2. + RCO3.
1.00E-10	(No T Dependence)			21	CL. + PHEN = HCL + 0.15 RO2-NP. + 0.85 RO2-R. + 0.2 GLY + 4.7 -C + RO2.
1.00E-10	(No T Dependence)			21	CL. + CRES = HCL + 0.15 RO2-NP. + 0.85 RO2-R. + 0.2 MGLY + 5.5 -C + RO2.
1.00E-10	(No T Dependence)			21	CL. + BALD = HCL + BZ-CO-O2. + RCO3.
1.00E-10	(No T Dependence)			21	CL. + AFG2 = HCL + C2CO-O2. + RCO3.
2.00E-10	(No T Dependence)			22	CL. + ALK1 = 0.911 RO2-R. + 0.074 RO2-N. + 0.005 RO2-XN. + 0.011 HO2. + 0.575 R2O2. + 1.564 RO2. + 0.065 HCHO + 0.339 CCHO + 0.196 RCHO + 0.322 ACET + 0.448 MEK + 0.024 CO + 0.025 GLY + 0.051 -C + HCL
4.00E-10	(No T Dependence)			22	CL. + ALK2 = 0.749 RO2-R. + 0.249 RO2-N. + 0.002 RO2-XN. + 0.891 R2O2. + 1.891 RO2. + 0.029 HCHO + 0.048 CCHO + 0.288 RCHO + 0.028 ACET + 1.105 MEK + 0.043 CO + 0.018 CO2 + 1.268 -C + HCL
6.00E-12	(No T Dependence)			22	CL. + ARO1 = HCL + RO2-R. + BALD + RO2.
1.20E-10	(No T Dependence)			22	CL. + ARO2 = HCL + RO2-R. + BALD + RO2.
2.41E-10	(No T Dependence)			22	CL. + OLE2 = 0.4 HO2. + 0.5 RCHO + 0.5 MEK + 1.657 -C + HCL
2.70E-10	(No T Dependence)			22	CL. + OLE3 = 0.4 HO2. + 0.5 RCHO + 0.5 MEK + 2.205 -C + HCL
<u>Reactions used to Represent Chamber-Dependent Processes [g]</u>					
(Parameter = O3W)					O3 =
(Parameter = N25I)					N2O5 = 2 NOX-WALL
(Parameter = N25S)					N2O5 + H2O = 2 NOX-WALL
(Parameter = NO2W)					NO2 = (yHONO) HONO + (1-yHONO) NOX-WALL
(Parameter = XSHC)					HO. = HO2.
(Phot. Set = NO2) x RS/K1					HV = HO.
(Phot. Set = NO2) x E-NO2/K1					HV = NO2 + -1 NOX-WALL

[a] Except as noted, expression for rate constant is $k = A e^{E_a/RT} (T/300)^B$. Rate constants and A factor are in cm, molecule, sec. units, and Ea values are in kcal mole⁻¹. "Phot Set" means this is a photolysis reaction, with the absorption coefficients and quantum yields given in Table A-3. If "(overall qy)" is given on the

Table A-2 (concluded)

- following line, then the photolysis data given in Table A-3 are only for the absorption cross sections, and the quantum yield given is assumed for all wavelengths. In addition, if "#(number)" or "#(parameter)" is given as a reactant, then the value of that number or parameter is multiplied by the result in the "rate constant expression" columns to obtain the rate constant used.
- [b] The Format of reaction listing same as used in documentation of the detailed mechanism (Carter 1990). Brackets ("{...}") around a set of reactants mean that they all have the same product yield coefficient. If a coefficient is given within the brackets, the coefficient for the product is the product of the coefficient x the coefficient outside the brackets.
- [c] Documentation notes for ClO_x or TCE reactions are as follows. For all other reactions, the rate constants and mechanisms are from the updated version of the Carter (1990) mechanism as described in the text.
1. Rate constant recommended by Atkinson (1994)
 2. See text for discussion of the mechanism.
 3. Rate constant of Atkinson and Aschmann (1987)
 4. Rate constant of Atkinson et al (1987)
 5. Radicals and products formed assumed to react with similar mechanism as those formed in the Cl + TCE reaction (see text). "-N" refers to the nitrogen lost in this representation, and is used to account for nitrogen balance.
 6. Model "A": Upper limit rate constant is $3 \times 10^{-20} \text{ cm}^3 \text{ molec}^{-1} \text{ s}^{-1}$ (Atkinson et al, 1982). Rate constant shown is essentially a guess. Model "B": Adjusted to fit environmental chamber experiments as discussed in the text and footnote [e], below.
 7. Rate constant is adjusted based on model simulations of selected experiments as discussed in the text and footnote [e], below. Model "A": adjusted value obtained assuming that the O₃ + TCE rate constant is $1.0 \times 10^{-22} \text{ cm}^3 \text{ molec}^{-1} \text{ s}^{-1}$. Model "B": if the O₃ + TCE is adjusted to fit the data, optimizations indicate that this rate constant is sufficiently low that this reaction can be neglected.
 8. Rate constant is estimated to be half that for OH + glyoxal.
 9. Rate constant is estimated to be half that for Cl + formaldehyde. (No rate constant available for Cl + glyoxal.)
 10. Assumed to have similar absorption cross sections to glyoxal. The overall quantum yield is adjusted based on model simulations of selected experiments as discussed in the text. The relatively low value is expected based on the low overall glyoxal quantum yield of 0.03 used in the standard mechanism. Adjusted values for Models "A" and "B" are slightly different, as shown.
 11. Assumed to photodecompose with the same rate as HCO-CO-Cl.
 12. "RO2-Cl." a chemical operator used to represent the effect of reactions of peroxy radicals which react to form alkoxy radicals which decompose to form Cl atoms. It is analogous to the "RO2-R." operator discussed by Carter (1990) except that it ultimately forms Cl atoms rather than HO₂ radicals.
 13. Rate constant from NASA evaluation (NASA, 1994).
 14. The kinetic parameters are for the equilibrium constant, which was derived from the low pressure chlorine nitrate decomposition rate constant of Schonle et al. (1979), combined with the low pressure rate constant for the reverse reaction.
 15. This reaction is neglected because it is of negligible importance compared with the ClO + NO_x and HO₂ reactions under the conditions of the simulations discussed here.
 16. Rate constants given by Aschmann and Atkinson (1995).
 17. Relative rate constant from Atkinson and Aschmann (1985); placed on an absolute basis using the Cl + n-butane rate constant used by Aschmann and Atkinson (1995) for deriving absolute Cl + alkane rate constants. The toluene rate constant is in good agreement with value of Wallington et al. (1988).
 18. Abstraction from the methyl group is expected to dominate over addition to the aromatic ring, so the representation of the products formed is modified accordingly.
 19. Rate constant from Wallington et al. (1988).
 20. Rate constant estimated from Cl + propene rate constant (Atkinson and Aschmann, 1985) and the estimation method derived for Cl + alkanes by Aschmann and Atkinson (1995).
 21. The rate constants for these organic product + chlorine reaction are unknown and are approximately estimated. They are not expected to be highly important in affecting the results of the simulations because much more of the Cl reacts with the alkanes which are present.
 22. Rate constants used are approximately those of the explicitly represented VOCs which are representative of this group (see Table A-1.) These are as follows: ALK1: n-butane; ALK2: n-octane; ARO1: toluene; ARO2: m-xylene; OLE1: propene; and OLE3: trans-2-butene.
- [d] Rate constants and product yield parameters based on the mixture of species in the base ROG mixture which are being represented.
- [e] As discussed in the text, two mechanisms, designated "A" and "B" were used. Rate constants or parameters which differ depending on the mechanism are indicated with a A or B in the first column. Parameters or rate constants which were adjusted were derived using a nonlinear optimization program to minimize the sum-of-squares differences between experimental and calculated d(O₃-NO) and TCE data in runs DTC-313(A), 314(A), 314(B), and 303(B). In the simulations of run DTC-313(A) background levels of 2 ppm methane, 3 ppb ethane and 2 ppb n-butane were assumed (see text).
- [f] Rate constants and absorption cross sections and quantum yields taken from the IUPAC (Atkinson et al, 1996) evaluation except where indicated otherwise.
- [g] See Table A-4 for the values of the parameters used for the specific chamber modeled in this study.

Table A-3. Absorption cross sections and quantum yields for photolysis reactions.

WL (nm)	Abs (cm ²)	QY	WL (nm)	Abs (cm ²)	QY	WL (nm)	Abs (cm ²)	QY	WL (nm)	Abs (cm ²)	QY	WL (nm)	Abs (cm ²)	QY
Photolysis File = NO2														
250.0	2.83E-20	1.000	255.0	1.45E-20	1.000	260.0	1.90E-20	1.000	265.0	2.05E-20	1.000	270.0	3.13E-20	1.000
275.0	4.02E-20	1.000	280.0	5.54E-20	1.000	285.0	6.99E-20	1.000	290.0	8.18E-20	0.999	295.0	9.67E-20	0.998
300.0	1.17E-19	0.997	305.0	1.66E-19	0.996	310.0	1.76E-19	0.995	315.0	2.25E-19	0.994	320.0	2.54E-19	0.993
325.0	2.79E-19	0.992	330.0	2.99E-19	0.991	335.0	3.45E-19	0.990	340.0	3.88E-19	0.989	345.0	4.07E-19	0.988
350.0	4.10E-19	0.987	355.0	5.13E-19	0.986	360.0	4.51E-19	0.984	365.0	5.78E-19	0.983	370.0	5.42E-19	0.981
375.0	5.35E-19	0.979	380.0	5.99E-19	0.975	381.0	5.98E-19	0.974	382.0	5.97E-19	0.973	383.0	5.96E-19	0.972
384.0	5.95E-19	0.971	385.0	5.94E-19	0.969	386.0	5.95E-19	0.967	387.0	5.96E-19	0.966	388.0	5.98E-19	0.964
389.0	5.99E-19	0.962	390.0	6.00E-19	0.960	391.0	5.98E-19	0.959	392.0	5.96E-19	0.957	393.0	5.93E-19	0.953
394.0	5.91E-19	0.950	395.0	5.89E-19	0.942	396.0	6.06E-19	0.922	397.0	6.24E-19	0.870	398.0	6.41E-19	0.820
399.0	6.59E-19	0.760	400.0	6.76E-19	0.695	401.0	6.67E-19	0.635	402.0	6.58E-19	0.560	403.0	6.50E-19	0.485
404.0	6.41E-19	0.425	405.0	6.32E-19	0.350	406.0	6.21E-19	0.290	407.0	6.10E-19	0.225	408.0	5.99E-19	0.185
409.0	5.88E-19	0.153	410.0	5.77E-19	0.130	411.0	5.88E-19	0.110	412.0	5.98E-19	0.094	413.0	6.09E-19	0.083
414.0	6.19E-19	0.070	415.0	6.30E-19	0.059	416.0	6.29E-19	0.048	417.0	6.27E-19	0.039	418.0	6.26E-19	0.030
419.0	6.24E-19	0.023	420.0	6.23E-19	0.018	421.0	6.18E-19	0.012	422.0	6.14E-19	0.008	423.0	6.09E-19	0.004
424.0	6.05E-19	0.000	425.0	6.00E-19	0.000									
Photolysis File = NO3NO														
585.0	2.77E-18	0.000	590.0	5.14E-18	0.250	595.0	4.08E-18	0.400	600.0	2.83E-18	0.250	605.0	3.45E-18	0.200
610.0	1.48E-18	0.200	615.0	1.96E-18	0.100	620.0	3.58E-18	0.100	625.0	9.25E-18	0.050	630.0	5.66E-18	0.050
635.0	1.45E-18	0.030	640.0	1.11E-18	0.000									
Photolysis File = NO3NO2														
400.0	0.00E+00	1.000	405.0	3.00E-20	1.000	410.0	4.00E-20	1.000	415.0	5.00E-20	1.000	420.0	8.00E-20	1.000
425.0	1.00E-19	1.000	430.0	1.30E-19	1.000	435.0	1.80E-19	1.000	440.0	1.90E-19	1.000	445.0	2.20E-19	1.000
450.0	2.80E-19	1.000	455.0	3.30E-19	1.000	460.0	3.70E-19	1.000	465.0	4.30E-19	1.000	470.0	5.10E-19	1.000
475.0	6.00E-19	1.000	480.0	6.40E-19	1.000	485.0	6.90E-19	1.000	490.0	8.80E-19	1.000	495.0	9.50E-19	1.000
500.0	1.01E-18	1.000	505.0	1.10E-18	1.000	510.0	1.32E-18	1.000	515.0	1.40E-18	1.000	520.0	1.45E-18	1.000
525.0	1.48E-18	1.000	530.0	1.94E-18	1.000	535.0	2.04E-18	1.000	540.0	1.81E-18	1.000	545.0	1.81E-18	1.000
550.0	2.36E-18	1.000	555.0	2.68E-18	1.000	560.0	3.07E-18	1.000	565.0	2.53E-18	1.000	570.0	2.54E-18	1.000
575.0	2.74E-18	1.000	580.0	3.05E-18	1.000	585.0	2.77E-18	1.000	590.0	5.14E-18	0.750	595.0	4.08E-18	0.600
600.0	2.83E-18	0.550	605.0	3.45E-18	0.400	610.0	1.45E-18	0.300	615.0	1.96E-18	0.250	620.0	3.58E-18	0.200
625.0	9.25E-18	0.150	630.0	5.66E-18	0.050	635.0	1.45E-18	0.000						
Photolysis File = O3O3P														
280.0	3.97E-18	0.100	281.0	3.60E-18	0.100	282.0	3.24E-18	0.100	283.0	3.01E-18	0.100	284.0	2.73E-18	0.100
285.0	2.44E-18	0.100	286.0	2.21E-18	0.100	287.0	2.01E-18	0.100	288.0	1.76E-18	0.100	289.0	1.58E-18	0.100
290.0	1.41E-18	0.100	291.0	1.26E-18	0.100	292.0	1.10E-18	0.100	293.0	9.89E-19	0.100	294.0	8.59E-19	0.100
295.0	7.70E-19	0.100	296.0	6.67E-19	0.100	297.0	5.84E-19	0.100	298.0	5.07E-19	0.100	299.0	4.52E-19	0.100
300.0	3.92E-19	0.100	301.0	3.42E-19	0.100	302.0	3.06E-19	0.100	303.0	2.60E-19	0.100	304.0	2.37E-19	0.100
305.0	2.01E-19	0.112	306.0	1.79E-19	0.149	307.0	1.56E-19	0.197	308.0	1.38E-19	0.259	309.0	1.25E-19	0.339
310.0	1.02E-19	0.437	311.0	9.17E-20	0.546	312.0	7.88E-20	0.652	313.0	6.77E-20	0.743	314.0	6.35E-20	0.816
315.0	5.10E-20	0.872	316.0	4.61E-20	0.916	317.0	4.17E-20	0.949	318.0	3.72E-20	0.976	319.0	2.69E-20	0.997
320.0	3.23E-20	1.000	330.0	6.70E-21	1.000	340.0	1.70E-21	1.000	350.0	4.00E-22	1.000	355.0	0.00E+00	1.000
400.0	0.00E+00	1.000	450.0	1.60E-22	1.000	500.0	1.34E-21	1.000	550.0	3.32E-21	1.000	600.0	5.06E-21	1.000
650.0	2.45E-21	1.000	700.0	8.70E-22	1.000	750.0	3.20E-22	1.000	800.0	1.60E-22	1.000	900.0	0.00E+00	1.000
Photolysis File = O3O1D														
280.0	3.97E-18	0.900	281.0	3.60E-18	0.900	282.0	3.24E-18	0.900	283.0	3.01E-18	0.900	284.0	2.73E-18	0.900
285.0	2.44E-18	0.900	286.0	2.21E-18	0.900	287.0	2.01E-18	0.900	288.0	1.76E-18	0.900	289.0	1.58E-18	0.900
290.0	1.41E-18	0.900	291.0	1.26E-18	0.900	292.0	1.10E-18	0.900	293.0	9.89E-19	0.900	294.0	8.59E-19	0.900
295.0	7.70E-19	0.900	296.0	6.67E-19	0.900	297.0	5.84E-19	0.900	298.0	5.07E-19	0.900	299.0	4.52E-19	0.900
300.0	3.92E-19	0.900	301.0	3.42E-19	0.900	302.0	3.06E-19	0.900	303.0	2.60E-19	0.900	304.0	2.37E-19	0.900
305.0	2.01E-19	0.888	306.0	1.79E-19	0.851	307.0	1.56E-19	0.803	308.0	1.38E-19	0.741	309.0	1.25E-19	0.661
310.0	1.02E-19	0.563	311.0	9.17E-20	0.454	312.0	7.88E-20	0.348	313.0	6.77E-20	0.257	314.0	6.35E-20	0.184
315.0	5.10E-20	0.128	316.0	4.61E-20	0.084	317.0	4.17E-20	0.051	318.0	3.72E-20	0.024	319.0	2.69E-20	0.003
320.0	3.23E-20	0.000												
Photolysis File = HONO														
311.0	0.00E+00	1.000	312.0	2.00E-21	1.000	313.0	4.20E-21	1.000	314.0	4.60E-21	1.000	315.0	4.20E-21	1.000
316.0	3.00E-21	1.000	317.0	4.60E-21	1.000	318.0	3.60E-20	1.000	319.0	6.10E-20	1.000	320.0	2.10E-20	1.000
321.0	4.27E-20	1.000	322.0	4.01E-20	1.000	323.0	3.93E-20	1.000	324.0	4.01E-20	1.000	325.0	4.04E-20	1.000
326.0	3.13E-20	1.000	327.0	4.12E-20	1.000	328.0	7.55E-20	1.000	329.0	6.64E-20	1.000	330.0	7.29E-20	1.000
331.0	8.70E-20	1.000	332.0	1.38E-19	1.000	333.0	5.91E-20	1.000	334.0	5.91E-20	1.000	335.0	6.45E-20	1.000
336.0	5.91E-20	1.000	337.0	4.58E-20	1.000	338.0	1.91E-19	1.000	339.0	1.63E-19	1.000	340.0	1.05E-19	1.000
341.0	8.70E-20	1.000	342.0	3.35E-19	1.000	343.0	2.01E-19	1.000	344.0	1.02E-19	1.000	345.0	8.54E-20	1.000
346.0	8.32E-20	1.000	347.0	8.20E-20	1.000	348.0	7.49E-20	1.000	349.0	7.13E-20	1.000	350.0	6.83E-20	1.000
351.0	1.74E-19	1.000	352.0	1.14E-19	1.000	353.0	3.71E-19	1.000	354.0	4.96E-19	1.000	355.0	2.46E-19	1.000
356.0	1.19E-19	1.000	357.0	9.35E-20	1.000	358.0	7.78E-20	1.000	359.0	7.29E-20	1.000	360.0	6.83E-20	1.000
361.0	6.90E-20	1.000	362.0	7.32E-20	1.000	363.0	9.00E-20	1.000	364.0	1.21E-19	1.000	365.0	1.33E-19	1.000
366.0	2.13E-19	1.000	367.0	3.52E-19	1.000	368.0	4.50E-19	1.000	369.0	2.93E-19	1.000	370.0	1.19E-19	1.000
371.0	9.46E-20	1.000	372.0	8.85E-20	1.000	373.0	7.44E-20	1.000	374.0	4.77E-20	1.000	375.0	2.70E-20	1.000
376.0	1.90E-20	1.000	377.0	1.50E-20	1.000	378.0	1.90E-20	1.000	379.0	5.80E-20	1.000	380.0	7.78E-20	1.000
381.0	1.14E-19	1.000	382.0	1.40E-19	1.000	383.0	1.72E-19	1.000	384.0	1.99E-19	1.000	385.0	1.90E-19	1.000
386.0	1.19E-19	1.000	387.0	5.65E-20	1.000	388.0	3.20E-20	1.000	389.0	1.90E-20	1.000	390.0	1.20E-20	1.000
391.0	5.00E-21	1.000	392.0	0.00E+00	1.000									
Photolysis File = H2O2														
250.0	8.30E-20	1.000	255.0	6.70E-20	1.000	260.0	5.20E-20	1.000	265.0	4.20E-20	1.000	270.0	3.20E-20	1.000
275.0	2.50E-20	1.000	280.0	2.00E-20	1.000	285.0	1.50E-20	1.000	290.0	1.13E-20	1.000	295.0	8.70E-21	1.000
300.0	6.60E-21	1.000	305.0	4.90E-21	1.000	310.0	3.70E-21	1.000	315.0	2.80E-21	1.000	320.0	2.00E-21	1.000
325.0	1.50E-21	1.000	330.0	1.20E-21	1.000	335.0	9.00E-22	1.000	340.0	7.00E-22	1.000	345.0	5.00E-22	1.000
350.0	3.00E-22	1.000	355.0	0.00E+00	1.000									

Table A-3. (continued)

WL (nm)	Abs (cm ²)	QY	WL (nm)	Abs (cm ²)	QY	WL (nm)	Abs (cm ²)	QY	WL (nm)	Abs (cm ²)	QY	WL (nm)	Abs (cm ²)	QY
Photolysis File = CO2H														
210.0	3.75E-19	1.000	220.0	2.20E-19	1.000	230.0	1.38E-19	1.000	240.0	8.80E-20	1.000	250.0	5.80E-20	1.000
260.0	3.80E-20	1.000	270.0	2.50E-20	1.000	280.0	1.50E-20	1.000	290.0	9.00E-21	1.000	300.0	5.80E-21	1.000
310.0	3.40E-21	1.000	320.0	1.90E-21	1.000	330.0	1.10E-21	1.000	340.0	6.00E-22	1.000	350.0	4.00E-22	1.000
360.0	0.00E+00	1.000												
Photolysis File = HCHONEWR														
280.0	2.49E-20	0.590	280.5	1.42E-20	0.596	281.0	1.51E-20	0.602	281.5	1.32E-20	0.608	282.0	9.73E-21	0.614
282.5	6.76E-21	0.620	283.0	5.82E-21	0.626	283.5	9.10E-21	0.632	284.0	3.71E-20	0.638	284.5	4.81E-20	0.644
285.0	3.95E-20	0.650	285.5	2.87E-20	0.656	286.0	2.24E-20	0.662	286.5	1.74E-20	0.668	287.0	1.13E-20	0.674
287.5	1.10E-20	0.680	288.0	2.62E-20	0.686	288.5	4.00E-20	0.692	289.0	3.55E-20	0.698	289.5	2.12E-20	0.704
290.0	1.07E-20	0.710	290.5	1.35E-20	0.713	291.0	1.99E-20	0.717	291.5	1.56E-20	0.721	292.0	8.65E-21	0.724
292.5	5.90E-21	0.727	293.0	1.11E-20	0.731	293.5	6.26E-20	0.735	294.0	7.40E-20	0.738	294.5	5.36E-20	0.741
295.0	4.17E-20	0.745	295.5	3.51E-20	0.749	296.0	2.70E-20	0.752	296.5	1.75E-20	0.755	297.0	1.16E-20	0.759
297.5	1.51E-20	0.763	298.0	3.69E-20	0.766	298.5	4.40E-20	0.769	299.0	3.44E-20	0.773	299.5	2.02E-20	0.776
300.0	1.06E-20	0.780	300.4	7.01E-21	0.780	300.6	8.63E-21	0.779	300.8	1.47E-20	0.779	301.0	2.01E-20	0.779
301.2	2.17E-20	0.779	301.4	1.96E-20	0.779	301.6	1.54E-20	0.778	301.8	1.26E-20	0.778	302.0	1.03E-20	0.778
302.2	8.53E-21	0.778	302.4	7.13E-21	0.778	302.6	6.61E-21	0.777	302.8	1.44E-20	0.777	303.0	3.18E-20	0.777
303.2	3.81E-20	0.777	303.4	5.57E-20	0.777	303.6	6.91E-20	0.776	303.8	6.58E-20	0.776	304.0	6.96E-20	0.776
304.2	5.79E-20	0.776	304.4	5.24E-20	0.776	304.6	4.30E-20	0.775	304.8	3.28E-20	0.775	305.0	3.60E-20	0.775
305.2	5.12E-20	0.775	305.4	4.77E-20	0.775	305.6	4.43E-20	0.774	305.8	4.60E-20	0.774	306.0	4.01E-20	0.774
306.2	3.28E-20	0.774	306.4	2.66E-20	0.774	306.6	2.42E-20	0.773	306.8	1.95E-20	0.773	307.0	1.58E-20	0.773
307.2	1.37E-20	0.773	307.4	1.19E-20	0.773	307.6	1.01E-20	0.772	307.8	9.01E-21	0.772	308.0	8.84E-21	0.772
308.2	2.08E-20	0.772	308.4	2.39E-20	0.772	308.6	3.08E-20	0.771	308.8	3.39E-20	0.771	309.0	3.18E-20	0.771
309.2	3.06E-20	0.771	309.4	2.84E-20	0.771	309.6	2.46E-20	0.770	309.8	1.95E-20	0.770	310.0	1.57E-20	0.770
310.2	1.26E-20	0.767	310.4	9.26E-21	0.764	310.6	7.71E-21	0.761	310.8	6.05E-21	0.758	311.0	5.13E-21	0.755
311.2	4.82E-21	0.752	311.4	4.54E-21	0.749	311.6	6.81E-21	0.746	311.8	1.04E-20	0.743	312.0	1.43E-20	0.740
312.2	1.47E-20	0.737	312.4	1.35E-20	0.734	312.6	1.13E-20	0.731	312.8	9.86E-21	0.728	313.0	7.82E-21	0.725
313.2	6.48E-21	0.722	313.4	1.07E-20	0.719	313.6	2.39E-20	0.716	313.8	3.80E-20	0.713	314.0	5.76E-20	0.710
314.2	6.14E-20	0.707	314.4	7.45E-20	0.704	314.6	5.78E-20	0.701	314.8	5.59E-20	0.698	315.0	4.91E-20	0.695
315.2	4.37E-20	0.692	315.4	3.92E-20	0.689	315.6	2.89E-20	0.686	315.8	2.82E-20	0.683	316.0	2.10E-20	0.680
316.2	1.66E-20	0.677	316.4	2.05E-20	0.674	316.6	4.38E-20	0.671	316.8	5.86E-20	0.668	317.0	6.28E-20	0.665
317.2	5.07E-20	0.662	317.4	4.33E-20	0.659	317.6	4.17E-20	0.656	317.8	3.11E-20	0.653	318.0	2.64E-20	0.650
318.2	2.24E-20	0.647	318.4	1.70E-20	0.644	318.6	1.24E-20	0.641	318.8	1.11E-20	0.638	319.0	7.70E-21	0.635
319.2	6.36E-21	0.632	319.4	5.36E-21	0.629	319.6	4.79E-21	0.626	319.8	6.48E-21	0.623	320.0	1.48E-20	0.620
320.2	1.47E-20	0.614	320.4	1.36E-20	0.608	320.6	1.69E-20	0.601	320.8	1.32E-20	0.595	321.0	1.49E-20	0.589
321.2	1.17E-20	0.583	321.4	1.15E-20	0.577	321.6	9.64E-21	0.570	321.8	7.26E-21	0.564	322.0	5.94E-21	0.558
322.2	4.13E-21	0.552	322.4	3.36E-21	0.546	322.6	2.39E-21	0.539	322.8	2.01E-21	0.533	323.0	1.76E-21	0.527
323.2	2.82E-21	0.521	323.4	4.65E-21	0.515	323.6	7.00E-21	0.508	323.8	7.80E-21	0.502	324.0	7.87E-21	0.496
324.2	6.59E-21	0.490	324.4	5.60E-21	0.484	324.6	4.66E-21	0.477	324.8	4.21E-21	0.471	325.0	7.77E-21	0.465
325.2	2.15E-20	0.459	325.4	3.75E-20	0.453	325.6	4.10E-20	0.446	325.8	6.47E-20	0.440	326.0	7.59E-20	0.434
326.2	6.51E-20	0.428	326.4	5.53E-20	0.422	326.6	5.76E-20	0.415	326.8	4.43E-20	0.409	327.0	3.44E-20	0.403
327.2	3.22E-20	0.397	327.4	2.13E-20	0.391	327.6	1.91E-20	0.384	327.8	1.42E-20	0.378	328.0	9.15E-21	0.372
328.2	6.79E-21	0.366	328.4	4.99E-21	0.360	328.6	4.77E-21	0.353	328.8	1.75E-20	0.347	329.0	3.27E-20	0.341
329.2	3.99E-20	0.335	329.4	5.13E-20	0.329	329.6	4.00E-20	0.322	329.8	3.61E-20	0.316	330.0	3.38E-20	0.310
330.2	3.08E-20	0.304	330.4	2.16E-20	0.298	330.6	2.09E-20	0.291	330.8	1.41E-20	0.285	331.0	9.95E-21	0.279
331.2	7.76E-21	0.273	331.4	6.16E-21	0.267	331.6	4.06E-21	0.260	331.8	3.03E-21	0.254	332.0	2.41E-21	0.248
332.2	1.74E-21	0.242	332.4	1.33E-21	0.236	332.6	2.70E-21	0.229	332.8	1.65E-21	0.223	333.0	1.17E-21	0.217
333.2	9.84E-22	0.211	333.4	8.52E-22	0.205	333.6	6.32E-22	0.198	333.8	5.21E-22	0.192	334.0	1.46E-21	0.186
334.2	1.80E-21	0.180	334.4	1.43E-21	0.174	334.6	1.03E-21	0.167	334.8	7.19E-22	0.161	335.0	4.84E-22	0.155
335.2	2.73E-22	0.149	335.4	1.34E-22	0.143	335.6	1.62E-22	0.136	335.8	1.25E-22	0.130	336.0	4.47E-22	0.124
336.2	1.23E-21	0.118	336.4	2.02E-21	0.112	336.6	3.00E-21	0.105	336.8	2.40E-21	0.099	337.0	3.07E-21	0.093
337.2	2.29E-21	0.087	337.4	2.46E-21	0.081	337.6	2.92E-21	0.074	337.8	8.10E-21	0.068	338.0	1.82E-20	0.062
338.2	3.10E-20	0.056	338.4	3.24E-20	0.050	338.6	4.79E-20	0.043	338.8	5.25E-20	0.037	339.0	5.85E-20	0.031
339.2	4.33E-20	0.025	339.4	4.20E-20	0.019	339.6	3.99E-20	0.012	339.8	3.11E-20	0.006	340.0	2.72E-20	0.000
Photolysis File = HCHONEWM														
280.0	2.49E-20	0.350	280.5	1.42E-20	0.346	281.0	1.51E-20	0.341	281.5	1.32E-20	0.336	282.0	9.73E-21	0.332
282.5	6.76E-21	0.327	283.0	5.82E-21	0.323	283.5	9.10E-21	0.319	284.0	3.71E-20	0.314	284.5	4.81E-20	0.309
285.0	3.95E-20	0.305	285.5	2.87E-20	0.301	286.0	2.24E-20	0.296	286.5	1.74E-20	0.291	287.0	1.13E-20	0.287
287.5	1.10E-20	0.282	288.0	2.62E-20	0.278	288.5	4.00E-20	0.273	289.0	3.55E-20	0.269	289.5	2.12E-20	0.264
290.0	1.07E-20	0.260	290.5	1.35E-20	0.258	291.0	1.99E-20	0.256	291.5	1.56E-20	0.254	292.0	8.65E-21	0.252
292.5	5.90E-21	0.250	293.0	1.11E-20	0.248	293.5	6.26E-20	0.246	294.0	7.40E-20	0.244	294.5	5.36E-20	0.242
295.0	4.17E-20	0.240	295.5	3.51E-20	0.238	296.0	2.70E-20	0.236	296.5	1.75E-20	0.234	297.0	1.16E-20	0.232
297.5	1.51E-20	0.230	298.0	3.69E-20	0.228	298.5	4.40E-20	0.226	299.0	3.44E-20	0.224	299.5	2.02E-20	0.222
300.0	1.06E-20	0.220	300.4	7.01E-21	0.220	300.6	8.63E-21	0.221	300.8	1.47E-20	0.221	301.0	2.01E-20	0.221
301.2	2.17E-20	0.221	301.4	1.96E-20	0.221	301.6	1.54E-20	0.222	301.8	1.26E-20	0.222	302.0	1.03E-20	0.222
302.2	8.53E-21	0.222	302.4	7.13E-21	0.222	302.6	6.61E-21	0.223	302.8	1.44E-20	0.223	303.0	3.18E-20	0.223
303.2	3.81E-20	0.223	303.4	5.57E-20	0.223	303.6	6.91E-20	0.224	303.8	6.58E-20	0.224	304.0	6.96E-20	0.224
304.2	5.79E-20	0.224	304.4	5.24E-20	0.224	304.6	4.30E-20	0.225	304.8	3.28E-20	0.225	305.0	3.60E-20	0.225
305.2	5.12E-20	0.225	305.4	4.77E-20	0.225	305.6	4.43E-20	0.226	305.8	4.60E-20	0.226	306.0	4.01E-20	0.226
306.2	3.28E-20	0.226	306.4	2.66E-20	0.226	306.6	2.42E-20	0.227	306.8	1.95E-20	0.227	307.0	1.58E-20	0.227
307.2	1.37E-20	0.227	307.4	1.19E-20	0.227	307.6	1.01E-20	0.228	307.8	9.01E-21	0.228	308.0	8.84E-21	0.228
308.2	2.08E-20	0.228	308.4	2.39E-20										

Table A-3. (continued)

WL (nm)	Abs (cm ²)	QY	WL (nm)	Abs (cm ²)	QY	WL (nm)	Abs (cm ²)	QY	WL (nm)	Abs (cm ²)	QY	WL (nm)	Abs (cm ²)	QY
319.2	6.36E-21	0.368	319.4	5.36E-21	0.371	319.6	4.79E-21	0.374	319.8	6.48E-21	0.377	320.0	1.48E-20	0.380
320.2	1.47E-20	0.386	320.4	1.36E-20	0.392	320.6	1.69E-20	0.399	320.8	1.32E-20	0.405	321.0	1.49E-20	0.411
321.2	1.17E-20	0.417	321.4	1.15E-20	0.423	321.6	9.64E-21	0.430	321.8	7.26E-21	0.436	322.0	5.94E-21	0.442
322.2	4.13E-21	0.448	322.4	3.36E-21	0.454	322.6	2.39E-21	0.461	322.8	2.01E-21	0.467	323.0	1.76E-21	0.473
323.2	2.82E-21	0.479	323.4	4.65E-21	0.485	323.6	7.00E-21	0.492	323.8	7.80E-21	0.498	324.0	7.87E-21	0.504
324.2	6.59E-21	0.510	324.4	5.60E-21	0.516	324.6	4.66E-21	0.523	324.8	4.21E-21	0.529	325.0	7.77E-21	0.535
325.2	2.15E-20	0.541	325.4	3.75E-20	0.547	325.6	4.10E-20	0.554	325.8	6.47E-20	0.560	326.0	7.59E-20	0.566
326.2	6.51E-20	0.572	326.4	5.53E-20	0.578	326.6	5.76E-20	0.585	326.8	4.43E-20	0.591	327.0	3.44E-20	0.597
327.2	3.22E-20	0.603	327.4	2.13E-20	0.609	327.6	1.91E-20	0.616	327.8	1.42E-20	0.622	328.0	9.15E-21	0.628
328.2	6.79E-21	0.634	328.4	4.99E-21	0.640	328.6	4.77E-21	0.647	328.8	1.75E-20	0.653	329.0	3.27E-20	0.659
329.2	3.99E-20	0.665	329.4	5.13E-20	0.671	329.6	4.00E-20	0.678	329.8	3.61E-20	0.684	330.0	3.38E-20	0.690
330.2	3.08E-20	0.694	330.4	2.16E-20	0.699	330.6	2.09E-20	0.703	330.8	1.41E-20	0.708	331.0	9.95E-21	0.712
331.2	7.76E-21	0.717	331.4	6.16E-21	0.721	331.6	4.06E-21	0.726	331.8	3.03E-21	0.730	332.0	2.41E-21	0.735
332.2	1.74E-21	0.739	332.4	1.33E-21	0.744	332.6	2.70E-21	0.748	332.8	1.65E-21	0.753	333.0	1.17E-21	0.757
333.2	9.84E-22	0.762	333.4	8.52E-22	0.766	333.6	6.32E-22	0.771	333.8	5.21E-22	0.775	334.0	1.46E-21	0.780
334.2	1.80E-21	0.784	334.4	1.43E-21	0.789	334.6	1.03E-21	0.793	334.8	7.19E-22	0.798	335.0	4.84E-22	0.802
335.2	2.73E-22	0.798	335.4	1.34E-22	0.794	335.6	0.00E+00	0.790	335.8	1.25E-22	0.786	336.0	4.47E-22	0.782
336.2	1.23E-21	0.778	336.4	2.02E-21	0.773	336.6	3.00E-21	0.769	336.8	2.40E-21	0.764	337.0	3.07E-21	0.759
337.2	2.29E-21	0.754	337.4	2.46E-21	0.749	337.6	2.92E-21	0.745	337.8	8.10E-21	0.740	338.0	1.02E-20	0.734
338.2	3.10E-20	0.729	338.4	3.24E-20	0.724	338.6	4.79E-20	0.719	338.8	5.25E-20	0.714	339.0	5.85E-20	0.709
339.2	4.33E-20	0.703	339.4	4.20E-20	0.698	339.6	3.99E-20	0.693	339.8	3.11E-20	0.687	340.0	2.72E-20	0.682
340.2	1.99E-20	0.676	340.4	1.76E-20	0.671	340.6	1.39E-20	0.666	340.8	1.01E-20	0.660	341.0	6.57E-21	0.655
341.2	4.83E-21	0.649	341.4	3.47E-21	0.643	341.6	2.23E-21	0.638	341.8	1.55E-21	0.632	342.0	3.70E-21	0.627
342.2	4.64E-21	0.621	342.4	1.08E-20	0.616	342.6	1.14E-20	0.610	342.8	1.79E-20	0.604	343.0	2.33E-20	0.599
343.2	1.72E-20	0.593	343.4	1.55E-20	0.588	343.6	1.46E-20	0.582	343.8	1.38E-20	0.576	344.0	1.00E-20	0.571
344.2	8.26E-21	0.565	344.4	6.32E-21	0.559	344.6	4.28E-21	0.554	344.8	3.22E-21	0.548	345.0	2.54E-21	0.542
345.2	1.60E-21	0.537	345.4	1.15E-21	0.531	345.6	8.90E-22	0.525	345.8	6.50E-22	0.520	346.0	5.09E-22	0.514
346.2	5.15E-22	0.508	346.4	3.45E-22	0.503	346.6	3.18E-22	0.497	346.8	3.56E-22	0.491	347.0	3.24E-22	0.485
347.2	3.34E-22	0.480	347.4	2.88E-22	0.474	347.6	2.84E-22	0.468	347.8	9.37E-22	0.463	348.0	9.70E-22	0.457
348.2	7.60E-22	0.451	348.4	6.24E-22	0.446	348.6	4.99E-22	0.440	348.8	4.08E-22	0.434	349.0	3.39E-22	0.428
349.2	1.64E-22	0.423	349.4	1.49E-22	0.417	349.6	8.30E-23	0.411	349.8	2.52E-23	0.406	350.0	2.57E-23	0.400
350.2	0.00E+00	0.394	350.4	5.16E-23	0.389	350.6	0.00E+00	0.383	350.8	2.16E-23	0.377	351.0	7.07E-23	0.371
351.2	3.45E-23	0.366	351.4	1.97E-22	0.360	351.6	4.80E-22	0.354	351.8	3.13E-21	0.349	352.0	6.41E-21	0.343
352.2	8.38E-21	0.337	352.4	1.55E-20	0.331	352.6	1.86E-20	0.326	352.8	1.94E-20	0.320	353.0	2.78E-20	0.314
353.2	1.96E-20	0.309	353.4	1.67E-20	0.303	353.6	1.75E-20	0.297	353.8	1.63E-20	0.291	354.0	1.36E-20	0.286
354.2	1.07E-20	0.280	354.4	9.82E-21	0.274	354.6	8.66E-21	0.269	354.8	6.44E-21	0.263	355.0	4.84E-21	0.257
355.2	3.49E-21	0.251	355.4	2.41E-21	0.246	355.6	1.74E-21	0.240	355.8	1.11E-21	0.234	356.0	7.37E-22	0.229
356.2	4.17E-22	0.223	356.4	1.95E-22	0.217	356.6	1.50E-22	0.211	356.8	8.14E-23	0.206	357.0	0.00E+00	0.200
Photolysis File = CCHOR														
260.0	2.00E-20	0.310	270.0	3.40E-20	0.390	280.0	4.50E-20	0.580	290.0	4.90E-20	0.530	295.0	4.50E-20	0.480
300.0	4.30E-20	0.430	305.0	3.40E-20	0.370	315.0	2.10E-20	0.170	320.0	1.80E-20	0.100	325.0	1.10E-20	0.040
330.0	6.90E-21	0.000												
Photolysis File = RCHO														
280.0	5.26E-20	0.960	290.0	5.77E-20	0.910	300.0	5.05E-20	0.860	310.0	3.68E-20	0.600	320.0	1.66E-20	0.360
330.0	6.49E-21	0.200	340.0	1.44E-21	0.080	345.0	0.00E+00	0.020						
Photolysis File = ACET-93C														
250.0	2.37E-20	0.760	260.0	3.66E-20	0.800	270.0	4.63E-20	0.640	280.0	5.05E-20	0.550	290.0	4.21E-20	0.300
300.0	2.78E-20	0.150	310.0	1.44E-20	0.050	320.0	4.80E-21	0.026	330.0	8.00E-22	0.017	340.0	1.00E-22	0.000
350.0	3.00E-23	0.000	360.0	0.00E+00	0.000									
Photolysis File = KETONE														
210.0	1.10E-21	1.000	220.0	1.20E-21	1.000	230.0	4.60E-21	1.000	240.0	1.30E-20	1.000	250.0	2.68E-20	1.000
260.0	4.21E-20	1.000	270.0	5.54E-20	1.000	280.0	5.92E-20	1.000	290.0	5.16E-20	1.000	300.0	3.44E-20	1.000
310.0	1.53E-20	1.000	320.0	4.60E-21	1.000	330.0	1.10E-21	1.000	340.0	0.00E+00	1.000			
Photolysis File = GLYOXAL1														
230.0	2.87E-21	1.000	235.0	2.87E-21	1.000	240.0	4.30E-21	1.000	245.0	5.73E-21	1.000	250.0	8.60E-21	1.000
255.0	1.15E-20	1.000	260.0	1.43E-20	1.000	265.0	1.86E-20	1.000	270.0	2.29E-20	1.000	275.0	2.58E-20	1.000
280.0	2.87E-20	1.000	285.0	3.30E-20	1.000	290.0	3.15E-20	1.000	295.0	3.30E-20	1.000	300.0	3.58E-20	1.000
305.0	2.72E-20	1.000	310.0	2.72E-20	1.000	312.5	2.87E-20	1.000	315.0	2.29E-20	1.000	320.0	1.43E-20	1.000
325.0	1.15E-20	1.000	327.5	1.43E-20	1.000	330.0	1.15E-20	1.000	335.0	2.87E-21	1.000	340.0	0.00E+00	1.000
Photolysis File = GLYOXAL2														
355.0	0.00E+00	1.000	360.0	2.29E-21	1.000	365.0	2.87E-21	1.000	370.0	8.03E-21	1.000	375.0	1.00E-20	1.000
380.0	1.72E-20	1.000	382.0	1.58E-20	1.000	384.0	1.49E-20	1.000	386.0	1.49E-20	1.000	388.0	2.87E-20	1.000
390.0	3.15E-20	1.000	391.0	3.24E-20	1.000	392.0	3.04E-20	1.000	393.0	2.23E-20	1.000	394.0	2.63E-20	1.000
395.0	3.04E-20	1.000	396.0	2.63E-20	1.000	397.0	2.43E-20	1.000	398.0	3.24E-20	1.000	399.0	3.04E-20	1.000
400.0	2.84E-20	1.000	401.0	3.24E-20	1.000	402.0	4.46E-20	1.000	403.0	5.27E-20	1.000	404.0	4.26E-20	1.000
405.0	3.04E-20	1.000	406.0	3.04E-20	1.000	407.0	2.84E-20	1.000	408.0	2.43E-20	1.000	409.0	2.84E-20	1.000
410.0	6.08E-20	1.000	411.0	5.07E-20	1.000	411.5	6.08E-20	1.000	412.0	4.86E-20	1.000	413.0	8.31E-20	1.000
413.5	6.48E-20	1.000	414.0	7.50E-20	1.000	414.5	8.11E-20	1.000	415.0	8.11E-20	1.000	415.5	6.89E-20	1.000
416.0	4.26E-20	1.000	417.0	4.86E-20	1.000	418.0	5.88E-20	1.000	419.0	6.69E-20	1.000	420.0	3.85E-20	1.000
421.0	5.67E-20	1.000	421.5	4.46E-20	1.000	422.5	5.27E-20	1.000	422.5	1.05E-19	1.000	423.0	8.51E-20	1.000
424.0	6.08E-20	1.000	425.0	7.29E-20	1.000	426.0	1.18E-19	1.000	426.5	1.30E-19	1.000	427.0	1.07E-19	1.000
428.0	1.66E-19	1.000	429.0	4.05E-20	1.000	430.0	5.07E-20	1.000	431.0	4.86E-20	1.000	432.0	4.05E-20	1.000
433.0	3.65E-20	1.000	434.0	4.05E-20	1.000	434.5	6.08E-20	1.000	435.0	5.07E-20	1.000	436.0	8.11E-20	1.000
436.5	1.13E-19	1.000	437.0	5.27E-20	1.000	438.0	1.01E-19	1.000	438.5	1.38E-19	1.000	439.0	7.70E-20	1.000
440.0	2.47E-19	1.000	441.0	8.11E-20	1.000	442.0	6.08E-20	1.000	443.0	7.50E-20	1.000	444.0	9.32E-20	1.000
445.0	1.13E-19	1.000	446.0	5.27E-20	1.000	447.0	2.43E-20	1.000	448.0	2.84E-20	1.000	449.0	3.85E-20	1.000
450.0	6.08E-20	1.000	451.0	1.09E-19	1.000	451.5	9.32E-20	1.000	452.0	1.22E-19	1.000	453.0	2.39E-19	1.000
454.0	1.70E-19	1.000	455.0	3.40E-19	1.000	455.5	4.05E-1							

Table A-3. (continued)

WL (nm)	Abs (cm ²)	QY	WL (nm)	Abs (cm ²)	QY	WL (nm)	Abs (cm ²)	QY	WL (nm)	Abs (cm ²)	QY	WL (nm)	Abs (cm ²)	QY
458.0	1.22E-20	1.000	458.5	1.42E-20	1.000	459.0	4.05E-21	1.000	460.0	4.05E-21	1.000	460.5	6.08E-21	1.000
461.0	2.03E-21	1.000	462.0	0.00E+00	1.000									
Photolysis File = GLYOXAL (consists of GLYOXAL1 for wavelengths below 350 nm and GLYOXAL2 for wavelengths above 350 nm)														
Photolysis File = MEGLYOX1														
220.0	2.10E-21	1.000	225.0	2.10E-21	1.000	230.0	4.21E-21	1.000	235.0	7.57E-21	1.000	240.0	9.25E-21	1.000
245.0	8.41E-21	1.000	250.0	9.25E-21	1.000	255.0	9.25E-21	1.000	260.0	9.67E-21	1.000	265.0	1.05E-20	1.000
270.0	1.26E-20	1.000	275.0	1.43E-20	1.000	280.0	1.51E-20	1.000	285.0	1.43E-20	1.000	290.0	1.47E-20	1.000
295.0	1.18E-20	1.000	300.0	1.14E-20	1.000	305.0	9.25E-21	1.000	310.0	6.31E-21	1.000	315.0	5.47E-21	1.000
320.0	3.36E-21	1.000	325.0	1.68E-21	1.000	330.0	8.41E-22	1.000	335.0	0.00E+00	1.000			
Photolysis File = MEGLYOX2														
350.0	0.00E+00	1.000	354.0	4.21E-22	1.000	358.0	1.26E-21	1.000	360.0	2.10E-21	1.000	362.0	2.10E-21	1.000
364.0	2.94E-21	1.000	366.0	3.36E-21	1.000	368.0	4.21E-21	1.000	370.0	5.47E-21	1.000	372.0	5.89E-21	1.000
374.0	7.57E-21	1.000	376.0	7.99E-21	1.000	378.0	8.83E-21	1.000	380.0	1.01E-20	1.000	382.0	1.09E-20	1.000
384.0	1.35E-20	1.000	386.0	1.51E-20	1.000	388.0	1.72E-20	1.000	390.0	2.06E-20	1.000	392.0	2.10E-20	1.000
394.0	2.31E-20	1.000	396.0	2.48E-20	1.000	398.0	2.61E-20	1.000	400.0	2.78E-20	1.000	402.0	2.99E-20	1.000
404.0	3.20E-20	1.000	406.0	3.79E-20	1.000	408.0	3.95E-20	1.000	410.0	4.33E-20	1.000	412.0	4.71E-20	1.000
414.0	4.79E-20	1.000	416.0	4.88E-20	1.000	418.0	5.05E-20	1.000	420.0	5.21E-20	1.000	422.0	5.30E-20	1.000
424.0	5.17E-20	1.000	426.0	5.30E-20	1.000	428.0	5.21E-20	1.000	430.0	5.55E-20	1.000	432.0	5.13E-20	1.000
434.0	5.68E-20	1.000	436.0	6.22E-20	1.000	438.0	6.06E-20	1.000	440.0	5.47E-20	1.000	441.0	6.14E-20	1.000
442.0	5.47E-20	1.000	443.0	5.55E-20	1.000	443.5	6.81E-20	1.000	444.0	5.97E-20	1.000	445.0	5.13E-20	1.000
446.0	4.88E-20	1.000	447.0	5.72E-20	1.000	448.0	5.47E-20	1.000	449.0	6.56E-20	1.000	450.0	5.05E-20	1.000
451.0	3.03E-20	1.000	452.0	4.29E-20	1.000	453.0	2.78E-20	1.000	454.0	2.27E-20	1.000	456.0	1.77E-20	1.000
458.0	8.41E-21	1.000	460.0	4.21E-21	1.000	464.0	1.68E-21	1.000	468.0	0.00E+00	1.000			
Photolysis File = BZCHO														
299.0	1.78E-19	1.000	304.0	7.40E-20	1.000	306.0	6.91E-20	1.000	309.0	6.41E-20	1.000	313.0	6.91E-20	1.000
314.0	6.91E-20	1.000	318.0	6.41E-20	1.000	325.0	8.39E-20	1.000	332.0	7.65E-20	1.000	338.0	8.88E-20	1.000
342.0	8.88E-20	1.000	346.0	7.89E-20	1.000	349.0	7.89E-20	1.000	354.0	9.13E-20	1.000	355.0	8.14E-20	1.000
364.0	5.67E-20	1.000	368.0	6.66E-20	1.000	369.0	8.39E-20	1.000	370.0	8.39E-20	1.000	372.0	3.45E-20	1.000
374.0	3.21E-20	1.000	376.0	2.47E-20	1.000	377.0	2.47E-20	1.000	380.0	3.58E-20	1.000	382.0	9.90E-21	1.000
386.0	0.00E+00	1.000												
Photolysis File = ACRROLEIN														
250.0	1.80E-21	1.000	252.0	2.05E-21	1.000	253.0	2.20E-21	1.000	254.0	2.32E-21	1.000	255.0	2.45E-21	1.000
256.0	2.56E-21	1.000	257.0	2.65E-21	1.000	258.0	2.74E-21	1.000	259.0	2.83E-21	1.000	260.0	2.98E-21	1.000
261.0	3.24E-21	1.000	262.0	3.47E-21	1.000	263.0	3.58E-21	1.000	264.0	3.93E-21	1.000	265.0	4.67E-21	1.000
266.0	5.10E-21	1.000	267.0	5.38E-21	1.000	268.0	5.73E-21	1.000	269.0	6.13E-21	1.000	270.0	6.64E-21	1.000
271.0	7.20E-21	1.000	272.0	7.77E-21	1.000	273.0	8.37E-21	1.000	274.0	8.94E-21	1.000	275.0	9.55E-21	1.000
276.0	1.04E-20	1.000	277.0	1.12E-20	1.000	278.0	1.19E-20	1.000	279.0	1.27E-20	1.000	280.0	1.27E-20	1.000
281.0	1.26E-20	1.000	282.0	1.26E-20	1.000	283.0	1.28E-20	1.000	284.0	1.33E-20	1.000	285.0	1.38E-20	1.000
286.0	1.44E-20	1.000	287.0	1.50E-20	1.000	288.0	1.57E-20	1.000	289.0	1.63E-20	1.000	290.0	1.71E-20	1.000
291.0	1.78E-20	1.000	292.0	1.86E-20	1.000	293.0	1.95E-20	1.000	294.0	2.05E-20	1.000	295.0	2.15E-20	1.000
296.0	2.26E-20	1.000	297.0	2.37E-20	1.000	298.0	2.48E-20	1.000	299.0	2.60E-20	1.000	300.0	2.73E-20	1.000
301.0	2.85E-20	1.000	302.0	2.99E-20	1.000	303.0	3.13E-20	1.000	304.0	3.27E-20	1.000	305.0	3.39E-20	1.000
306.0	3.51E-20	1.000	307.0	3.63E-20	1.000	308.0	3.77E-20	1.000	309.0	3.91E-20	1.000	310.0	4.07E-20	1.000
311.0	4.25E-20	1.000	312.0	4.39E-20	1.000	313.0	4.44E-20	1.000	314.0	4.50E-20	1.000	315.0	4.59E-20	1.000
316.0	4.75E-20	1.000	317.0	4.90E-20	1.000	318.0	5.05E-20	1.000	319.0	5.19E-20	1.000	320.0	5.31E-20	1.000
321.0	5.43E-20	1.000	322.0	5.52E-20	1.000	323.0	5.60E-20	1.000	324.0	5.67E-20	1.000	325.0	5.67E-20	1.000
326.0	5.62E-20	1.000	327.0	5.63E-20	1.000	328.0	5.71E-20	1.000	329.0	5.76E-20	1.000	330.0	5.80E-20	1.000
331.0	5.95E-20	1.000	332.0	6.23E-20	1.000	333.0	6.39E-20	1.000	334.0	6.38E-20	1.000	335.0	6.24E-20	1.000
336.0	6.01E-20	1.000	337.0	5.79E-20	1.000	338.0	5.63E-20	1.000	339.0	5.56E-20	1.000	340.0	5.52E-20	1.000
341.0	5.54E-20	1.000	342.0	5.53E-20	1.000	343.0	5.47E-20	1.000	344.0	5.41E-20	1.000	345.0	5.40E-20	1.000
346.0	5.48E-20	1.000	347.0	5.90E-20	1.000	348.0	6.08E-20	1.000	349.0	6.00E-20	1.000	350.0	5.53E-20	1.000
351.0	5.03E-20	1.000	352.0	4.50E-20	1.000	353.0	4.03E-20	1.000	354.0	3.75E-20	1.000	355.0	3.55E-20	1.000
356.0	3.45E-20	1.000	357.0	3.46E-20	1.000	358.0	3.49E-20	1.000	359.0	3.41E-20	1.000	360.0	3.23E-20	1.000
361.0	2.95E-20	1.000	362.0	2.81E-20	1.000	363.0	2.91E-20	1.000	364.0	3.25E-20	1.000	365.0	3.54E-20	1.000
366.0	3.30E-20	1.000	367.0	2.78E-20	1.000	368.0	2.15E-20	1.000	369.0	1.59E-20	1.000	370.0	1.19E-20	1.000
371.0	8.99E-21	1.000	372.0	7.22E-21	1.000	373.0	5.86E-21	1.000	374.0	4.69E-21	1.000	375.0	3.72E-21	1.000
376.0	3.57E-21	1.000	377.0	3.55E-21	1.000	378.0	2.83E-21	1.000	379.0	1.69E-21	1.000	380.0	8.29E-24	1.000
381.0	0.00E+00	1.000												
Photolysis File = CL2														
260.0	2.00E-21	1.000	270.0	8.20E-21	1.000	280.0	2.60E-20	1.000	290.0	6.20E-20	1.000	300.0	1.19E-19	1.000
310.0	1.85E-19	1.000	320.0	2.37E-19	1.000	330.0	2.55E-19	1.000	340.0	2.35E-19	1.000	350.0	1.88E-19	1.000
360.0	1.32E-19	1.000	370.0	8.40E-20	1.000	380.0	5.00E-20	1.000	390.0	2.90E-20	1.000	400.0	1.80E-20	1.000
410.0	1.30E-20	1.000	420.0	9.60E-21	1.000	430.0	7.30E-21	1.000	440.0	5.40E-21	1.000	450.0	3.80E-21	1.000
460.0	2.60E-21	1.000	470.0	1.60E-21	1.000	480.0	0.00E+00	1.000						
Photolysis File = CLNO														
190.0	4.32E-17	1.000	192.0	5.34E-17	1.000	194.0	6.15E-17	1.000	196.0	6.48E-17	1.000	198.0	6.31E-17	1.000
200.0	5.86E-17	1.000	202.0	5.25E-17	1.000	204.0	4.54E-17	1.000	206.0	3.84E-17	1.000	208.0	3.21E-17	1.000
210.0	2.63E-17	1.000	212.0	2.18E-17	1.000	214.0	1.76E-17	1.000	216.0	1.40E-17	1.000	218.0	1.11E-17	1.000
220.0	8.96E-18	1.000	222.0	7.07E-18	1.000	224.0	5.52E-18	1.000	226.0	4.36E-18	1.000	228.0	3.39E-18	1.000
230.0	2.66E-18	1.000	232.0	2.12E-18	1.000	234.0	1.64E-18	1.000	236.0	1.28E-18	1.000	238.0	1.01E-18	1.000
240.0	8.25E-19	1.000	242.0	6.72E-19	1.000	244.0	5.51E-19	1.000	246.0	4.52E-19	1.000	248.0	3.77E-19	1.000
250.0	3.17E-19	1.000	252.0	2.74E-19	1.000	254.0	2.37E-19	1.000	256.0	2.13E-19	1.000	258.0	1.90E-19	1.000
260.0	1.75E-19	1.000	262.0	1.65E-19	1.000	264.0	1.53E-19	1.000	266.0	1.44E-19	1.000	268.0	1.36E-19	1.000
270.0	1.29E-19	1.000	272.0	1.23E-19	1.000	274.0	1.18E-19	1.000	276.0	1.13E-19	1.000	278.0	1.07E-19	1.000
280.0	1.06E-19	1.000	282.0	1.02E-19	1.000	284.0	9.99E-20	1.000	286.0	9.84E-20	1.000	288.0	9.71E-20	1.000
290.0	9.64E-20	1.000	292.0	9.63E-20	1.000	294.0	9.69E-20	1.000	296.0	9.71E-20	1.000	298.0	9.89E-20	1.000

Table A-3. (continued)

WL (nm)	Abs (cm ²)	QY	WL (nm)	Abs (cm ²)	QY	WL (nm)	Abs (cm ²)	QY	WL (nm)	Abs (cm ²)	QY	WL (nm)	Abs (cm ²)	QY
300.0	1.00E-19	1.000	302.0	1.03E-19	1.000	304.0	1.05E-19	1.000	306.0	1.08E-19	1.000	308.0	1.11E-19	1.000
310.0	1.15E-19	1.000	312.0	1.19E-19	1.000	314.0	1.22E-19	1.000	316.0	1.25E-19	1.000	318.0	1.30E-19	1.000
320.0	1.34E-19	1.000	322.0	1.36E-19	1.000	324.0	1.40E-19	1.000	326.0	1.43E-19	1.000	328.0	1.46E-19	1.000
330.0	1.47E-19	1.000	332.0	1.49E-19	1.000	334.0	1.51E-19	1.000	336.0	1.53E-19	1.000	338.0	1.53E-19	1.000
340.0	1.52E-19	1.000	342.0	1.53E-19	1.000	344.0	1.51E-19	1.000	346.0	1.51E-19	1.000	348.0	1.49E-19	1.000
350.0	1.45E-19	1.000	355.0	1.36E-19	1.000	360.0	1.29E-19	1.000	365.0	1.20E-19	1.000	370.0	1.10E-19	1.000
375.0	9.95E-20	1.000	380.0	8.86E-20	1.000	385.0	7.82E-20	1.000	390.0	6.86E-20	1.000	395.0	5.97E-20	1.000
400.0	5.13E-20	1.000	405.0	4.40E-20	1.000	410.0	3.83E-20	1.000	415.0	3.38E-20	1.000	420.0	2.89E-20	1.000
425.0	2.45E-20	1.000	430.0	2.21E-20	1.000	435.0	2.20E-20	1.000	440.0	2.20E-20	1.000	445.0	2.07E-20	1.000
450.0	1.87E-20	1.000	455.0	1.79E-20	1.000	460.0	1.95E-20	1.000	465.0	2.25E-20	1.000	470.0	2.50E-20	1.000
475.0	2.61E-20	1.000	480.0	2.53E-20	1.000	485.0	2.33E-20	1.000	490.0	2.07E-20	1.000	495.0	1.78E-20	1.000
500.0	1.50E-20	1.000	505.0	0.00E+00	1.000									
Photolysis File = CLONO														
235.0	2.15E-18	1.000	240.0	1.76E-18	1.000	245.0	1.37E-18	1.000	250.0	1.06E-18	1.000	255.0	6.50E-19	1.000
260.0	6.46E-19	1.000	265.0	6.93E-19	1.000	270.0	9.03E-19	1.000	275.0	1.10E-18	1.000	280.0	1.32E-18	1.000
285.0	1.44E-18	1.000	290.0	1.44E-18	1.000	295.0	1.42E-18	1.000	300.0	1.29E-18	1.000	305.0	1.14E-18	1.000
310.0	1.05E-18	1.000	315.0	9.81E-19	1.000	320.0	8.03E-19	1.000	325.0	7.54E-19	1.000	330.0	5.87E-19	1.000
335.0	5.77E-19	1.000	340.0	4.37E-19	1.000	345.0	3.75E-19	1.000	350.0	2.69E-19	1.000	355.0	2.29E-19	1.000
360.0	1.61E-19	1.000	365.0	1.13E-19	1.000	370.0	9.00E-20	1.000	375.0	6.90E-20	1.000	380.0	4.10E-20	1.000
385.0	3.30E-20	1.000	390.0	2.20E-20	1.000	395.0	1.50E-20	1.000	400.0	6.00E-21	1.000	405.0	0.00E+00	1.000
Photolysis File = CLNO2														
190.0	2.69E-17	1.000	200.0	4.68E-18	1.000	210.0	3.20E-18	1.000	220.0	3.39E-18	1.000	230.0	2.26E-18	1.000
240.0	1.33E-18	1.000	250.0	9.06E-19	1.000	260.0	6.13E-19	1.000	270.0	3.53E-19	1.000	280.0	2.20E-19	1.000
290.0	1.73E-19	1.000	300.0	1.49E-19	1.000	310.0	1.21E-19	1.000	320.0	8.87E-20	1.000	330.0	5.84E-20	1.000
340.0	3.54E-20	1.000	350.0	2.04E-20	1.000	360.0	1.15E-20	1.000	370.0	6.90E-21	1.000	380.0	0.00E+00	1.000
Photolysis File = CLONO2														
200.0	2.82E-18	1.000	205.0	2.84E-18	1.000	210.0	3.14E-18	1.000	215.0	3.42E-18	1.000	220.0	3.32E-18	1.000
225.0	2.78E-18	1.000	230.0	2.08E-18	1.000	235.0	1.48E-18	1.000	240.0	1.05E-18	1.000	245.0	7.64E-19	1.000
250.0	5.60E-19	1.000	255.0	4.32E-19	1.000	260.0	3.38E-19	1.000	265.0	2.65E-19	1.000	270.0	2.05E-19	1.000
275.0	1.57E-19	1.000	280.0	1.19E-19	1.000	285.0	8.80E-20	1.000	290.0	6.41E-20	1.000	295.0	4.38E-20	1.000
300.0	3.13E-20	1.000	305.0	2.24E-20	1.000	310.0	1.60E-20	1.000	315.0	1.14E-20	1.000	320.0	8.31E-21	1.000
325.0	6.13E-21	1.000	330.0	4.66E-21	1.000	335.0	3.67E-21	1.000	340.0	3.02E-21	1.000	345.0	2.58E-21	1.000
350.0	2.29E-21	1.000	355.0	2.08E-21	1.000	360.0	2.00E-21	1.000	365.0	1.80E-21	1.000	370.0	1.59E-21	1.000
375.0	1.41E-21	1.000	380.0	1.21E-21	1.000	385.0	1.37E-21	1.000	390.0	9.10E-22	1.000	395.0	7.60E-22	1.000
400.0	6.40E-22	1.000	405.0	5.40E-22	1.000	410.0	4.40E-22	1.000	415.0	3.60E-22	1.000	420.0	3.20E-22	1.000
425.0	2.30E-22	1.000	430.0	1.90E-22	1.000	435.0	0.00E+00	1.000						
Photolysis File = HOCL														
200.0	7.10E-20	1.000	205.0	5.50E-20	1.000	210.0	5.70E-20	1.000	215.0	7.00E-20	1.000	220.0	9.70E-20	1.000
225.0	1.28E-19	1.000	230.0	1.64E-19	1.000	235.0	1.92E-19	1.000	240.0	2.07E-19	1.000	245.0	2.00E-19	1.000
250.0	1.73E-19	1.000	255.0	1.39E-19	1.000	260.0	1.05E-19	1.000	265.0	7.80E-20	1.000	270.0	6.00E-20	1.000
275.0	5.00E-20	1.000	280.0	4.70E-20	1.000	285.0	4.80E-20	1.000	290.0	5.30E-20	1.000	295.0	5.70E-20	1.000
300.0	6.00E-20	1.000	305.0	6.00E-20	1.000	310.0	5.90E-20	1.000	315.0	5.50E-20	1.000	320.0	4.90E-20	1.000
325.0	4.20E-20	1.000	330.0	3.50E-20	1.000	335.0	2.90E-20	1.000	340.0	2.40E-20	1.000	345.0	1.80E-20	1.000
350.0	1.50E-20	1.000	355.0	1.20E-20	1.000	360.0	8.00E-21	1.000	365.0	9.00E-21	1.000	370.0	8.00E-21	1.000
375.0	8.00E-21	1.000	380.0	8.00E-21	1.000	385.0	0.00E+00	1.000						

Table A-4. Values of chamber-dependent parameters used in the model simulations of the experiments for this study. [a]

Parm.	Value(s)	Discussion
k(1)	0.218 → 0.217 min ⁻¹	Derived by fitting results of quartz tube NO ₂ actinometry measurements to curve similar to that derived for other blacklight chambers by Carter et al. (1995b). The results of the actinometry measurements during this study were within the uncertainty range of this extrapolation.
k(O3W)	1.5x10 ⁻⁴ min ⁻¹	The results of the O ₃ dark decay experiments in this chamber are consistent with the recommended default of Carter et al. (1995b) for Teflon bag chambers in general.
k(N25I) k(N25S)	2.8 x10 ⁻³ min ⁻¹ , 1.5x10 ⁻⁶ - k _g ppm ⁻¹ min ⁻¹	Based on the N ₂ O ₅ decay rate measurements in a similar chamber (Tuazon et al. 1983). Although we previously estimated their rate constants were lower in the larger Teflon bag chambers (Carter and Lurmann, 1990, 1991), we now consider it more reasonable to use the same rate constants for all such chambers (Carter et al., 1995b).
k(NO2W) yHONO	1.6x10 ⁻⁴ min ⁻¹ 0.2	Based on dark NO ₂ decay and HONO formation measured in a similar chamber by Pitts et al. (1984). Assumed to be the same in all Teflon bag chambers (Carter et al, 1995b).
k(XSHC)	250 min ⁻¹	Estimated by modeling pure air irradiations. Not an important parameter affecting model predictions except for pure air or NO _x -air runs.
RS/K1	3.27x10 ⁶ e ^{-7297/T} ppm	Based on model simulations of n-butane - NO _x experiments. The temperature dependence is derived from simulating outdoor experiments as discussed by Carter et al. (1995b).
E-NO2/K1	0.03 ppb	Based on model simulations of pure air experiments.

[a] See Table A-2 for definition of parameters.